UNITED STATES DEPARTMENT OF COMMERCE
HENRY A. WALLACE, Secretary
NATIONAL BUREAU OF STANDARDS
E. U. Condon, Director

✦

Journal of Research

of the

National Bureau of Standards

✦

Volume 35, Number 4

October 1945

[Published with approval of the Director of the Budget]

UNITED STATES
GOVERNMENT PRINTING OFFICE
WASHINGTON : 1945

For sale by the Superintendent of Documents, U. S. Government Printing Office
Washington 25, D. C. - Price 30 cents, $3.50 per year on subscription

The prices of the separate Research Papers appearing in this JOURNAL are given on the front cover page. If 100 or more copies of any separate are ordered, a discount of 25 percent is allowed. Those who desire copies of separate Research Papers should send their orders and remittances without delay to the Superintendent of Documents, U. S. Government Printing Office, Washington 25, D. C. Research Papers are not printed from electrotypes, and usually no more reprints can be had when the first and only printing is exhausted.

MATHEMATICAL TABLES

A list of the mathematical tables now obtainable from the National Bureau of Standards is printed on pages 3 and 4 of the JOURNAL cover. New tables will be announced from time to time as they become available. An order blank is available on the last page of this issue.

U. S. Department of Commerce National Bureau of Standards

RESEARCH PAPER RP1671

Part of Journal of Research of the National Bureau of Standards, Volume 35, October 1945

COLOR STANDARD FOR RUBY MICA

By Deane B. Judd

ABSTRACT

At the request of the Metals Reserve Company and the War Production Board, a study has been made of the color classification of mica used by the mica-consuming industry. This classification has been found to be consistent and can be reproduced from the chromaticity of the mica specimen and its daylight transmission considered in relation to thickness. A method of defining ruby mica in these terms is described, and as it does not depend upon the physical integrity of any material color standard, this definition constitutes a fundamental color standard for ruby mica. This standard is particularly for application to micas close to the border line between ruby and nonruby.

CONTENTS

	Page
I. Introduction	245
II. Selection of borderline specimens	246
III. Method of measurement	247
IV. Derivation of a hue and a lightness index for mica colors	248
V. Derivation and validification of a color standard for ruby mica	251
VI. Procedure used in color grading mica	255

I. INTRODUCTION

Mica is a critical material for the manufacture of electrical equipment for the armed forces because it is a good insulator and can be split to desirable thicknesses. Capacitor manufacturers prefer "ruby" mica because they find that the better qualities (clear, clear and slightly stained, fair stained, good stained)[1] are of satisfactory power factor and easy to split, whereas the "nonruby" micas of the same qualities often tend to be brittle, and much of it is found to have undesirably high power factor. At the request of the War Production Board and the Metals Reserve Company, a study has been made of the system of determining the color of mica by visual inspection used by the mica-consuming industry. There are micas of many colors: light green, green, rum, ruby, and intermediates between them, so that classification into ruby and nonruby often depends upon color differences so small as to be scarcely perceptible. As there have been no formally accepted standards for ruby mica the inspector must develop from his experience an idea of the borderline colors, and remember them. Furthermore, a given borderline mica will exhibit a progression of colors from nearly colorless through yellowish gray to dark

[1] Standard methods of test for grading and classification of natural mica, Am. Soc. Testing Materials, Standards, part III, Nonmetallic Materials, p. 504 (1944) D 351-38.

brown, inclining more toward red as the thickness of the specimen viewed is increased; so the inspector must take into account the thickness of the specimen in order to arrive at a judgment characteristic of the mica independent of its thickness. This he does by viewing the mica in several ways; single specimens of various thicknesses viewed against the sky, a handful of specimens viewed against the sky, single specimens of various thicknesses placed on a white surface and viewed by light that passes through each specimen twice, once to illuminate the white surface, once to reach the eye of the observer, and finally directly in the stock box or barrel in an opaque layer by light reflected from the nearly parallel faces of the various specimens in random position at various depths in the pile. His judgment is complicated by the fact that mica from a single mine to be classified exhibits more or less variation in color from specimen to specimen and from spot to spot within the same specimen.

In spite of these difficulties there has become established by trade practice a fairly definite idea of what is acceptable to the mica-consuming industry as ruby mica. An experienced inspector of mica comes to remember the family of colors corresponding to specimens of various thicknesses by constant intercomparison of members of such families. He disregards small variations such as air or mineral inclusions, or cloudy or stained areas of a specimen, makes a mental average of the colors of various specimens from a given lot or mine, and makes a mental comparison with a mental border line between ruby and nonruby that is surprisingly reliable and consistent.

It is the purpose of this paper to set up in fundamental terms the color standard for ruby mica, heretofore existent only in the memories of mica inspectors, and to show how this fundamental standard may be applied, particularly to specimens so close to the border line between ruby and nonruby as to make doubtful their classifications by direct visual inspection.

II. SELECTION OF BORDERLINE SPECIMENS

At the request of the War Production Board an industry task committee familiar with the visual classification of mica met in Asheville, N. C., on December 4, 1944, to review the classification of 35 lots of mica, classed as nonruby or doubtful, at the southern headquarters of the Colonial Mica Corporation, set up as agent for the Metals Reserve Company to ensure so far as possible a maximum supply of domestic mica for war industries. One-pound samples were taken of each of these lots and an extra sample of three of them. In addition, specimens characteristic of near-borderline mica from nine mines and eight stock boxes were also selected. These 17 specimens were visually intercompared, and it was noted that the color grading was consistent to a high degree. After correction of one small inconsistency in the color grading by consultation with George Purcell, Wm. J. Alexander, and Bradley Johnson of the Colonial Mica Corporation, with due regard to the judgments of the industry task committee, five specimens were selected to represent the border line between ruby and nonruby mica. These specimens were cut in two and each half marked respectively as follows: No. 2 quality border line, No. 1 quality border line, No. 1 quality ruby, No. 37 green, and No. 17 border line. One half of each was left at the Asheville offices as a

physical standard defining ruby mica. The other half of each was measured to provide a fundamental definition of the border line between ruby and nonruby mica.

III. METHOD OF MEASUREMENT

The approximate thicknesses of the five standard specimens were found by means of a direct-reading micrometer.

The five specimens were illuminated perpendicularly by artificial daylight (incandescent lamp combined with Corning Daylite glass of such thickness as to yield a color temperature of 6,500° K) in the chromaticity-difference colorimeter [2] and the chromaticity difference between the incident and emergent light was determined for each specimen in terms of the chromaticity coordinates (x, y) of the stand-

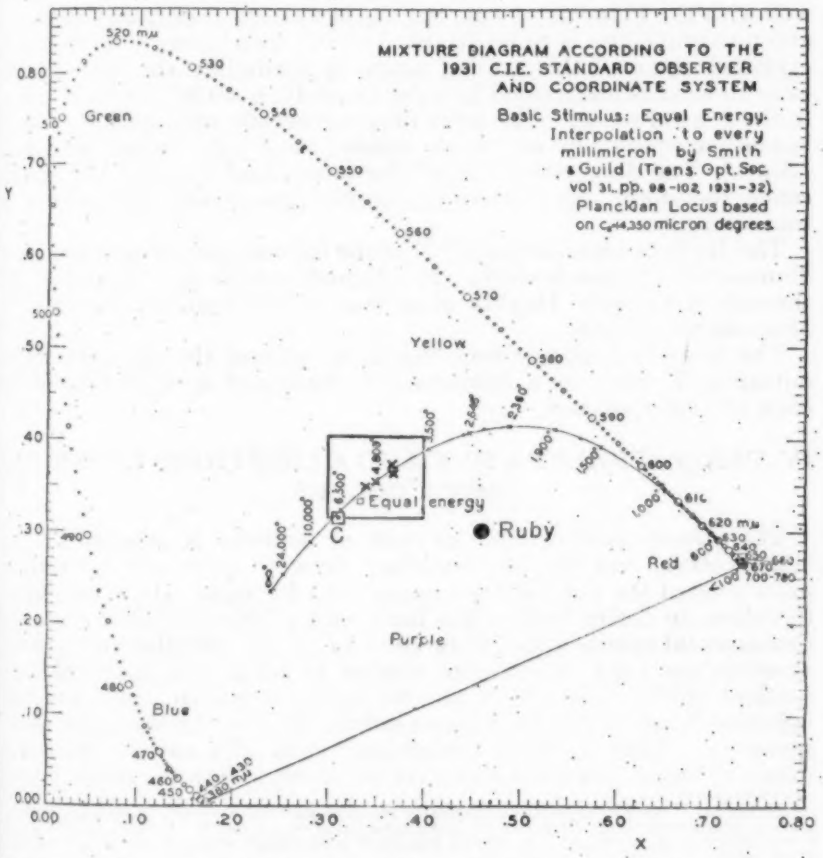

FIGURE 1.—*Chromaticity (x, y) diagram showing borderline mica specimens (crosses) compared to standard illuminant C (square), to ruby color (solid dot) and to the spectrum colors (small circles).*

These mica specimens have chromaticities corresponding to weak yellow and pale brown, and are to be considered close to "ruby" only in accord with the meaning of the term in trade practice. These chromaticities by a coincidence happen to fall close to those of the ideal radiator at about 4,800° K.

[1] D. B. Judd, Specification of uniform color tolerances for textiles, Textile Research **9**, 258 (1939).

ard ICI colorimetric coordinate system.[3] The chromaticity coordinates (x, y) for each specimen were estimated for ICI standard illuminant C (representative of average daylight) by adding the x-difference (Δx) to the x-coordinate (0.3101) for illuminant C, and by adding the y-difference (Δy) to the y-coordinate (0.3163); that is, x for each specimen was computed as $0.3101+\Delta x$, and y was computed as $0.3163+\Delta y$. Figure 1 shows the chromaticity diagram formed by plotting y against x. The chromaticities of the standard specimens are shown by crosses in relation to those (small circles) of the spectrum and the point (indicated by a square) representing illuminant C, which corresponds to a colorless mica. It may be noted that the range of chromaticities covered by the five specimens is relatively small, and it happens that the points fall close to the Planckian locus in the neighborhood of 4,800° K. Thus by a coincidence the borderline between ruby and nonruby mica agrees fairly well with the Planckian locus, but the agreement is only approximate, and no significance is to be attached to the coincidence. As might be expected, none of this limited range of borderline chromaticities is close to what is understood by ruby ($x=0.46$, $y=0.30$; see solid circle) in the general sense.[4] The color names generally appropriate to these borderline specimens are weak yellow, very pale brown, and pale brown.[5] The designation "ruby" for colors near to these has significance, therefore, only relative to classification of mica in accord with trade practice.

The daylight transmittance,[6] T, of the lightest part of each specimen illuminated perpendicularly by incandescent-lamp light filtered through a Corning Daylite glass was determined by means of a Martens photometer.

The two chromaticity coordinates (x, y) and the daylight transmittance, T, serve as a fundamental, three-part specification of the color of each specimen.

IV. DERIVATION OF A HUE AND A LIGHTNESS INDEX FOR MICA COLORS

The classification of mica as ruby or nonruby is primarily a hue classification,[7] but the hue boundary between ruby and nonruby is more toward the red for dark micas than for light. It is necessary, therefore, to derive both a hue index and a lightness index from the fundamental specification of the color (T, x, y). Furthermore, as the classification ruby or nonruby applies to mica as a material independent of the thickness of the particular specimen, these hue and lightness indices must likewise be independent of the thickness of the specimen. That is, from transmission and chromaticity measurements of any specimen of whatever thickness within the range (factor

[3] Proceedings of the Eighth Session, Commission Internationale de l'Éclairage, Cambridge, England, p. 19 (September 1931); D. B. Judd, The 1931 ICI standard observer and coordinate system for colorimetry, J. Opt. Soc. Am. **23**, 359 (1933); A. C. Hardy, Handbook of colorimetry (Technology Press, Cambridge, Mass., 1936).

[4] See, for example, the color designated as ruby (6 G 6) by A. Maerz and M. Rea Paul, A dictionary of color, (McGraw-Hill Book Co., Inc., New York, N. Y., 1930).

[5] D. B. Judd, and K. L. Kelly, Method of designating colors, J. Research NBS **23**, 355 (1939) RP1239.

[6] Transmittance is the ratio of transmitted to incident flux; formerly, transmission. See Physical concepts; radiant energy and its measurement, Committee on Colorimetry, J. Opt. Soc. Am. **34**, 188 (1944).

[7] Hue is the attribute of color that determines whether the color is red, yellow, green, blue, purple, or the like.

Lightness is the attribute that permits an object-color to be classified as equivalent to some member of the series of grays ranging between black and white. See ASTM Tentative Definitions of Terms Relating to Paint, Varnish, Lacquer and Related Products, D16–42T.

of about 10) suitable for test, it should be possible to find the same hue and lightness indices within the uncertainties of the measurements.

As a basis for choosing functions of daylight transmittance, T, and chromaticity coordinates (x, y) that could serve as these indices, measurements were made upon six specimens selected at random from five different mica mines ranging from a specimen found to be ruby by a large margin to one that is very green, and including some that are close to the border line. These specimens, except for 110R and 117R arbitrarily numbered, are identified by the number of the lot from which they were chosen followed by an "R" to indicate that they are random choices. After each specimen was measured it was split so as to provide new specimens of about one-third and two-thirds, respectively, of the original thickness. And one such specimen after measurement was again split, yielding measurements at five different thicknesses. One specimen (No. 35) exhibited two distinct and uniform color areas side by side; these areas are designated "35 red" and "35 green," respectively, and were measured separately.

TABLE 1.—*Dependence of lightness index and hue index on thickness of specimen*

Specimen No.	Thickness (hundredths of an inch)	Daylight transmittance, T	Daylight absorption coefficient (lightness index)	Chromaticity coordinates		Dominant wavelength (in μ)	Hue index, $-\Delta G/\Delta Y$
				x	y		
6R	1.8	0.44	0.27	0.385	0.381	579.7	0.309
	1.1			.357	.361	578.5	.294
	0.6			.339	.344	578.2	.300
	.4	.67	.29	.327	.334	577.5	.292
	.2	.76	.28	.322	.328	577.6	.301
17R	1.2			.352	.355	578.7	.318
	0.8	.53	.26	.337	.342	578.5	.332
	.4	.68	.26	.325	.331	578.0	.321
35, red	1.7			.375	.371	579.8	.332
	1.1	.59	.15	.352	.354	579.1	.341
	0.5	.72	.15	.333	.337	578.5	.338
35, green	1.7			.360	.366	577.7	.256
	1.1	.56	.17	.342	.350	577.1	.253
	0.5	.70	.18	.327	.334	576.7	.271
110R	2.4	.09	.41	.408	.416	577.5	.156
	1.7	.17	.39	.389	.401	576.6	.151
	0.6	.51	.39	.337	.349	575.0	.151
117R	3.3	.30	.14	.391	.378	581.4	.377
	2.4	.42	.13	.371	.366	580.4	.377
	0.9	.71	.10	.332	.336	578.9	.365

Table 1 gives for these specimens not only the thickness in hundredths of an inch, the daylight transmittance, T, and the chromaticity coordinates (x, y), but also the dominant wavelength computed from the chromaticity coordinates,[8] and the ratio of the negative logarithm of internal transmittance to the thickness, d. The internal transmittance is obtained from the measured transmittance by correcting for the losses of light by reflection at the two surfaces and has been computed as $T/0.90$, the constant 0.90 corresponding to the reflection losses for a plate of refractive index equal to 1.59. The ratio of the negative logarithm of internal transmittance to the thickness may be called the daylight absorption coefficient.

Dominant wavelength is an index of hue that is expected to increase somewhat with increasing thickness of mica specimen, and daylight absorption coefficient is an index of lightness that is expected to

[8] OSA Committee on Colorimetry, The psychophysics of color, J. Opt. Soc. Am. 34, 265 (1944); see also footnote 3.

vary slightly with thickness of specimen. However, reference to table 1 shows that this latter variation is in fact less than the uncertainty of the determination; hence daylight absorption coefficient is a satisfactory index of the lightness or darkness of mica color. On the other hand, the expected increase in dominant wavelength is seen to be significant. For each of the six specimens, a regular increase may be noted greater than the uncertainty of the determination. It is worthwhile, therefore, to search for another hue index less dependent upon thickness of specimen.

On the chromaticity diagram of figure 1 constant dominant wavelengths correspond to straight lines intersecting at the point representing a colorless specimen ($x=0.3101$, $y=0.3163$). The progressive increase of dominant wavelength with thickness is represented on a chromaticity diagram as a curved line similar to the Planckian locus. The points corresponding to the chromaticity coordinates (x, y) are plotted in figure 2, which is the section of the (x, y)-diagram inclosed by the rectangle on figure 1 shown to an enlarged scale. The points corresponding to each specimen are connected by a smooth dotted line. The generally regular curvature toward red for increasing thickness is evident, and it appears from these specimens that the

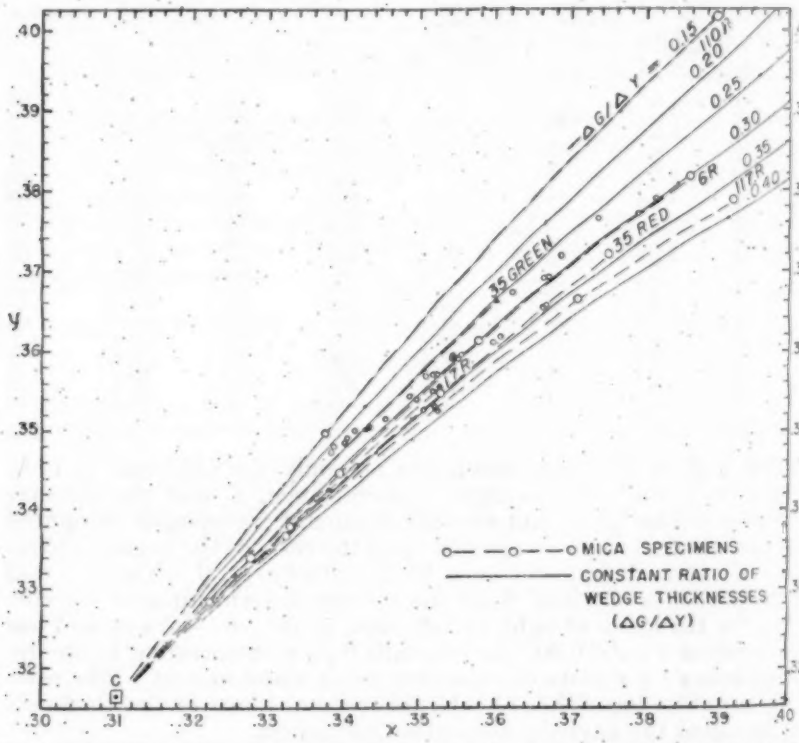

FIGURE 2.—*Variation of the chromaticity of mica specimens (dashed lines) with thickness shown on an enlarged scale on a portion of the (x, y) chromaticity diagram; see rectangle on figure 1.*

Closely the same chromaticity variations are produced on the colorimeter by holding constant the thickness ratio of bluish green wedge to yellow wedge (solid lines), and on this account this ratio is used as the hue index for mica.

direction of this curvature is constant and its amount reasonably constant. This direction corresponds to that characteristic of any light-absorbing medium whose spectral transmittance increases in a general way with wavelength. Each solid curve shown on figure 2 corresponds to a series of two-component filters, a yellow component and a red component, both of known spectral transmittance [9]; in which the ratio of thicknesses of the components is held constant, whereas the total thickness varies. The yellow component is that comprising the yellow wedge of the chromaticity-difference colorimeter. The red component is a hypothetical filter having the same effect in combination with the yellow component as that of the bluish-green wedge of the colorimeter combined with the specimen. The amount of the yellow component is indicated by the symbol ΔY, which is proportional to the thickness of yellow glass required for setting up a chromaticity match involving the mica specimen. The amount of the red component is similarly indicated by the symbol $-\Delta G$, which is proportional to the thickness of the bluish-green glass required to be combined with the mica specimen to duplicate the chromaticity of the yellow component. The minus sign is prefixed to the symbol ΔG to indicate that the bluish-green glass to produce a chromaticity match has to be combined with the mica specimen instead of with the yellow component. An unusually large value of $-\Delta G$ indicates an unusually reddish mica specimen.

Each solid curve of figure 2 is identified by the ratio of the amounts of the two components, $-\Delta G/\Delta Y$, expressed in terms of the arbitrary scales on the wedges. This ratio is taken as the hue index; and values of this hue index are given for all specimens in table 1. It will be noted that the variations in hue index are irregular and therefore within the experimental uncertainty.

A lightness index and a hue index have therefore been found for mica, both indices being independent of thickness of the specimen. The lightness index is the ratio of the negative logarithm of internal transmittance of the mica specimen to its thickness, $[-\log (T/0.90)]/d$. The hue index is the ratio of the red component to the yellow component in the filter required to duplicate the chromaticity of the mica specimen, $-\Delta G/\Delta Y$.

V. DERIVATION AND VALIDIFICATION OF A COLOR STANDARD FOR RUBY MICA

As a guide to the use of the hue and lightness indices in setting up a color standard for ruby mica, these indices have been determined not only for the 5 borderline specimens but also for representative specimens selected from the most doubtful of the 35 lots whose classification was reviewed by the industry task committee and for 4 specimens of ruby mica selected at the same time as the borderline specimens. Table 2 gives the results of these measurements in the same form as table 1. Figure 3 shows on the (x, y)-diagram the chromaticities of these specimens together with those for two thicknesses of the "35 red" specimen see table 1. A straight line has been drawn between points representing the extreme borderline standards; this straight line is drawn solid between the extremes and is shown dashed beyond them as an approximate indication of the border line

[9] D. B. Judd, Specification of uniform color tolerances for textiles, Textile Research **9**, 260 (1939).

between the chromaticities of ruby and nonruby mica. It will be noted that this straight line divides the mica specimens somewhat in accord with accepted color grading. Nonruby mica specimens tend to be represented above this line; ruby, below. There are exceptions, however; one measurement of No. 1-quality ruby standard yields a point on the wrong side of the line, two representative specimens from the nonruby lot No. 35 fall on the ruby side, the thick "35 red" specimen falls on the green side. These exceptions, particularly the last one, are important, and indicate that the color grading of mica is not based upon this line. Furthermore, there is no simple curved line (such as the Planckian locus, see figure 1) to serve as a border line that will eliminate these discrepancies. This is the evidence that showed that the color grading of mica is based on other factors than chromaticity and led to the search for a lightness index.

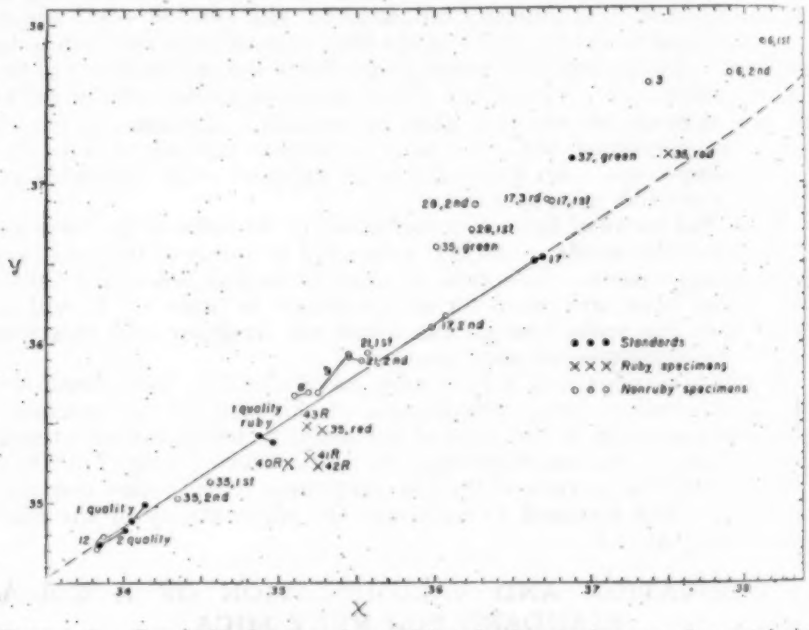

FIGURE 3.—*Correlation between chromaticity of mica specimens and accepted color classification of the lots from which the specimens were drawn.*

The straight line separates the (x, y) chromaticity diagram into an upper left and a lower right section which correlates roughly with the accepted color classification. An important exception is lot No. 35 composed partly of ruby and partly of nonruby mica; the "35 red" specimen has a chromaticity represented on the same side of the line as the "35 green" and other nonruby specimens (circles). This graph proves that color grading of mica according to trade practice is based partly but not wholly on chromaticity.

Figure 4 is a plot of lightness index against hue index for the same specimens shown in figure 3. On this plot the lightness index is plotted with a descending scale, so that specimens of light-colored mica are represented near the top of the plot. Reddish mica is represented near the right of the plot; greenish, near the left. As on figure 3 a straight line has been drawn to connect the points representing the extremes of the borderline specimens. This line is shown solid as a basis for interpolation between the extremes, and is continued by dotted lines to indicate the most reasonable basis for extrapolation

TABLE 2—*Thickness, daylight transmittance, chromaticity coordinates, lightness index, and hue index for 5 standards and 23 mica specimens*

Specimen No.	Thickness (hundredths of an inch)	Daylight transmittance, T	Daylight-absorption coefficient (lightness index)	Chromaticity coordinates		Dominant wavelength (in mμ)	Hue index, $-\Delta G/\Delta Y$
				x	*y*		
2 quality border line	1.3$_8$	0.65$_9$	0.10$_3$	0.340$_1$	0.348$_3$	576.7	0.237
				.338$_8$	.347$_4$	576.3	.224
1 quality border line	1.4$_7$	.60$_2$	.11$_8$	.341$_4$	.349$_9$	576.6	.231
				.340$_1$	.348$_9$	576.6	.229
1 quality ruby	1.8$_3$	.52$_8$	.12$_8$	.349$_1$	.353$_8$	578.4	.303
				.348$_7$	.354$_3$	577.9	.283
37, green	2.1$_8$	.36$_1$	.18$_1$	.368$_8$	.371$_6$	578.4	.277
17, border line	1.8$_2$	.37$_1$	.21$_3$	.366$_9$	.365$_4$	579.6	.339
		.37$_6$	.20$_8$	.366$_4$	.365$_2$	579.6	.338
3	1.8$_1$	.32$_3$	.24$_6$	.373$_7$	.376$_3$	578.4	.265
6, 1st	1.6$_9$	.33$_6$	.25$_3$	.381$_4$	.378$_6$	579.4	.300
6, 2d	1.7$_3$	.28$_9$	.29$_7$	.379$_9$	.376$_9$	579.4	.301
8	1.2$_9$	.45$_7$	.22$_3$	.351$_9$	.356$_9$	578.0	.283
				.351$_9$	.356$_7$	577.8	.273
9	1.3$_3$	.40$_9$	.25$_3$	.352$_8$	.356$_9$	578.2	.293
				.354$_8$	.359$_3$	578.0	.280
12	1.2$_8$	.64$_3$	.11$_5$	.338$_3$	.347$_1$	576.4	.222
17, 1st	1.5$_7$	.31$_7$	.28$_9$	.367$_3$	.368$_9$	578.8	.297
17, 2d	1.7$_8$	.29$_3$	.28$_8$	.360$_7$	.361$_7$	579.1	.327
17, 3d	1.8$_9$	.32$_3$	.24$_3$	.359$_1$	.361$_0$	579.1	.325
				.367$_1$	.369$_0$	578.7	.294
19, 1st	1.6$_2$	.26$_9$	.33$_3$	.382$_3$	.388$_0$	577.7	.214
19, 2d	1.5$_8$	.26$_2$	.34$_6$	.383$_2$	.386$_2$	578.2	.237
21, 1st	1.7$_9$	.45$_1$	.17$_7$	.355$_7$	.359$_4$	578.4	.296
		.44$_3$	.18$_9$				
21, 2d	1.6$_8$	.42$_7$	.19$_3$	.354$_3$	.359$_1$	578.1	.286
		.44$_3$	.18$_3$	.355$_3$	.358$_9$	578.4	.298
28, 1st	1.4$_4$	.38$_3$	.25$_9$	.362$_4$	.367$_1$	578.0	.266
28, 2d	1.7$_3$	.34$_3$	.24$_1$	.362$_3$	.368$_7$	577.7	.247
35, 1st	1.7$_3$	.53$_4$	.13$_8$	.345$_8$	.351$_2$	577.8	.284
35, 2d	1.4$_8$	.55$_7$	.14$_3$	.343$_3$	.350$_8$	577.4	.264
40R	1.6$_8$	.51$_9$	.14$_4$	.350$_8$	.352$_8$	579.2	.346
41R	1.5$_9$	.59$_3$	.12$_1$	.352$_9$	.352$_9$	579.5	.363
42R	1.5$_9$	.51$_9$	.15$_9$	.352$_3$	.352$_3$	579.9	.385
43R	1.7$_3$	.48$_4$	.15$_4$	.351$_3$	.354$_3$	578.7	.319

beyond the extremes represented by the borderline samples. It should be noted that this straight line departs considerably from the vertical; that is, the grading of mica as ruby or nonruby according to trade practice departs considerably from grading purely on the basis of hue alone. A specimen of light-colored mica can be considerably greener than the dark borderline specimen and still be graded ruby.

It should also be noted that the correlation between location of points on this diagram relative to the borderline and color grading by the industry task committee and experts of the Colonial Mica Corporation is nearly perfect. The "37 green" standard (solid circle) falls well below the border line. The "1 quality ruby" falls well above the border line. The "35 red" specimen and the six specimens (40R to 43R) picked at random from lots graded "ruby" are all represented well above the border line. Seventeen of the 18 specimens chosen as representative of the lot graded by the industry task committee as nonruby are represented below the line, as are also the "35 green" and "110R" specimens. The only exception is the first specimen chosen as representative of lot No. 35; this specimen falls above the border line. It is worth noting that the second specimen chosen as representative of this lot is represented slightly below the line in accord with the judgment of the industry task committee. From this correlation it may be concluded that figure 4 is successful in reproducing

the grading of mica into ruby and nonruby groups in accord with trade practice.

From the points representing the repeat measurements recorded in table 2, an estimate may be made of the uncertainty of the determinations in hue index and lightness index. This uncertainty is seen to be about 0.02 in the former and 0.01 in the latter; it is ascribable chiefly to experimental error of the colorimetric and photometric settings, and to nonuniformity of the specimens. The two dot-dash

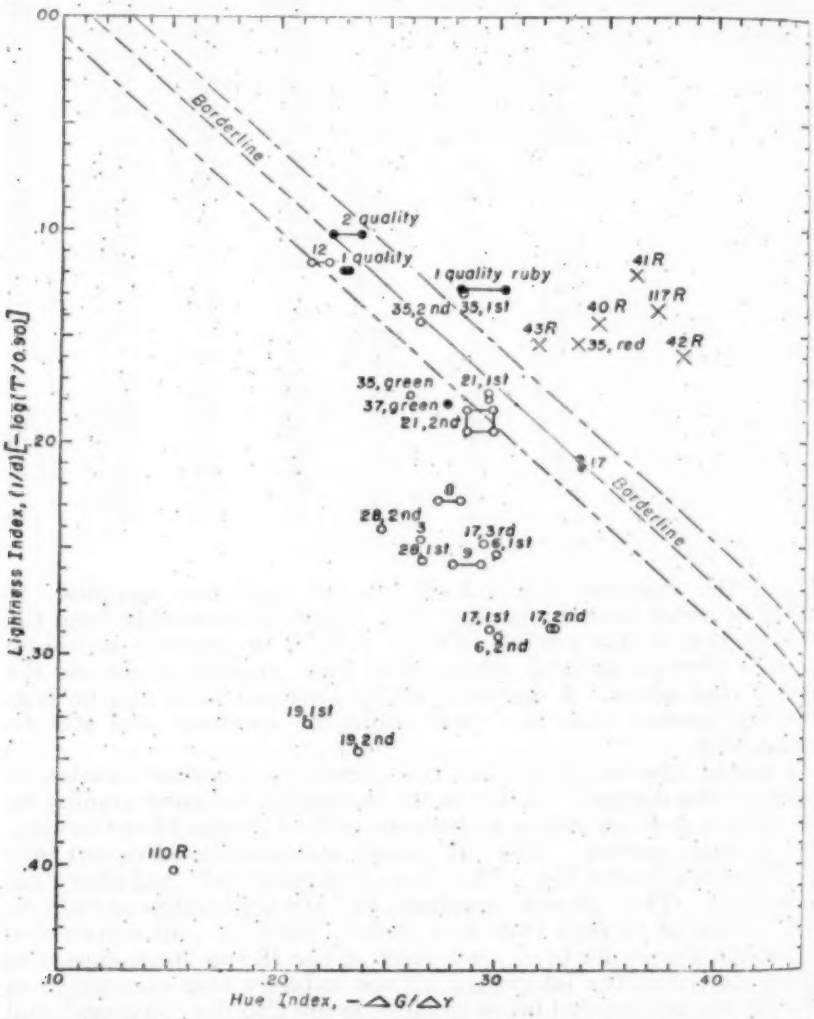

FIGURE 4.—*Lightness indices of 3 borderline, 7 ruby and 19 nonruby mica specimens plotted against their hue indices.*

The solid straight line passes close to the points representing the three borderline specimens. Note that the six specimens of ruby mica chosen at random (crosses) are represented above the line together with the "1 quality ruby" standard. Also note that the "37 green" standard and all but one of the specimens chosen as representative from nonruby lots of mica (circles) are represented below the line. The dot-dash lines represent color distinctions from the border line (solid and dotted) just distinguishable with certainty by one determination according to the method used. These lines are used as the basis for classifying lots of mica as ruby, nonruby, or border line.

lines drawn on figure 4 therefore delineate what may be called a borderline area of the diagram. Mica specimens represented by points within this area are considered to be border line in the sense that it is not definitely known whether they should be classed as ruby or nonruby. It may be noted that all of the borderline specimens are represented by points within this area, as is also the first specimen selected as representative of lot No. 21 and the second specimen selected as representative of lot No. 35. Repeated measurements of these specimens would decide whether they are ruby or nonruby according to the arbitrary solid line shown; and such repeat measurements were made on specimens drawn from lots No. 12 and No. 21. But so great is the variation in color within a given lot that it is usually more significant to draw another sample, choose a representative specimen, and measure that. Note that the third specimen from lot No. 17 differed in lightness index from the first and second specimens by nearly 0.04, as did also the first and second specimens chosen from lot No. 6. Figure 4 has been used in the classification of mica samples into the three classes: ruby, nonruby, border line.

VI. PROCEDURE USED IN COLOR GRADING MICA

1. From the lot to be graded there is selected, a few pieces at a time from 8 to 10 parts of the pile, a sample of approximately 1 pound.

2. The specimens comprising this sample are spread out, a few at a time, on a large white surface and arranged approximately according to luminous transmission; that is, all light-colored specimens are placed at one end of a series, dark-colored at the other end, and the intermediate specimens are also arranged approximately according to lightness of the color. Unusually reddish or unusually greenish specimens are set aside.

3. By means of a direct-reading micrometer 20 specimens are selected with thicknesses between 0.015 and 0.020 inch. The arrangement in a light-to dark series facilitates this selection, and the casting out of unusually reddish and unusually greenish specimens insures that the specimens selected are representative of the sample. The required range of thicknesses is favorable for the measurements which differentiate the color of one lot of mica from another.

4. The 20 specimens so selected are spread out on a large white surface, illuminated by light from the north sky, and arranged by visual inspection into a two-dimensional array, light-colored specimens to the top, dark-colored to the bottom, reddish specimens to the right, greenish to the left.

5. This array of colors is studied visually for nonuniformities in spacing, which might cause a centrally located specimen to be nonrepresentative in color, and a representative specimen is chosen with due regard to all 20 specimens.

6. The thickness, d, and the daylight transmittance, T, are measured for the representative specimen as described in section III; the lightness index, $[-\log (T/0.90)]/d$, is computed as described in section IV.

7. The chromaticity coordinates (x, y) of the representative specimen for ICI illuminant C are determined by whatever means are available, the point corresponding to these coordinates is plotted on figure 3, and the hue index, $-\Delta G/\Delta Y$, is read from the family of solid curves thereon; or, alternatively, if the chromaticity-difference colori-

meter referred to in section III is used, the hue index, $-\Delta G/\Delta Y$, is found directly without obtaining the chromaticity coordinates.

8. The point defined by the lightness index plotted against the hue index on figure 4 determines the classification of the mica specimen measured. If the point falls between the two dot-dash lines, the specimen is classed as border line; if it falls above both, ruby; if below both, nonruby.

Analytically expressed, if H be the hue index and L, the lightness index, the specimen is classed as ruby if $0.927H-L-0.104$ is greater than 0.019; nonruby if $0.927H-L-0.104$ is less than -0.019; and border line if $0.927H-L-0.104$ is between 0.019 and -0.019. The equation of the solid line on figure 4 is $0.927H-L-0.104=0$.

9. The class of the lot of mica to be color graded is taken to be the same as the class of the specimen chosen as representative by steps 1 to 5.

WASHINGTON, July 6, 1945.

U. S. Department of Commerce National Bureau of Standards

RESEARCH PAPER RP1672

Part of Journal of Research of the National Bureau of Standards, Volume 35, October 1945

COMPRESSION OF SOLE LEATHER

By Charles E. Weir

ABSTRACT

Specimens of sole leather were subjected to indentation tests and compressive tests. Comparisons between compression data and the indentation numbers of the original dry leather show that compression may be used as a measure of indentation. Compression of dry leather gives results showing better correlation between the methods and eliminates distortions occurring when moist leather is compressed. Compression data show satisfactory reproducibility. Compression for a three-minute period is adequate for test purposes, all changes being completed in this interval with the exception of a very minute compression proceeding at a slow rate. Compensation for variations in thickness of specimens may be effected by expressing the results in terms of percentage compression. Area and shape of specimens do not affect the compression appreciably. Compression-decompression curves show large hysteresis loops. The effect of tannery rolling in compressing leather is estimated to be equivalent to that produced by pressures of from 2,000 to 3,000 lb/in^2. Based upon the data obtained in the compressive tests, the lower limit of the coefficient of compressibility of leather is estimated to be 33×10^{-6} bar^{-1}.

CONTENTS

	Page
I. Introduction	258
II. Instruments for measuring indentation and compression	258
1. ASTM rubber hardness tester	258
2. McBurney indentation tester	258
3. Sigler indentation tester	259
4. Hydraulic press	259
5. Hydraulic testing machine	259
6. Thickness gage	259
III. Preparation of specimens and experimental procedure	260
1. Indentation of dry leather and compression of moist leather	260
2. Indentation and compression of dry leather	260
3. Stress-strain measurements	260
IV. Results and discussion	261
1. Compression of moist specimens	261
2. Compression of dry specimens	262
3. Reproducibility of compression data	264
4. Effect of duration of the pressure	264
5. Effect of thickness of the specimen	265
6. Effect of area and shape of the specimen	266
7. Stress-strain curves for leather	267
8. Estimation of tannery rolling pressures	269
V. Conclusion	270
VI. References	271

I. INTRODUCTION

This investigation was undertaken to obtain information on the compressive characteristics of commercial sole leather and to determine the correlation existing between the results of compressive tests and the results of the usual types of indentation tests.

The resistance of sole leather to indentation may be determined by forcing a spherical or a plane circular indenter into the surface of the sample. The depth of penetration under a given load or the increase in depth of penetration produced by an increment of load is taken as the measure of the indentation. Such methods are satisfactory if the material being tested is homogeneous, but are of dubious value for materials that are not uniform. Leather is not homogeneous. It exhibits numerous surface irregularities, and the results of indentation measurements may show a wide variation at neighboring points on a leather specimen. In order to minimize this variation, a method was developed in which a slab of sole leather is subjected to pressure between plane metal plates. This method is described in Federal Specification for Leather and Leather Products, General Specifications, KK–L–311.

Recent studies at this Bureau have shown that additional compression of sole leather improves the wearing quality [1].[1] Conabere [2] concluded that the greater the resistance of sole leather to indentation, the better the wear resistance. As additional compression increases the resistance of sole leather both to further compression and also to indentation, the two methods appear to measure closely related properties of leather that are associated with the ability to resist wear.

In this study the change in thickness resulting from compression of sole leather was compared with the indentation results obtained with each of three indentation instruments. Factors that might influence compression, such as thickness, area, and shape of the specimen, were also investigated.

II. INSTRUMENTS FOR MEASURING INDENTATION AND COMPRESSION

1. ASTM RUBBER HARDNESS TESTER

The ASTM rubber hardness tester [3] consists essentially of an indenting rod, $\frac{3}{32}$ in. in diameter, which protrudes through a flat presser foot. The indenter, which has a hemispherical indenting surface with a radius of curvature of $\frac{3}{64}$ in. actuates a dial micrometer that indicates the depth of penetration of the rod. In these tests a load of 5 lb was applied to the indenter.

The indentation number is the difference in reading of the dial micrometer, expressed in thousandths of an inch, between the value indicated when the instrument is placed on a plane glass surface and the value indicated when it is placed on the specimen.

2. McBURNEY INDENTATION TESTER

The McBurney instrument [4] consists of an indenting rod, $\frac{1}{4}$ in. in diameter, which protrudes through a flat presser foot. The indenter,

[1] Figures in brackets indicate the literature references at the end of this paper.

which has a hemispherical indenting surface with a radius of curvature of ⅛ in., actuates a dial micrometer that indicates the depth of penetration of the rod. The zero setting of the dial micrometer is obtained on the specimen under test with a load of 2 lb on the indenter.

The indentation number is the difference in the reading of the dial micrometer, expressed in thousandths of an inch, between the value indicated when a load of 2 lb is applied to the indenter and the value indicated when a load of 30 lb is applied to the indenter.

3. SIGLER INDENTATION TESTER

The Sigler indentation instrument [5] differs from the instruments previously described in that it uses interchangeable flat-surfaced indenters that may be loaded as desired. In these tests a load of 180 lb was applied to plane-ended rod, ⅛ in. in diameter. As the dial micrometer which indicates the position of the indenter is adjusted to read zero when the indenter is in contact with the base plate, it is necessary to measure the thickness of the specimen independently to obtain a value for indentation. This measurement was made with a dial micrometer instrument, which carried a load of ¼ lb on a presser foot ⅛ in. in diameter.

The indentation number is the difference, in thousandths of an inch, between the thickness of the specimen and the reading of the dial micrometer of the indentation instrument at the conclusion of the indentation period.

4. HYDRAULIC PRESS

Loads were applied to the plane platens, between which the samples were loaded during the compression tests by means of a hydraulic jack operated by a motor-driven pump. The capacity of the press was 50 tons. Loads were indicated by a Bourdon tube gage.

5. HYDRAULIC TESTING MACHINE

A 30-ton capacity hydraulic testing machine was used to obtain stress-strain measurements. The load was applied by means of a hydraulic jack operated by a motor-driven pump and was indicated by a pointer that moved around a graduated circular scale.

The compression was measured by means of two dial micrometers, which indicated the movement of one circular compression platen with respect to the other. The two dial micrometers were located at the opposite ends of a diameter of the platens. The compression was considered to be the average of the compressions indicated by the two micrometers.

Stress-strain measurements were made at a rate of loading of 10,000 lb/min.

6. THICKNESS GAGE

A dial micrometer was used for measurements of thickness of specimens before and after compression. A load of 450 g was applied to a plane presser foot ⅜ in. in diameter.

665730—45——2

III. PREPARATION OF SPECIMENS AND EXPERIMENTAL PROCEDURE

1. INDENTATION OF DRY LEATHER AND COMPRESSION OF MOIST LEATHER

Specimens of sole leather were cut to a size of 2 by 4 in. by means of a steel die, and were conditioned at 72° F and 65-percent relative humidity for 72 hr. The indentation numbers of each specimen were determined on the Sigler indentation tester at eight points, i. e., two rows of four points, each ¾ in. from the longer edge and spaced approximately ¾ in. apart. The average of these eight measurements was considered to be the indentation number of the specimen.

The thickness of each specimen was measured at eight marked points, and the average of these measurements was taken as the thickness of the specimen. Each specimen was weighed and then immersed in water until 10 percent ±1 percent by weight of water was absorbed. The moist specimen was conditioned at 72° F and 100-percent relative humidity for 48 hr, compressed for 3 min at a pressure of 3,000 lb/in.^{2} and dried at 72° F and 65-percent relative humidity. The thickness of the dry specimen was redetermined at the marked points and the average taken. The difference between the original and the final thickness was considered to be the compression.

2. INDENTATION AND COMPRESSION OF DRY LEATHER

The dry specimens for compressive tests were prepared in a similar manner and conditioned at 72° F and 65-percent relative humidity. The indentation numbers of each specimen were determined on the ASTM instrument at eight points, spaced as previously described, and on the Sigler indentation tester at eight points adjacent to the points used for the measurements on the ASTM gage. The indentation was then determined on the McBurney instrument at four points, spaced ¾ in. apart on the longer center line of the specimen. All indentation measurements were made 30 sec after application of the load. The averages of the measurements with each instrument were taken as the indentation numbers of the specimen.

The thickness of each specimen was measured at eight marked points, and the average was taken as the thickness of the specimen. Each specimen was compressed for 3 min at a pressure of 3,000 lb/in.^{2}, and the load was removed. The thickness was redetermined immediately at the marked points. The specimens were conditioned for 24 hr at 72° F and 65-percent relative humidity, and the thickness was redetermined. The thickness of some specimens was measured for the third time at the conclusion of 30 days.

3. STRESS-STRAIN MEASUREMENTS

For stress-strain measurements, 2- by 4-in. specimens were halved with a band saw to give 2- by 2-in. blocks; and the irregularities of the edge, caused by the die and the saw, were removed by buffing. This treatment gave specimens that were uniform in area and that had approximately vertical edges. One-inch blocks were cut by a band saw and buffed, and disks having approximately vertical edges were

cut by a circular die. These specimens were conditioned for 24 hr at 77° F and 50-percent relative humidity. The area of each specimen was measured with a planimeter. The measurements made on these specimens were varied and will be described subsequently.

IV. RESULTS AND DISCUSSION

1. COMPRESSION OF MOIST SPECIMENS

The results of the compression of the moist specimens are shown in figure 1, where the change in thickness resulting from compression is plotted as the ordinate and the Sigler indentation number as the abscissa. The figure shows that, although there appears to be some relationship between the indentation of leather when dry and the compression when moist, the relationship is not well defined.

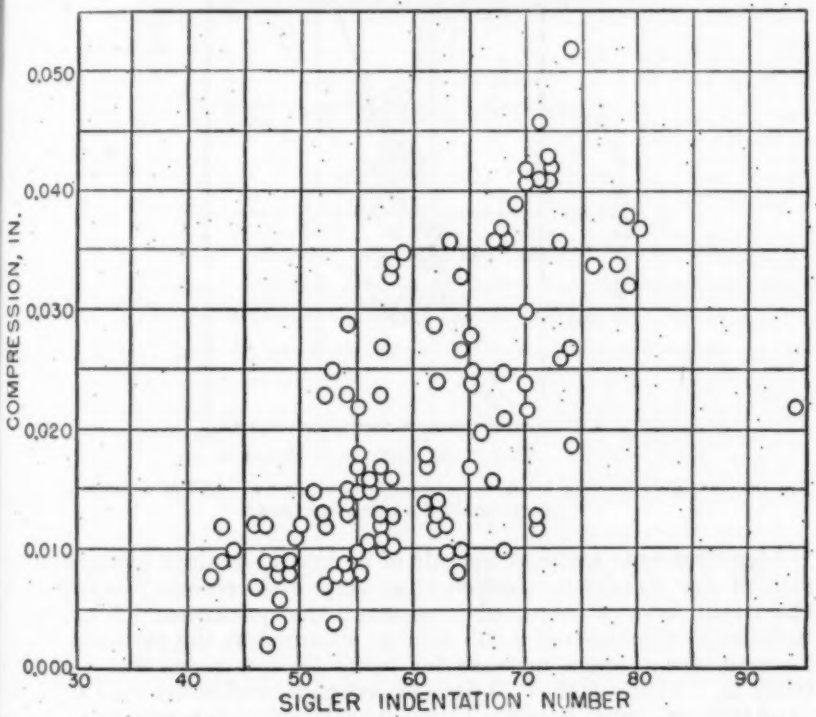

FIGURE 1.—*Relationship between compression values for moist leather and Sigler indentation numbers obtained on the same specimens in a dry condition.*

Two objectionable features were connected with the compression of moist leather. During the compression, water soluble material was squeezed from the leather, and the resulting specimen was probably chemically different from the original leather. After compression most specimens were warped and could not be measured accurately. Apparently, the grain layer undergoes more lateral expansion than the flesh layer under pressure, as the specimen is invariably convex as viewed from the grain surface. Neither of these objections is manifest when dry leather is compressed.

2. COMPRESSION OF DRY SPECIMENS

Comparisons between the results of compression of dry leather and the results of indentation are shown in figures 2, 3, and 4, where the compressions are plotted as ordinates and the indentation numbers as abscissas. All three figures contain an equal number of points representing data obtained on the same specimens. The lines were fitted to the points by inspection. No attempt was made to differentiate between various leathers. Every available type of vegetable-tanned sole leather, irrespective of origin, tannage, thickness, or location, was tested; and all the results are shown in the figures. The points in the lower left portion of each figure, which represent leather much harder than is available commercially, were obtained by subjecting some specimens to compression before testing.

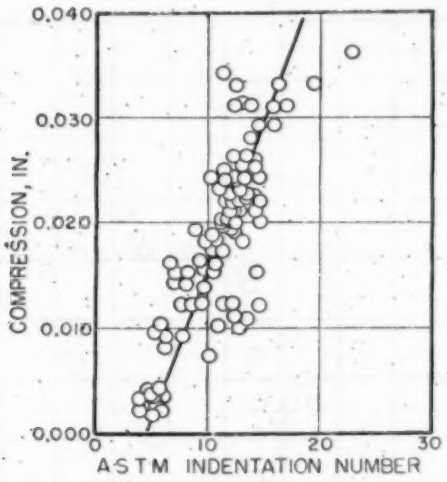

FIGURE 2.—*Relationship between compression values and ASTM indentation numbers obtained on dry specimens.*

Measurements made at periods of 24 hr and 30 days after compression of dry specimens showed that very little recovery occurs after the 1-min interval required to measure the specimens. A maximum increase in thickness of 0.003 in. was obtained at the expiration of 24 hr, and the average increase for some 50 specimens was less than 0.002 in. At the end of 30 days an average total increase in thickness of 0.003 in. was found. Consequently, the compression of dry leather gives a product that appears to be stable and, for testing purposes, is not too sensitive to the time factor.

The results show that correlation between the data obtained by compression of dry leather and the Sigler indentation numbers is better than that with the ASTM and McBurney numbers. Considering the compression as the dependent variable, the standard errors of the points from the lines are 0.006, 0.005, and 0.002 in., respectively, in figures 2, 3, and 4. A consideration of the mechanisms by which indentation occurs leads to the conclusion that this is to be expected. The Sigler instrument and the press compress the specimens between plane surfaces, whereas the ASTM and McBurney testers use hemi-

spherical indenters. Furthermore, the loads on the Olsen and McBurney indenters are so small that surface irregularities may have a significant influence on the indentation numbers obtained with these instruments.

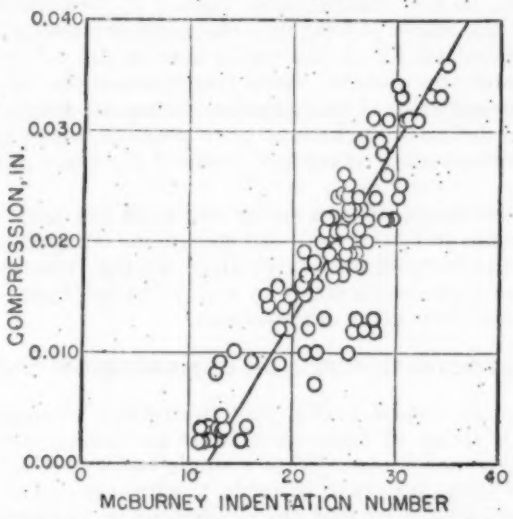

FIGURE 3.—*Relationship between compression values and McBurney indentation numbers obtained on dry specimens.*

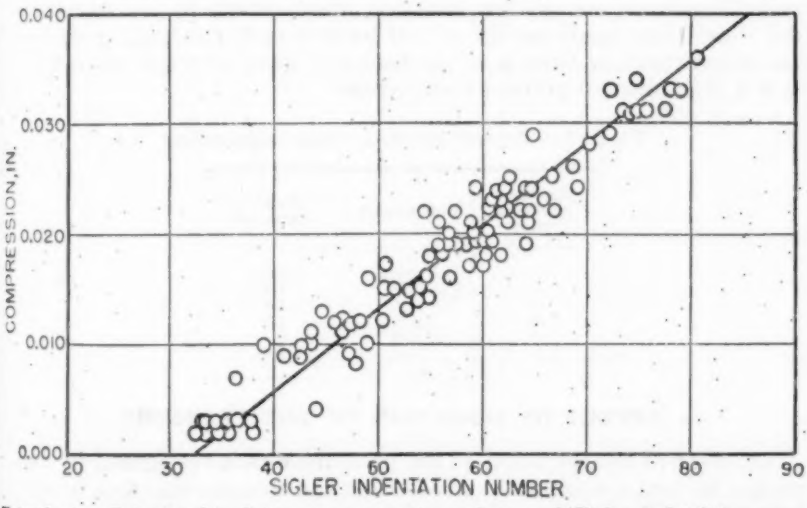

FIGURE 4.—*Relationship between compression values and Sigler indentation numbers obtained on dry specimens.*

Comparison of figures 1 and 4 shows that better agreement exists when dry, rather than moist, leather is compressed. As in one case both compression and indentation measurements were made on dry leather, and in the other case indentation measurements were made on dry leather and compression measurements on moist leather, this is

not surprising. The amount of water in the moist leather cannot be accurately controlled and the effect of the water on the structure of the leather is probably complex. If the voids in the specimen are filled with a relatively incompressible liquid such as water, the moist specimen should be less compressible than a corresponding dry specimen, provided the water is held in a chemical or adsorptive combination. If, on the other hand, the water acts in the role of a lubricant for the fibers and the platens, more compression should be obtained with moist specimens. Comparisons between similar specimens showed that no definite conclusions were possible, other than that dry and moist specimens showed compressions of the same order of magnitude.

It must not be assumed that compression of dry and moist leather results in the same end product. All specimens compressed in a moist condition became warped and rigid after drying, whereas dry specimens showed no appreciable warping and, although hard, still retained considerable flexibility after compression.

3. REPRODUCIBILITY OF COMPRESSION DATA

To determine the reproducibility of the results obtained from compressive tests a series of tests on similar specimens was performed. Each set of specimens was cut from a single bend of sole leather. The results of these tests are given in table 1, where the average compression of each set in percent and the coefficient of variation within the set are given. The variations shown are small in comparison with variations known to occur in other measurements on leather. Tensile-strength measurements, for instance, show much larger variations. Additional tests made on six sets of leather each containing six taps, selected at random from a single tannage, gave averages of 6.1, 6.4, 6.0, 6.9, 6.7, and 6.0 percent compression.

TABLE 1.—*Reproducibility of compression values*

Number of specimens tested	Compression	Coefficient of variation
	Percent	*Percent*
6	9.6	8.3
6	13.5	14.8
6	17.4	6.3
6	4.6	8.7
6	11.6	9.5

4. EFFECT OF DURATION OF THE PRESSURE

The effect of the duration of the pressure was investigated by compressing several specimens and recording the compression as a function of the time. To simulate the previous compressions, the pressure was applied as rapidly as possible, and then maintained for the duration of the test. The load was applied at the rate of 60,000 lb/min, and, after the desired load was reached, was held constant to within ± 50 lb.

Two typical curves are shown in figure 5, in which the percentage compression is plotted as a function of time. These curves show that compression has practically ceased at the conclusion of 3 min. This

length of time seems suitable for purposes of testing and was used in the previous experiments. The experimental irregularities shown are ascribed to the fact that the thickness measurements were obtained only to the nearest 0.001 in. Although the curves appear flat after the 3-min period, such is not the case. At the end of the longest period of pressure a very slow compression was observed to be proceeding.

5. EFFECT OF THICKNESS OF THE SPECIMEN

The thickness of the specimen has a decided effect on the compression. The effect of thickness was not discussed in connection with figures 2, 3, and 4 because the specimens did not differ appreciably in

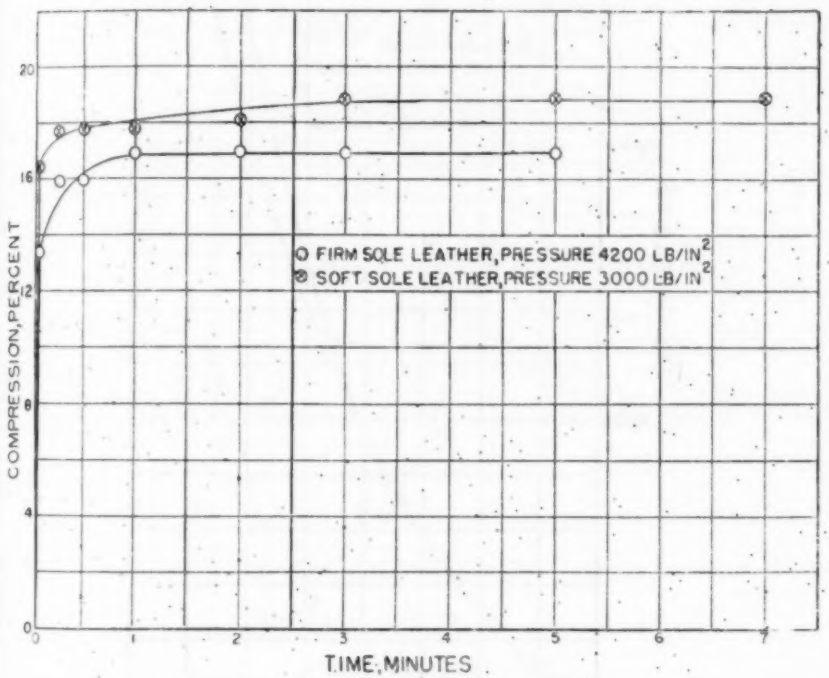

FIGURE 5.—*Effect of duration of compression.*

thickness, and the small variations which occurred should affect measurements of compression and indentation in essentially the same manner and tend to compensate. To compare the results of compression of different specimens, however, the thicknesses must be considered. The use of percentage compression, i. e., the change in thickness divided by the original thickness of the specimen multiplied by 100, gives results that agree when the thickness varies in a 2:1 ratio as shown by figures 6 and 7. Figure 6 shows the stress-strain diagrams obtained with a single block of leather and a block of double thickness, formed by placing two similar blocks together, flesh to grain. The curves in figure 7 were obtained with a normal block of leather and a thin block, formed by buffing the flesh surface of a similar block. The

compression values indicated by the curves agree within 3 percent compression at 3,000 lb/in².

6. EFFECT OF AREA AND SHAPE OF THE SPECIMEN

The area and shape of the specimen used for compressive tests have little effect on the compression value, as is shown in figure 8. This figure shows pressure-compression diagrams for two sizes of square

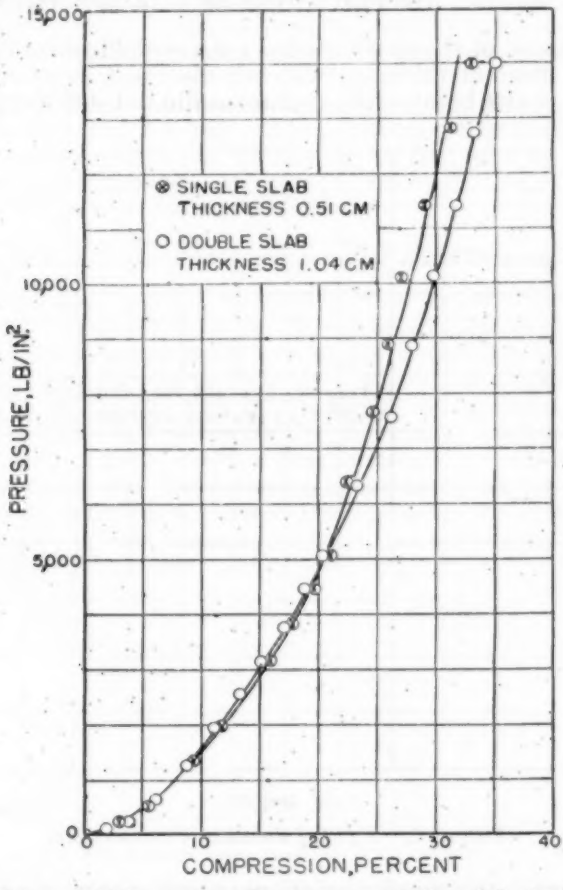

FIGURE 6.—*Effect of thickness of specimen on compression; slab of normal thickness and slab of double thickness.*

slabs and disks of the same leather. The results for the slabs and the larger disk are in excellent agreement, whereas the results for the smaller disk show a deviation of the order of 5 percent compression. This deviation may be due to variation of the leather, or may be experimental in nature. The area and shape of the specimen may be chosen to give a convenient load, although in order to reduce the effect of variation, it is desirable to test a large specimen.

It is to be noted that the structure of leather breaks down at a pressure of approximately 35,000 lb/in². This failure is indicated by

the broken lines shown in figure 8. At this pressure the specimens spread laterally under the vertical pressure in spite of the concentric grooves in the platens designed to resist lateral motion.

7. STRESS-STRAIN CURVES FOR LEATHER

Stress-strain diagrams for rolled and unrolled sole leather are shown in figure 9. The compression and decompression portions of the curves are denoted by arrows.

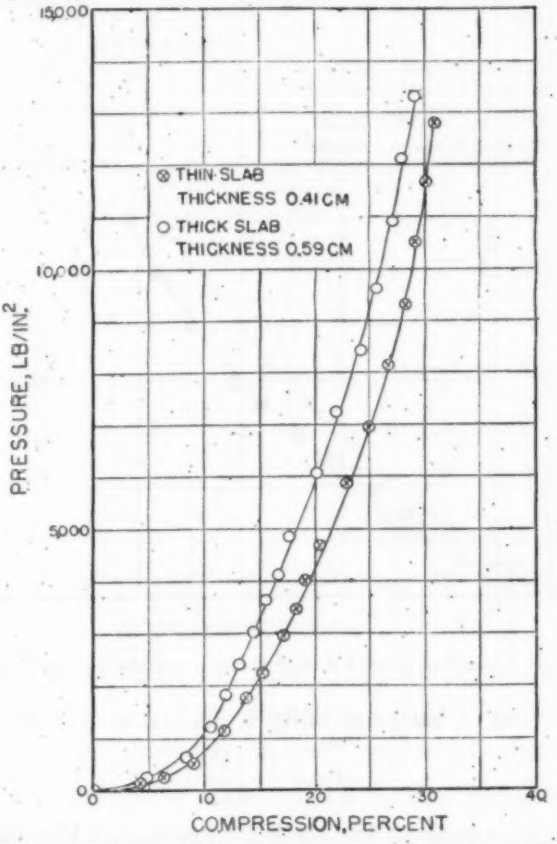

FIGURE 7.—*Effect of thickness of specimen on compression; normal slab and thin slab.*

The compression of leather consists in two main processes. First, a packing of the fibers resulting in the elimination of the interstitial voids; and second, the compression of the leather substance. As it is improbable that the voids can be completely eliminated, both processes probably occur simultaneously at all except the lowest pressures. When the pressure on the compressed specimen is reduced, the resultant decompression curve does not follow the compression curve, as shown by the large hysteresis loops in figure 9.

Reduction of pressure should result predominately in an expansion of the compressed leather substance until the pressure reaches a value

at which the fibers are able to separate. A linear relationship between pressure and percentage compression does not hold after this point is reached. This point occurs at a pressure of approximately 3,500 lb/in.^{2} in the curves shown in figure 9. The slopes of the linear portions of the decompression curves were found to be nearly the same for a wide variety of specimens. This indicates that the principal process occurring in this region of pressure is an expansion of the leather substance.

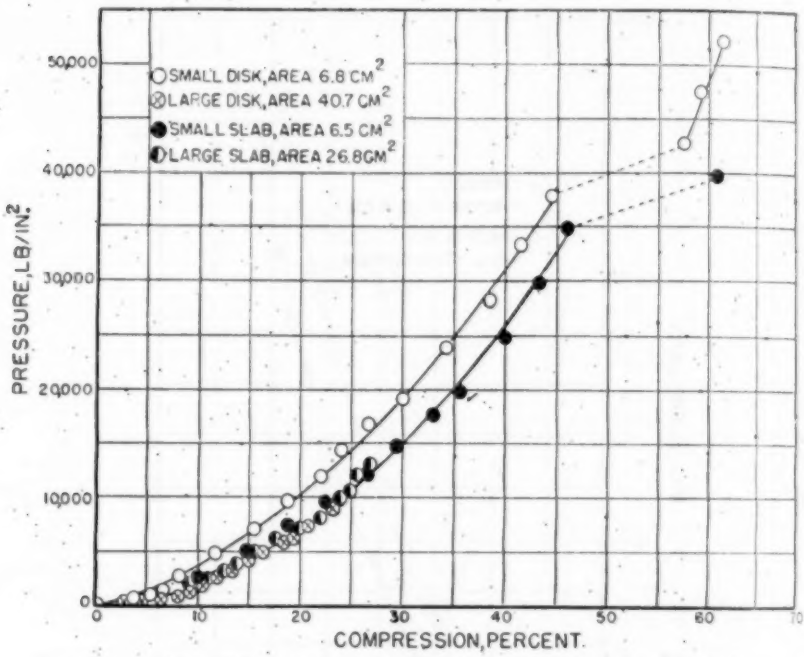

FIGURE 8.—*Effect of area and shape of specimen on compression.*

The coefficient of compressibility is defined as β in the equation

$$\beta = -\frac{1}{V}\frac{\Delta V}{\Delta P}, \tag{1}$$

where V is the volume of the leather substance, ΔV is the change in this volume, and ΔP is the change in pressure. The pressure defined by eq 1 is a force per unit area acting in all directions and may be realized experimentally only by fluid pressure.

The ratio of the length of the shortest side to the thickness of the specimen in these tests was at least 8:1. Measurements of the areas of specimens after compression indicated that any increase in area was less than the experimental accuracy of the area measurement and probably an effect of the second order. Errors resulting from the application of eq 1 to leather under vertical pressure will most probably result in too low a value for ΔV.

The true volume of the leather fibers, exclusive of void space, is not known. Measurements by J. R. Kanagy and E. L. Wallace [6] have

shown that the dimensional volume is in error by at least 20 percent after compressing leather at a pressure of 3,000 lb/in.^{2}

Use of the observed volume change and the dimensional volume in eq 1 will, therefore, lead to an estimate of the lower limit of the coefficient of compressibility of leather. The average value for this limit was found to be 33×10^{-6} bar^{-1}.

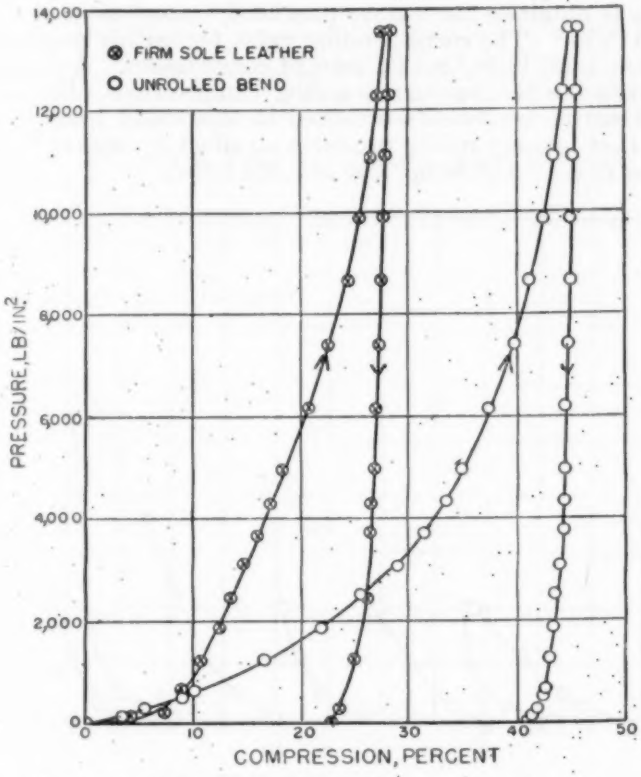

FIGURE 9.—*Compression-decompression curves for leather.*

8. ESTIMATION OF TANNERY ROLLING PRESSURES

The choice of the pressure of 3,000 lb/in.^{2} for purposes of testing was arbitrary. This pressure was considered to be available on ordinary presses with a specimen at least 4 in.^{2} in area. Although higher pressures produce larger compressions, a pressure of 3,000 lb/in.^{2} is adequate to produce measurable compressions of all commercial leather tested, and even of leather that had been compressed before testing, as shown in figures 2, 3, and 4.

The pressure exerted on the leather during the rolling operation at the tannery cannot be evaluated readily, yet it is of considerable interest. In order to estimate this pressure, a specimen of unrolled leather taken from the bend location of the hide was compressed consecutively to pressures of 1,000, 2,000, 3,000, and 4,000 lb/in.^{2}, and the stress-strain diagrams were drawn. These curves are shown in

figure 10, in which each curve has been displaced to reduce confusion of the points.

Comparison of the percentage compression at a given pressure shows that the magnitude of the compression is a measure of the compressive history of the leather. At 1,000 lb/in.^{2}, for instance, the percentage compressions stand in the ratios of 16:11:9:6 in the four curves. At a pressure of 3,000 lb/in.^{2} a value of 18.5 percent compression is obtained for leather previously compressed at a pressure of 2,000 lb/in.^{2} The corresponding value for leather previously compressed at 3,000 lb/in.^{2} is 12.5 percent compression. A comparison of these values with the corresponding compressions observed on all stress-strain measurements obtained in this study leads to the conclusion that tannery rolling produces an effect equivalent to that produced by pressures of from 2,000 to 3,000 lb/in^2.

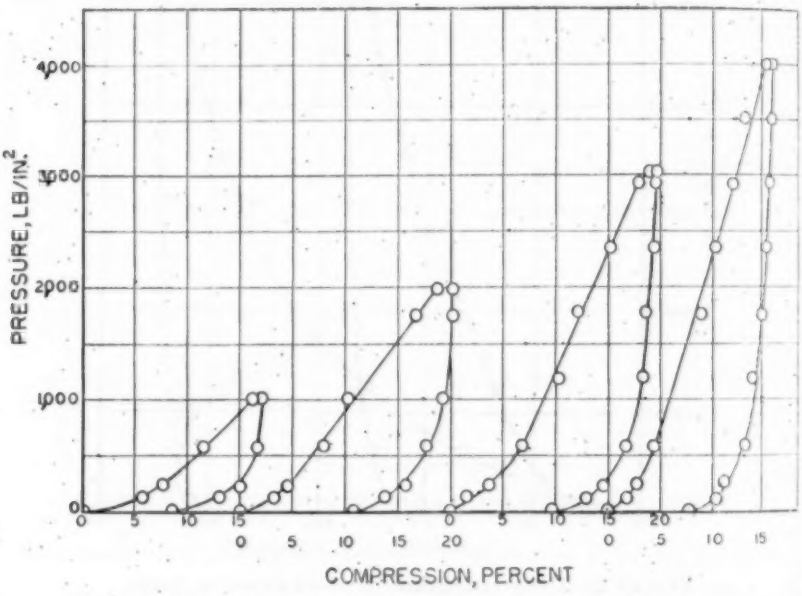

FIGURE 10.—*Effect of successive compressions on stress-strain curve.*

V. CONCLUSION

Comparisons between compressions resulting when sole leather is subjected to a pressure of 3,000 lb/in.^{2} and the indentation numbers of the original leather indicate that compression and indentation measure related properties of leather. To obtain best correlation between these methods, leather should be compressed in the dry state. A compression period of 3 min is adequate. The thickness, area, and shape of specimens have small effect on results of compression if results are expressed as percentage compression, although it is advisable to use specimens at least 4 in.^{2} in area to reduce the effect of possible variations within the specimen. The effect of tannery rolling in compressing leather is estimated to be equivalent to that produced

by pressures of from 2,000 to 3,000 lb/in.^{2}. Based upon the data obtained in the compressive tests, the lower limit of the coefficient of compressibility of leather is estimated to be 33×10^{-1} bar^{-6}.

VI. REFERENCES

[1] R. B. Hobbs and R. Kronstadt, Wearing quality of some vegetable-tanned sole leathers, J. Research NBS **34**, 33 (1945) RP1626.
[2] G. O. Conabere, Firmness, compressibility and abrasion resistance of sole leather, J. Int. Soc. Leather Trades' Chem. **28**, 25 (1944).
[3] Standard Method of Testing Hardness of Rubber, Am. Soc. Testing Materials, Standards, Pt. III, Nonmetallic Materials, p. 597 (1944) D314–39.
[4] J. W. McBurney, Indentation of asphalt tile, Proc. Am. Soc. Testing Materials **34**$_2$, 591 (1934).
[5] P. A. Sigler and Myrtle B. Woodward, Indentation and recovery of low-cost floor coverings, NBS Building Materials and Structures Report BMS14. (1939).
[6] J. R. Kanagy and E. L. Wallace, The density of leather and its significance, J. Am. Leather Chem. Assn. **38**, 314 (1943).

Washington, April 19, 1945.

U. S. Department of Commerce . National Bureau of Standards

RESEARCH PAPER RP1673

Part of Journal of Research of the National Bureau of Standards, Volume 35, October 1945

KNOCK RATINGS OF GASOLINE SUBSTITUTES

By Afton D. Puckett

ABSTRACT

Knock ratings of gaseous paraffins and olefins through C_4, and of carbon monoxide, were determined by current motor and aviation test methods. Auxiliary apparatus and modifications of test engines necessary to rate gases are described.

Antiknock qualities of ethyl and normal butyl alcohol and acetone, both alone and in blends, were determined by current motor-fuel rating procedures. Blending characteristics of these materials with straight run gasolines and naphthas were investigated.

Diethyl ether in ethyl alcohol blends showed a high positive sensitivity (Coordinating Fuel Research Committee (CFR) research minus American Society for Testing Materials (ASTM) motor octane number) for ether concentrations below 48 percent and a high negative sensitivity above that figure. The tests indicated that blends containing up to 45 percent of ether should give relatively knock-free performance under conditions of steady operation.

CONTENTS

	Page
I. Introduction	273
II. Methods of test	274
III. Knock ratings of gaseous fuels	276
1. Nonhydrocarbons	276
2. Hydrocarbons	277
IV. Nonhydrocarbon blends	277
1. Ethyl alcohol–diethyl ether blends	277
2. Blends containing *n*-butyl alcohol, acetone, and ethyl alcohol	278
V. Hydrocarbon fuels containing nonhydrocarbon components	279
1. Gasoline blends	279
2. Naphtha blends with nonhydrocarbons	282
VI. Conclusions	284

I. INTRODUCTION

As part of a program of investigation of the properties of various substitutes for gasoline as a fuel for internal-combustion engines, knock ratings were determined on a number of compounds and blends. The primary purpose of the major investigation was to ascertain whether, and to what extent, substitutes that could be produced in certain areas where petroleum products were scarce or entirely lacking could be used successfully. With this end in view, the antiknock qualities of a number of materials, both gaseous and liquid, were determined by the current CFR Research (CRC Designation F–1) the ASTM Motor D 357 (CRC Designation F–2), and the ASTM Aviation D 614 (CRC Designation F–3) methods. Included to give as complete information as possible were a number of

hydrocarbon gases ordinarily obtained from petroleum that obviously do not fall into the category of easily available gasoline substitutes.

Reliable knock ratings by current methods are presented that either were not hitherto reported in the literature, or, in some cases, were of questionable precision because of outmoded methods of test or other irregularities.

II. METHODS OF TEST

The unit currently approved for the knock rating of both motor and aviation gasolines has been designed and built to the specifications of the Cooperative Fuel Research Committee. It is a single-cylinder engine, belt connected to a synchronous motor generator, which maintains constant speed. Compression ratio is continuously variable between 4 and 10 and may be changed while the engine is operating.[1]

The CFR Research (CRC F–1), ASTM Motor (ASTM D 357, CRC F–2), and the ASTM Aviation (ASTM D 614, CRC F–3) methods differ in instrumentation and engine operating conditions. The F–1 and F–2 methods make use of a bouncing pin and knockmeter to detect and indicate knock intensity, whereas the F–3 method utilizes a standard thermocouple, or "thermal plug", and potentiometer to differentiate between knocking tendencies of the fuels. Engine operating conditions for the three methods are shown in table 1.

All determinations of antiknock quality of the liquid fuels tested were made in strict accordance with the standard test methods and on standard knock-test units. Before each run the engines were

TABLE 1.—*Engine operating conditions for standard methods of knock rating*

Test method	CFR research	ASTM motor	ASTM aviation
ASTM designation		D 357	D 614.
CRC designation	F-1	F-2	F-3.
Intake air temperature, ° F	125±2	75 to 125	125 ±5.
Mixture temperature, °F		300 ±2	220 ±2.
Coolant temperature, ° F	[a] 209 to 215	[a] 209 to 215	374 ±9.
Oil temperature, ° F			150 ±10.
Intake air humidity, grains per pound of dry air.	[b] 25 to 50	[b] 25 to 50	[b] 25 to 50.
Mixture ratio	Maximum knock	Maximum knock	Maximum knock.
Knock intensity [c]	Standard, specified by guide table.	Standard, specified by guide table.	Adjusted so that cp benzene is equal in thermal plug temperature to 87 octane number reference fuel.
Engine speed, rpm	600 ±6	900 ±9	1200 ±12.
Compression ratio	Variable with octane number.	Variable with octane number.	Variable with octane number.
Spark advance, °btc	13, fixed	Variable with compression ratio.	35, fixed.

[a] Constant to within 1° F.

[b] Usually controlled at 27 grains per pound of dry air by passing the intake air through an ice-packed humidity control tower of standard design.

[c] Standard knock intensity for the F–1 and F–2 methods is defined as that obtained with a blend of isooctane and normal heptane under the standard conditions of the methods and at a compression ratio corresponding to the blend used and to the prevailing barometric pressure in accordance with the standard knock intensity guide tables for the respective method; for the F–3 method the knock intensity is set by operating at a compression ratio to give a thermal-plug temperature in accordance with a "match temperature line" determined at the beginning of each day's testing.

[1] For detailed descriptions of the test apparatus and procedures see CRC Procedures F–1–1044, F–2–1044, and F–3–1044, Coordinating Research Council, 30 Rockefeller Plaza, New York 20, N. Y.; or ASTM Methods D 357 and D 614, ASTM Book of Standards, 1944, Part III, Nonmetallic Materials, American Society for Testing Materials, 260 S. Broad St., Philadelphia, Pa.

carefully checked and adjusted to give proper ratings on standardization fuels of known octane number. However, as the standard engines are not normally equipped to operate on gaseous fuels, it was necessary to modify the carburetors in order to obtain ratings on the gases tested. A connection was installed on the standard air-intake elbow of the carburetor, so that gas could be introduced into the air stream ahead of the venturi. To rate the gas samples, the carburetor fuel selector valve was turned to an "off" position, and the gas was admitted through this connection. By using this system, satisfactory engine operation was obtained, there was a minimum of deviation from either standard equipment or conditions, and the usual bracketing procedure was followed.

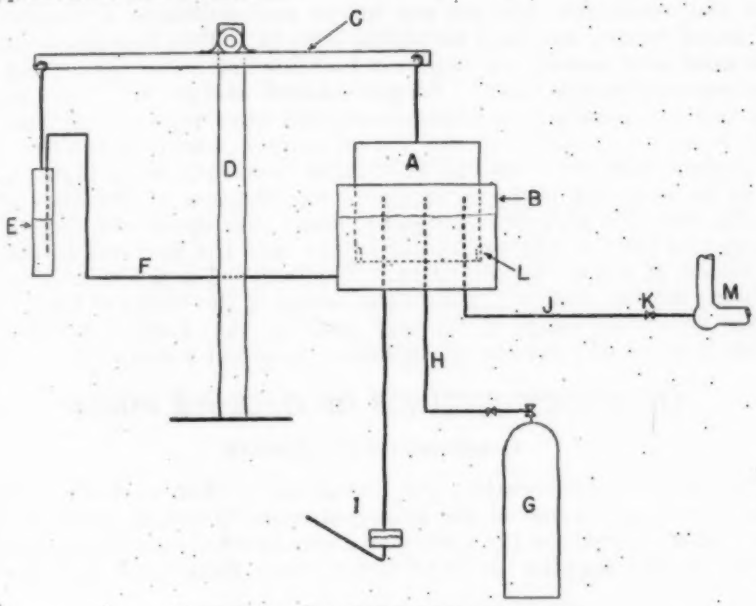

FIGURE 1.—*Constant pressure gasometer.*

A, Gasholder; *B*, water tank; *C*, ball-bearing-mounted beam; *D*, beam support; *E*, counterbalance bucket; *F*, siphon line; *G*, high-pressure gas cylinder; *H*, gas cylinder to gasometer connection; *I*, inclined single-leg manometer; *J*, gas line to engine; *K*, gas-throttling valve; *L*, lead weights; *M*, CFR carburetor air intake.

The F–1, F–2, and F–3 methods require that fuels be tested at the fuel-air ratio for maximum knock. Prerequisite to this condition is a rate of fuel flow which may be varied to give mixtures appreciably richer and appreciably leaner than that for maximum knock, and once set will remain constant long enough for the engine to reach equilibrium. These requirements were fulfilled by the use of the gasometer illustrated schematically in figure 1. The gas from cylinder *G* was led through line *H* into gas holder *A*, which was weighted with lead strips *L*, and thence through line *J* to the intake elbow *M*. *J* consisted of a section of ⅜-in. outside diameter copper tubing into *A* and a section of ⅜-in. inside diameter rubber tubing from the copper tube to the engine inlet connection. It was originally intended that *K* should be a standard ¼-in. globe valve, but such a valve was found to offer excessive resistance to flow. Consequently a screw-clamp-

type hose cock was tried and found to give excellent regulation. The gas holder was suspended on a knife edge from beam C, which was pivoted at its center on a ball bearing mounted on column D. A small bucket, E, also suspended from the beam opposite the gas holder, acted as a counterbalance. Line F was installed as a siphon from the water tank B and extended down into the counterbalance bucket thus maintaining equal liquid levels in the two. The cross-sectional area of E was such that any change in the submerged volume of the walls of A, and consequently of the buoyant force acting on the gas holder, was compensated by the change in the amount of water in E, and constant pressure was maintained in the gas holder regardless of its position. The inclined single-leg manometer was connected into the gas holder and indicated a pressure of 1.2 in. of water, constant to within 0.05 in. This low gas pressure was used as it was found to give a fuel flow sufficient for the richest mixture necessary for any of the gases tested except carbon monoxide, was not oversensitive to adjustment, and gave reproducible results.

It was impracticable to use the gasometer described for the runs on carbon monoxide, as the flow rates necessary were higher than could be obtained without extensive modification of the apparatus. In this case the high-pressure gas cylinder was connected directly to the special inlet on the carburetor intake, and the flow was controlled by means of a ⅛-in. needle valve. This method is not recommended as being precise, but in this case the rating of the material tested was so far above the range of the test methods that further precautions in the interest of precision of regulation were not warranted.

III. KNOCK RATINGS OF GASEOUS FUELS

1. NONHYDROCARBONS

The only nonhydrocarbon gas tested was carbon monoxide, which was of interest as one of the principal constituents of producer gas. The material used for the tests was a commercially available product stated by the supplier to be of better than 90-mole-percent purity.

TABLE 2.—*Knock ratings of gaseous fuels*

Fuel	Test method (CRC designation)		
	F-1	F-2	F-3
Nonhydrocarbon:			
Carbon monoxide (90+mole%)	[a]>6	[a]>6	[a]>6
Hydrocarbon:			
Paraffin—			
Methane (99+mole%)	[a]>6	[a]>6	[a]>6
Ethane (99+mole%)	[a] 4.6	105	99.0
Propane (99+mole%)	[a] 1.9	97.1	[a].08
n-Butane (99+mole%)	93.6	90.1	93.0
Isobutane (99+mole%)	[a].17	97.6	[a].02
Olefin—			
Ethylene (USP anesthesia grade)	[a].03	75.6	[b]
Propylene (99+mole%)	[a].24	84.9	77.5
Butene-1 (99+mole%)	97.4	81.7	74.9
Butene-2 (99+mole%)	99.6	86.5	76.2
Isobutylene (95+mole%)	[a].26	88.1	87.6

[a] TEL in isooctane, ml/gal.

[b] Ethylene could not be rated under the standard F-3 conditions. Ratings made at thermal-plug temperatures considerably above that prescribed by the method gave values of 70 and 74 octane number.

From the extremely high knock ratings listed in table 2, it is evident that as far as antiknock quality is concerned, the gas could be used with supercharge and in high-compression engines.

2. HYDROCARBONS

The normally gaseous paraffins and olefins rated were commercially available samples stated to be of the purity indicated in table 2. In any case where there was reason to question the precision of a rating, duplicate tests were run and an average value listed in the table.

IV. NONHYDROCARBON BLENDS

Liquid substitute fuels considered were ethyl alcohol, both 190- and 200-proof; acetone; normal butyl alcohol; and diethyl ether (all of technical grade). Ether, although known to be of very low octane number, was included in the list because of the possibility of its use to improve volatility characteristics of the other fuels.

1. ETHYL ALCOHOL-DIETHYL ETHER BLENDS

Both ASTM motor and CFR research octane numbers were determined on a series of ethyl alcohol-diethyl ether blends in order to ascertain how much ether could be added without reducing knock rating to objectionably low values. Knock ratings obtained for the blends are listed in table 3 and are plotted against composition in figure 2. Behavior of the blends is somewhat unusual in that decrease in octane number with increasing ether content becomes very rapid in the neighborhood of 45 percent by volume of ether and that for low concentrations of ether the sensitivity (difference between CFR research and ASTM motor octane numbers) is positive and high, whereas at concentrations of ether above 48 percent exactly the oppo-

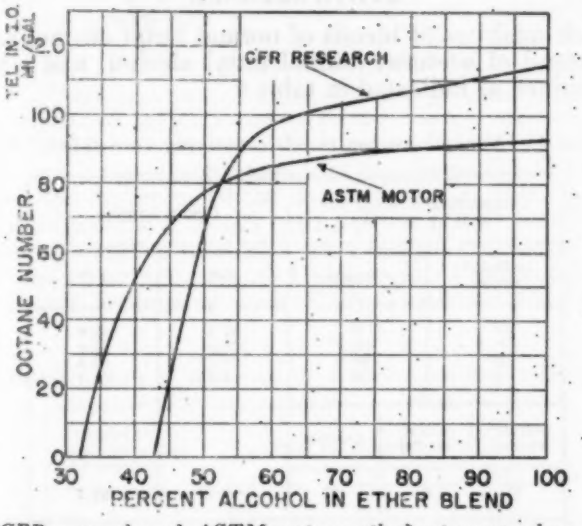

FIGURE 2.—*CFR research and ASTM motor method octane numbers of blends of 200-proof ethyl alcohol with diethyl ether.*

site is true. These tests indicate that blends of alcohol and ether containing as high as 45 percent of ether should give freedom from knock under conditions of steady operation. Road tests, however, have shown that blends containing 25 percent or more of ether will knock violently for one or two cycles if the throttle is opened quickly for rapid acceleration.

TABLE 3.—*CFR research and ASTM motor octane numbers of alcohol-ether blends*

Composition of blend, percent, by volume		Octane number	
200-proof alcohol	Diethyl ether	F-1	F-2
100	0	[a] 1.4	92.2
85	15	[a] .88	90.0
70	30	[a] .34	88.3
60	40	97.9	85.2
55	45	89.8	82.3
50	50	66.2	74.4
45	55	29.9	70.4
42.9	57.1	0	----------
40	60	----------	52.0
32	68	----------	0
190-proof alcohol	Diethyl ether		
100	0	[a] 2.7	93.8
70	30	[a] .60	89.2
50	50	91.1	83.8
40	60	----------	45.0
35	65	----------	10.9
33.4	66.6	----------	0

[a] TEL in isooctane, ml/gal.

2. BLENDS CONTAINING *n*-BUTYL ALCOHOL, ACETONE, AND ETHYL ALCOHOL

Antiknock qualities of blends of normal butyl alcohol and acetone and of a blend of acetone, normal butyl alcohol, and ethyl alcohol were determined as indicated in table 4.

TABLE 4.—*Nonhydrocarbon blends containing normal-butyl alcohol*

Composition of blend, percent by volume			Octane number	
n-Butyl alcohol	Acetone		F-1	F-2
100	0		99.5	85.6
71.5	28.5		100.0	87.0
50	50		[a] .17	89.5
0	100		[a] 3.4	[a] 3.1
n-Butyl alcohol	Ethyl alcohol	Acetone		
67	6	27	[a] 0.12	87.7

[a] TEL in isooctane, ml/gal.

V. HYDROCARBON FUELS CONTAINING NONHYDROCARBON COMPONENTS

1. GASOLINE BLENDS

To determine the practicability of extending supplies where some petroleum was available, fuels made up of varying amounts of ethyl alcohol, acetone, and/or normal butyl alcohol in gasoline or blending naphthas were investigated. Preliminary work along this line consisted of determining knock ratings by motor method of samples of 40, 50, and 60 octane number standard secondary reference fuels containing up to 40 percent by volume of alcohol. One object of these particular tests was to obtain an estimate of how much alcohol would have to be added to straight-run gasolines of 40, 50, or 60 octane number to bring their knock rating up to that of regular grade (70 ASTM motor octane number) fuel. As can be seen from the curves in figure 3, blends of these fuels containing 30, 20, and 12 per-

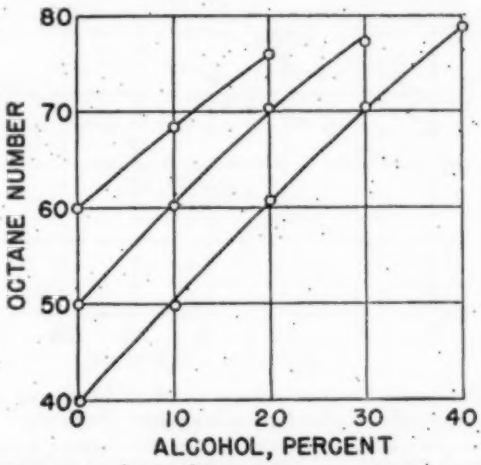

FIGURE 3.—*ASTM motor method octane numbers of blends of 200-proof ethyl alcohol with 40, 50, and 60 octane number standard reference fuels.*

cent of alcohol, respectively, met this requirement. Over the range of concentration investigated the use of alcohol in these fuels resulted in an average increase in knock rating of 1.0 octane number in the 40 and 50 octane number fuels and an average increase of 0.8 octane number in the 60 octane number fuel for each 1-percent increment of alcohol. Knock ratings of each of the blends tested are shown in table 5.

TABLE 5.—*Knock ratings of 200-proof ethyl alcohol-standard reference fuel blends*

Alcohol in blend, percent by volume	ASTM motor octane number		
0	40.0	50.0	60.0
10	49.8	60.2	68.4
20	60.8	70.3	75.9
30	70.4	77.2	----------
40	78.7	----------	----------

Tests were made by the motor method on a straight-run gasoline, typical of that furnished by a Texas Gulf Coast Refinery for nonmilitary use under lend-lease commitments, to determine the saving of tetraethyl lead that might result from the use of alcohol to raise the knock rating to that of a regular or a premium grade fuel. Results indicated that this material could be leaded to 70 and to 75 motor octane number with 0.25 and 1.1 milliliters of tetraethyl lead per gallon, respectively, and that the same ends could be accomplished through the use of blends containing 5.0 and 16.3 percent of alcohol in the finished products. On the basis of these data, it appeared feasible to ship this gasoline to countries requiring fuels of these octane numbers and possessing the alcohol with which to make the blends. Thus could be effected a saving in lead, and at the same time a reduction, by the amount of the alcohol used, in the tanker capacity needed. Properties of the gasoline and knock ratings of the alcohol blends are shown in table 6 and figure 4, respectively.

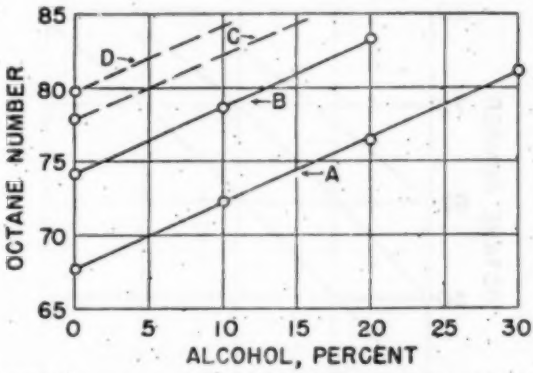

FIGURE 4.—*ASTM motor method octane numbers of blends of 200-proof ethyl alcohol with a typical lend-lease gasoline.*

Samples represented by curve A were clear, those by B, C, and D contained 1, 2, and 3 ml TEL/gal, respectively. Curves C and D were estimated from the octane numbers of the leaded gasoline and the slope of A and B.

TABLE 6.—*Lend-lease gasoline, inspection data*

Distillation:	
Initial boiling point, ° F	100
10% distilled, ° F	128
50% distilled, ° F	244
90% distilled, ° F	343
End point, ° F	381
Recovery, %	96.5
Loss, %	2.4
Residue, %	1.1
Reid vapor pressure, lb./in.²	10.0
ASTM gum	Trace
Sulfur, %	0.065
ASTM motor octane number:	
Clear	67.7
Leaded (1.0 ml. TEL/gal	74.2
Leaded (2.0 ml. TEL/gal	77.9
Leaded (3.0 ml. TEL/gal	79.8

Tests similar to the preliminary runs on alcohol–reference fuel blends were made on acetone–reference fuel blends, as indicated in table 7 and figure 5.

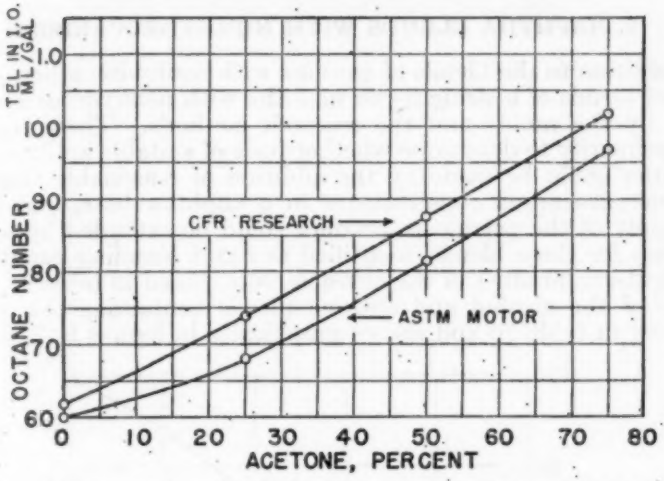

FIGURE 5.—*CFR research and ASTM motor method octane numbers of blends of acetone with a 60-motor octane number standard reference fuel.*

TABLE 7.—*Knock ratings of acetone–reference fuel blends*

Composition of blend, percent by volume		Octane number	
Acetone	Standard reference fuel (52% C–12/A–6)	F-1	F-2
0	100	61.7	60.0
25	75	73.8	68.0
50	50	87.5	81.4
75	25	[illegible]18	96.7

[illegible] TEL in isooctane, ml./gal.

The effect of the addition of alcohol and acetone to an Australian shale-oil motor fuel was studied, as indicated in table 8.

TABLE 8.—*Properties of Australian shale oil motor fuel*

Gravity, deg API	58.5
Reid vapor pressure, lb/in [illegible]	7.0
Distillation:	
Initial boiling point, °F	99
10% distilled, °F	149
50% distilled, °F	255
90% distilled, °F	342
End point, °F	378
Sulfur, %	0.20
Corrosion	Negative
ASTM gum, mg/100 ml	2
Bromine number, mg/100 g	78.6

Knock rating:

	Octane number					
	F-1			F-2		
TEL content, ml/gal	0	1	4	0	1	4
Shale-oil motor fuel	74.6	80.2	86.1	69.9	72.0	76.9
50% alcohol blend				83.0		85.4
25% acetone blend				76.9		82.3
50% acetone blend				84.0		90.7

2. NAPHTHA BLENDS WITH NONHYDROCARBONS

In addition to the blends of gasoline with nonhydrocarbons, several series of blends of a straight-run naphtha with nonhydrocarbons were tested by the motor and the research methods. These tests were made primarily to determine whether fuels of suitable antiknock characteristics could be made by the addition of reasonable amounts of the nonhydrocarbon constitutents to a naphtha base, and how far the supply of the petroleum product could be extended by so doing. The base for these blends, identified as Saxet blending naphtha, was a straight-run product of the characteristics listed in table 9. Knock ratings of the alcohol and acetone blends containing this material are listed in table 10 and shown graphically in figures 6, 7, 8, and 9.

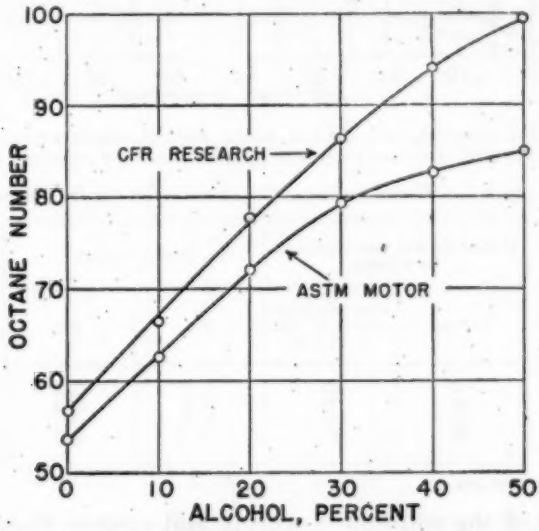

FIGURE 6.—*CFR research and ASTM motor method octane numbers of blends of 200-proof ethyl alcohol with Saxet naphtha.*

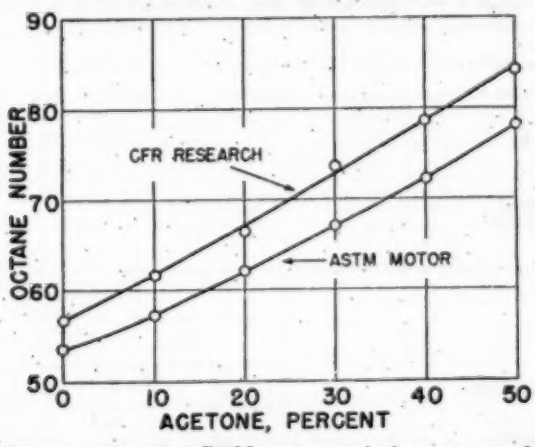

FIGURE 7.—*CFR research and ASTM motor method octane numbers of blends of acetone with Saxet naphtha.*

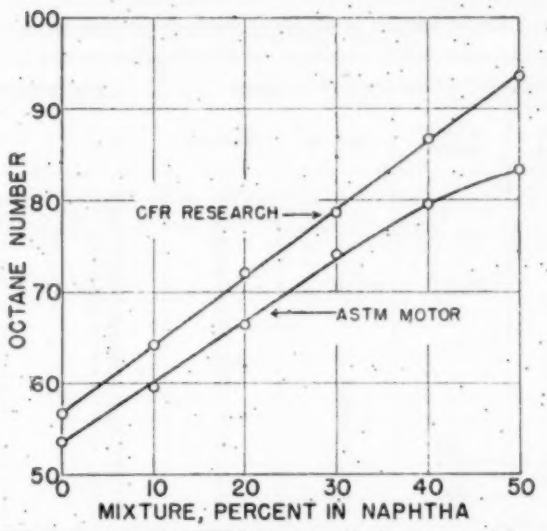

FIGURE 8.—*CFR research and ASTM motor method octane numbers of blends of a mixture of equal volumes of 200-proof alcohol and acetone with Saxet naphtha.*

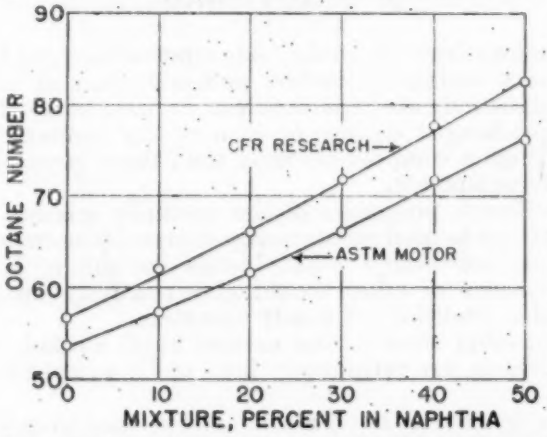

FIGURE 9.—*CFR research and ASTM motor method octane numbers of blends of a mixture of two volumes of n-butyl alcohol and one volume of acetone with Saxet naphtha.*

TABLE 9.—*Saxet naphtha, inspection data*

Gravity, deg API	55.4
Reid vapor pressure, lb/in.²	3.0
Distillation:	
Initial boiling point, °F	140
5% distilled, °F	176
10% distilled, °F	202
20% distilled, °F	227
30% distilled, °F	246
40% distilled, °F	263
50% distilled, °F	280
60% distilled, °F	295
70% distilled, °F	318
80% distilled, °F	337
90% distilled, °F	360
95% distilled, °F	381
End point, °F	397
Recovery, percent	98.1
Residue, percent	1.0

TABLE 10.—*Knock ratings of blends of nonhydrocarbons in sazet naphtha*

Composition of blend, percent by volume				Octane number	
Ethyl alcohol	n-Butyl alcohol	Acetone	Naphtha	F-1	F-2
.....	.....	.....	100	56.7	53.6
10	.....	.....	90	66.5	62.6
20	.....	.....	80	77.6	72.0
30	.....	.....	70	86.3	79.3
40	.....	.....	60	94.1	82.7
50	.....	.....	50	99.5	85.0
.....	.....	10	90	61.6	57.3
.....	.....	20	80	66.5	62.1
.....	.....	30	70	73.5	67.1
.....	.....	40	60	78.6	72.2
.....	.....	50	50	84.2	78.1
5	.....	5	90	64.1	59.6
10	.....	10	80	72.0	66.5
15	.....	15	70	78.7	74.1
20	.....	20	60	86.7	79.6
25	.....	25	50	93.7	83.4
.....	6⅔	3⅓	90	62.4	57.3
.....	13⅓	6⅔	80	66.1	61.5
.....	20	10	70	71.9	66.1
.....	26⅔	13⅓	60	77.8	71.8
.....	33⅓	16⅔	50	82.8	76.2

VI. CONCLUSIONS

The conclusions drawn from the tests reported herein are as follows:

1. The knock ratings of carbon monoxide and of the normally gaseous paraffins indicate that they can be used successfully as fuel in either supercharged engines or in normally aspirated engines of considerably higher compression ratio than those currently available in automotive equipment.

2. The antiknock properties of the normally gaseous olefins are such that they can be used satisfactorily in present automotive engines.

3. Ethyl alcohol–diethyl ether blends containing less than 45 percent by volume of ether should give relatively knock-free performance under conditions of steady operation.

4. Acetone, ethyl alcohol, and normal butyl alcohol, either separately or in blends, are satisfactory fuels as far as antiknock value is concerned.

5. Acetone or ethyl or butyl alcohol can be used to extend supplies of gasoline or can be blended with suitable petroleum naphthas to make motor fuels of satisfactory knock rating.

6. When up to 30 percent by volume of ethyl alcohol is blended with gasoline of 40 to 60 ASTM motor octane number, the improvement in knock rating is of the order of one octane unit for each percent of alcohol.

7. Acetone, though higher in octane number when tested neat, is less effective in blends than is ethyl alcohol.

WASHINGTON, August 3, 1945.

U. S. Department of Commerce National Bureau of Standards

RESEARCH PAPER RP1674

Part of Journal of Research of the National Bureau of Standards, Volume 35, October 1945

HYSTERESIS IN THE PHYSICAL ADSORPTION OF NITROGEN ON BONE CHAR AND OTHER ADSORBENTS[1,2]

By Leland F. Gleysteen and Victor R. Deitz[3]

ABSTRACT

An investigation has been made of some characteristics of hysteresis in the physical adsorption of nitrogen on bone char, activated carbon, silica gel, and coconut-shell charcoal at 77.4° K. It was found that hysteresis became less pronounced in the order given, occurring only slightly in coconut-shell charcoal and only from high relative pressures in the pressure range in which the Langmuir equation was not obeyed. It was shown that it was highly probable that a true steady state was attained in the pressure determinations and that the time dependency of adsorption and desorption are compatible with the requirements of diffusion processes. In this paper the theories of hysteresis are reviewed on the basis of capillary condensation, and an alternative interpretation is suggested in terms of the theory of multimolecular adsorption.

CONTENTS

	Page
I. Introduction	285
II. Experimental procedure	286
III. Experimental results and discussion	287
1. Rates of adsorption and desorption	287
2. Hysteresis determinations	291
IV. Theories of hysteresis in physical adsorption	300
1. Capillary condensation	300
2. Multimolecular adsorption	303
V. Summary	307
VI. References	307

I. INTRODUCTION

In many cases of physical adsorption of vapors, it has been observed that an adsorption isotherm determined for a system does not, in general, coincide with the desorption isotherm determined on the same system at the same temperature. This phenomenon is known as hysteresis in adsorption.

The possibility of hysteresis in the adsorption and desorption of nitrogen at 77.4° K, its normal boiling temperature, on bone char and other carbon adsorbents arose naturally in the course of a determination of the surface area per gram of these materials. In a previous publication [1][4] an analysis of a large number of adsorption isotherms

[1] This investigation has resulted from a joint research project undertaken by the United States and Canadian Cane Sugar Refiners, United States Bone Char Manufacturers, and the National Bureau of Standards.

[2] A portion of the material given in this paper was presented before the Division of Sugar Chemistry and Technology of the American Chemical Society at the Detroit meeting, April 1943.

[3] Research Associates at the National Bureau of Standards, representing the United States and Canadian Cane Sugar Refiners and the United States Bone Char Manufacturers.

[4] Figures in brackets indicate the literature references at the end of this paper.

by means of the multimolecular theory of physical adsorption [2] made possible the calculation of the surface areas available for the adsorption of nitrogen. As soon as it was established that hysteresis takes place in adsorption on bone char, it was thought to be desirable to pursue these experiments further and to determine what such investigations could contribute to our knowledge of the structure of carbon adsorbents.

Hysteresis has been studied by many observers in a wide variety of adsorbing systems. In many of these systems adsorbents were capable of swelling, and the adsorbed molecules were often complex. The investigation described in this paper has the advantage of dealing with the simple nitrogen molecule adsorbed on materials that are non-swelling, fairly rigid, and stable toward heating to relatively high temperatures (about 400° C) in vacuum. This evacuating and heating procedure is a necessary prerequisite for the elimination of non-reproducible hysteresis phenomena. In some cases it may even completely eliminate the phenomenon itself.

This paper presents the hysteresis phenomena observed in the adsorption and desorption of nitrogen, at 77° K, on a new bone char, a spent bone char, an activated carbon, two silica gels, and a coconut-shell charcoal. Studies of the approach to the equilibrium in both adsorption and desorption are presented as evidence that these examples of hysteresis are not consequences of failure to reach equilibrium. The explanations of hysteresis and of its possible dependence on the structure of the adsorbent are discussed on the basis of the theory of capillary condensation. An interpretation of hysteresis on the basis of the theory of multimolecular adsorption is suggested.

II. EXPERIMENTAL PROCEDURE

The apparatus used in these experiments was described in detail in a previous publication [1]. The method of determining the "dead space" in the sorption bulb and the procedure for obtaining the adsorption isotherms was also described. The procedure for obtaining the desorption points is essentially a reversal of that for obtaining the adsorption points. The nitrogen is removed from the sorption bulb by lowering the pressure in one of two ways: either the mercury level in the gas burette is lowered; or, with the stopcock connecting the gas burette to the sorption bulb closed, nitrogen is pumped out from the gas burette. The new pressure is read and the stopcock to the sorption bulb is again opened. The quantity of nitrogen removed by pumping is readily calculated from the initial and final pressures and the volume of the apparatus.

The adsorption bulbs were thermostated by immersion in a bath of boiling liquid nitrogen. At the time of reading the final pressure for each sorption point, the temperature of the bath was determined by means of a 10-junction copper-constantan thermopile. The liquid nitrogen was freshly prepared from a commercial tank of water-pumped nitrogen before each experiment. The weighed samples of adsorbent were sealed into the adsorption bulbs, which were then evacuated and heated at 400° C for about 18 hours. After the adsorbent had cooled, the dead space was measured with purified helium with the bath of liquid nitrogen in position around the tube. The helium was then removed by pumping, the adsorbent being at

room temperature. The adsorption and desorption isotherms were then determined.

The adsorbents used in these experiments are the same as previously described [3]. Char 2 is a new bone char containing 6.12 percent of carbon and 0.39 percent of hydrogen. Char 6 is an activated carbon containing 71.90 percent of carbon and 0.47 percent of hydrogen. Char 1 is a coconut-shell charcoal containing 93.88 percent of carbon and 0.63 percent of hydrogen. All materials had been ground and the portions passing through a No. 35 United States Standard Sieve and held on a No. 80 United States Standard Sieve were used.

In order to establish the presence of true equilibria, it is desirable to approach a given state from either side of the equilibrium. In the case of hysteresis this is not possible and it is, therefore, necessary to be sure that a reproducible steady state has been realized for each point. If, for example, in the physical adsorption of nitrogen on bone char, insufficient time had been allowed in both the adsorption and desorption measurements, the true isotherm would lie somewhere between the isotherms determined by such procedures and the indicated hysteresis would be an apparent rather than a true phenomenon. Several kinds of evidence indicate that the observed hysteresis is real and not apparent. This evidence includes data on the rates of adsorption and desorption at various pressures and on the reproducible characteristics of the hysteresis loops.

In observing the progress of adsorption and desorption with the apparatus used in these experiments, it was not possible to make accurate observations at the beginning stages of any point. The initial adsorption was always very rapid, and about 95 percent of the final quantity of gas was adsorbed in the first 2 minutes. With some practice it was found possible to note positions of the mercury levels of the manometer in about 1 minute. The particular volume of the gas burette was held fixed. In reading the manometer the high-pressure side was read at the time assigned to the reading and the vacuum side of the manometer, which shifts much more slowly, was read as soon thereafter as possible. The mercury level on the high-pressure side was kept nearly constant, and all data were corrected for the variation in volume caused by variations in this level. These variations were small compared to the total dead-space volume. The influence of changes in room temperature and in the temperature of the liquid-nitrogen bath was followed over the duration of the experiment.

III. EXPERIMENTAL RESULTS AND DISCUSSION

1. RATES OF ADSORPTION AND DESORPTION

It is generally recognized that physical adsorption takes place at a relatively rapid rate. There are two well-known factors that could decrease the rate of such a process. The first is a slow dissipation of the heat of adsorption that increases the time in which a given increment of adsorption takes place, as the extent of physical adsorption at a given pressure decreases markedly with increase of temperature. In the experiments reported in this paper, this factor is minimized because of the fact that all measurements were made in a pressure range where 90 percent or more of surface is covered with

adsorbed gas. Under conditions in which most of the adsorption is forming polymolecular layers, the heat of adsorption of nitrogen is but a few kilocalories per mole above the heat of liquefaction of nitrogen. The facilities for conducting these small heat evolutions to the surrounding bath are sufficient to prevent the heat developed from exceeding that which is conducted away.

The second factor retarding the rate of adsorption or that of desorption is the slow diffusion of gas molecules into the smaller interstices of the porous structure of the adsorbent. This possible effect of various pore-size distributions on the rate of physical adsorption of nitrogen was investigated by observing the rates on the three carbon adsorbents used in these experiments. It was known that the surface area per gram that was available to nitrogen molecules was greatest on coconut-shell charcoal–1 and that the adsorption isotherm for nitrogen on that material closely obeyed the Langmuir equation for monomolecular adsorption. New bone char–2, on the other hand, exhibited the least available surface, and the adsorption pursued an S-shaped isotherm typical of multimolecular adsorption. In comparison, the particular sample of activated carbon–6 was intermediate in these properties. Qualitatively, therefore, it might be expected that the ranges covered in the pore-size distributions of these adsorbents should increase in the following order: Coconut-shell charcoal, activated carbon, and bone char. The time required for these adsorbents to reach a steady state in adsorption, or desorption, should decrease in the same order.

The data presented in figure 1 relate to the dependency on time of the adsorption and of the desorption for these three samples. The curves present the change in the total amounts of gas adsorbed per gram of adsorbent with increase of time. The sharp bend of the curve is characteristic of a rapid approach to a steady state. A steady state is attained sooner, of course, for more rapid rates of adsorption or desorption than for less rapid rates. Consider first the progress of the adsorption on new bone char–2 at a relative pressure[5] of 0.74, for which data are presented in one of the upper curves of figure 1. It appears that a "steady state" is attained in about 20 minutes, and that during the next hour and a half there is no measurable drift toward increased adsorption. In other instances a very slight drift toward increased adsorption was observed, never amounting to more than 0.02 milliliter of nitrogen (STP)[6] per hour. Occasionally a slight drift in the opposite direction was observed. These drifts probably are consequences of changes in atmospheric pressure or other experimental conditions, as evidence now to be presented will indicate. It will be observed in the case of desorption from the bone char that a virtually steady state is attained in about 10 minutes. In another experiment in which the relative pressure was 0.77, desorption was observed over a longer time. In this instance, however, no satisfactory conclusions could be drawn as a rising barometer, and the possible dissolubility of oxygen in the liquid nitrogen bath, led to an increase in the temperature of the bath corresponding to an increase in the saturation pressure, p_0, amounting to several millimeters of mercury. In such cases both the increase in temperature and the consequent lowering of the relative pressure lead to further desorption.

[5] By relative pressure is meant the ratio of p to p_0, where p = experimental pressure, p_0 = saturation pressure at the temperature of the isotherm.

[6] Standard temperature and pressure, namely 0° C and 760 mm of Hg.

In this particular experiment the amount of adsorbed gas decreased continually, but always to a smaller extent than would have been required to compensate for the effect of the increase in p_0.

In addition to fluctuations resulting from variations in the temperature of the bath, the rate experiments are limited in sensitivity by the limits of precision of the gas-measuring apparatus. The reproducibility of determinations of volume—for example, that of the empty adsorption bulb—is no better than 0.02 milliliter. This sets a lower limit to the drift that could be observed.

Turning to the adsorption on activated carbon-6, figure 1 shows

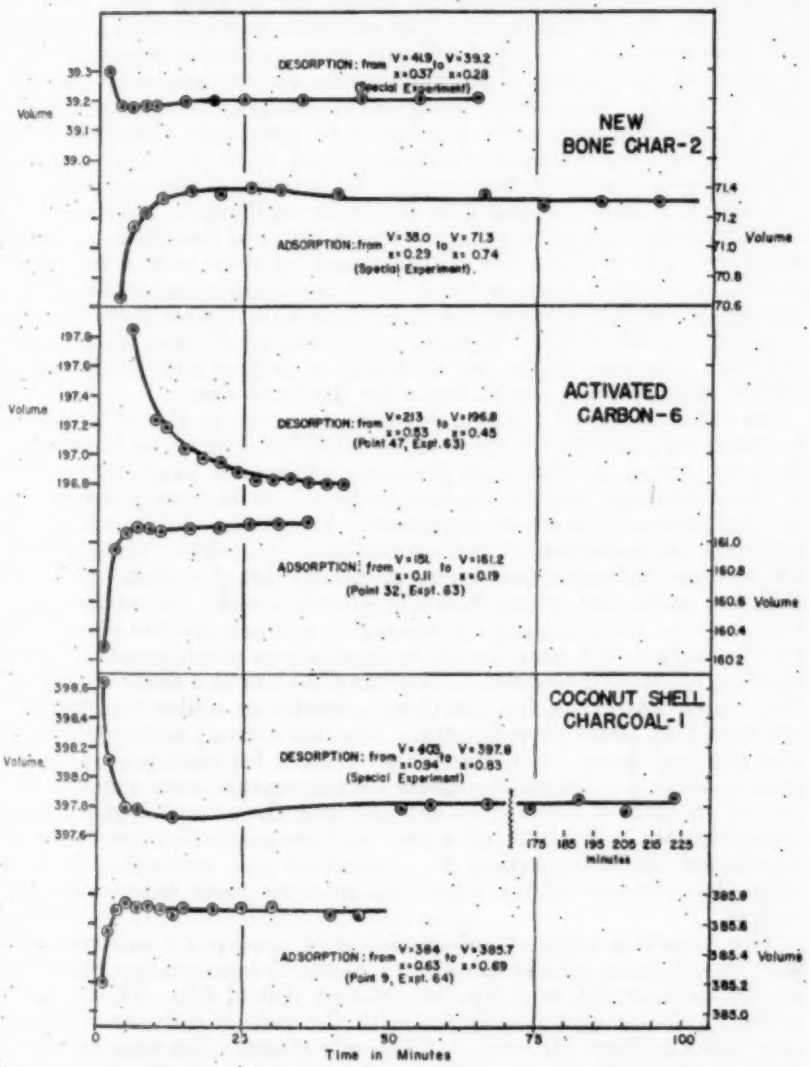

FIGURE 1.—*Adsorption and desorption of nitrogen on some carbon adsorbents at 77.4° K as a function of time.*

Volumes per gram of adsorbent, expressed as milliliters at standard temperature and pressure; time as minutes.

that very little change occurs after the first 10 minutes. Desorption seems to be a little slower, requiring 25 minutes to reach fairly steady values. The sample of coconut-shell charcoal-1 shows a prompt attainment of an apparently steady state, as is evident from the lower part of figure 1. Both adsorption and desorption become quite steady within 10 minutes. In considering all of these data, it may be said that if there is, in general, a continued drift of the adsorption or desorption with time, then that drift is too slow to be determined precisely with the present apparatus.

The surprising feature about these time-dependent curves is their similarity. The pore sizes to be attributed to bone chars are much larger than those characteristic of coconut-shell charcoal. To illustrate, coconut-shell charcoal exhibits monomolecular adsorption and, in terms of the theory of multimolecular adsorption, it is characterized by $n=1$. Bone char, however, is characterized by n values of 4 or 5 [1]. Therefore, the hindrance to gas-phase diffusion in the particles of coconut-shell charcoal might well be expected to be much greater than with bone char. In support of this point one may consider the nature of gas flow in single capillaries. Barrer [4] has assembled the equations for the various types of flow through various openings. All of these are characterized by some power term in the radius, r, ranging from a term in r^2 for simple molecular effusion through a circular opening in a thin plane wall to a term in r^4 for some types of turbulent flow. Consequently, the small pore sizes in coconut-shell charcoal might be expected to reduce materially the observed rates compared with those for the bone char.

An explanation of the approximate equality in the time required to reach equilibrium on these three adsorbents may be found in the dual nature of the diffusion process. Molecules may either diffuse to the adsorbing surface via the gas phase, or they may arrive there by the process of surface migration. Damköhler [5] considers both processes in operation at the same time. He shows that, although the volume diffusion coefficient is usually greater than the surface diffusion coefficient in capillaries of plausible radii, the surface migration may be the predominant term if the concentration of molecules on the surface of a unit length of capillary is much greater than the concentration of molecules in the gas phase in the same unit length. This condition exists for the three adsorbents under the conditions prevailing in these experiments. The bone char, activated carbon, and charcoal have large adsorbing surfaces for nitrogen, as may be seen in table 1. Moreover, these measurements were made with 90 percent or more of the surface covered with the adsorbed gas. Hence, according to this point of view, surface migration probably predominated in transporting the adsorbed gas molecules from the immediate exterior of the adsorbent into the more extensive interior surface.

The observed rates of adsorption and desorption are compatible with the theories of the kinetics of physical adsorption as developed by Damköhler [5] and by Barrer and Rideal [6]. These theories associate the rate of adsorption with the rate of diffusion of the gas into the capillary structure of the adsorbent. No matter whether surface migration or gas diffusion predominates in the transport of material to the adsorbing surface, the observed rates may be expected to vary according to some exponential law. As already mentioned,

the two possible processes are distinguished by the numerical values of the diffusion constants and in their interpretation. Barrer and Rideal predict that initially

$$|V_t^2 - V_i^2| = kt, \text{ and finally, when } |V_t - V_i| > |V_t - V_i|,$$

$$\log_e \frac{|V_e - V_i|}{|V_e - V_t|} = kt,$$

where V_t represents the volume adsorbed at time t, V_i the volume initially adsorbed, V_e the volume adsorbed at equilibrium, t is the time, and the k's are constants. The sorption is so rapid that in no experiments were data obtained that fit the first relationship. In order to plot the present data on carbon adsorbents according to the logarithmic expression, values for V_e were chosen by extrapolation of the rate curves. When these values and the data are substituted in the logarithmic expression and the appropriate plot is made, the points are scattered about straight lines. Thus, these data are compatible with Barrer and Rideal's theory and with Damköhler's theory also, as his equation is formally equivalent to the second equation of Barrer and Rideal.

The role of surface migration in the mechanism of gas adsorption and desorption has a particular significance in regard to an explanation of hysteresis in physical adsorption. This will be discussed after the presentation of the hysteresis data for the adsorbents under investigation.

2. HYSTERESIS DETERMINATIONS

It may be noted from the data on the rates of adsorption and desorption that the measurements are substantially constant for both adsorption and desorption points after about 20 minutes. This is in agreement with the observations of Beebe and Dowden [7], who found that the adsorption of nitrogen, as well as five other gases, on chromic oxide at −183° C was usually complete in 20 minutes. They further state: "The amount of gas adorbed in the interval between 2 and 20 minutes after admission was never more than 2 percent of the total increment adsorbed, and in most cases much less than that." In the experiments reported in this part of the present paper each point was observed for at least 20 minutes. It is estimated that the final measurements for each point accounted for about 99.5 percent of the increment that would have been absorbed if the previously defined steady state were attained.

The hysteresis loops that were observed in these experiments are presented in figures 2, 3, 4, 5, and 7. Relative pressures are plotted as abscissas, and the quantities of nitrogen adsorbed, expressed in milliliters at STP, are plotted as ordinates.

The isotherms for bone chars are given in figures 2 and 3. In figure 2 the adsorption isotherm was observed in experiment 61 up to a relative pressure of 0.99 by points 1 to 18. Points 19 to 30 represent the desorption isotherm observed immediately after point 18. The hysteresis loop closes at a relative pressure between 0.3 and 0.4, this serving as a check on the numerous experimental manipulations. Throughout most of the hysteresis loop, the points on the desorption isotherm lie roughly 10 percent above the corresponding adsorption

values. It is to be noted that both the adsorption and desorption isotherms are of the type termed S-shaped and, between relative pressures 0.05 and 0.3, the data conform quite accurately to the linear plot of the multimolecular theory, as we have previously shown [2]. Between 0.95 and 0.99 in relative pressure there is some evidence that adsorption and desorption isotherms again coincide. In this

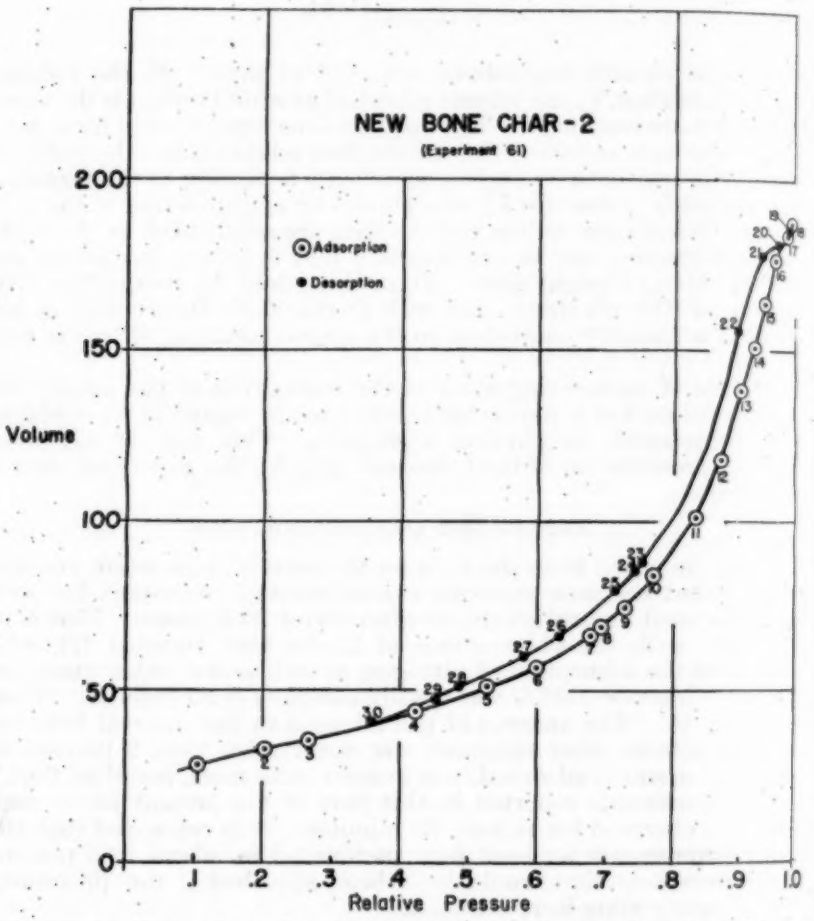

FIGURE 2.—*Hysteresis in the physical adsorption of nitrogen on bone char-2 at 77.4° K.*

Ordinates represent volume adsorbed, per gram of adsorbent, expressed as milliliters at standard temperature and pressure. Abscissas, relative pressure, i. e., equilibrium pressures divided by the saturation pressure.

range there appears to be a leveling off of the isotherm such as occurs definitely in some other systems at a somewhat lower relative pressure.

Figure 3 presents additional data from four different experiments on bone chars, three on samples of the new bone char-2 employed in procuring the data given in figure 2, and a fourth on a sample of spent bone char-27. The ordinate in figure 3 is the ratio V/V_m, and despite the wide difference in V_m for these two bone chars (see table 1),

the two adsorption isotherms superimpose on each other in this type of plot. Similar cases were reported in more detail in a previous publication [1]. In experiment 45a, points 1 to 9 represent the observations on adsorption, and points 10 to 13 those on desorption. This cycle was again repeated in experiment 45b, in which points 14 to 18 represent measurements on adsorption and points 19 to 24 on desorp-

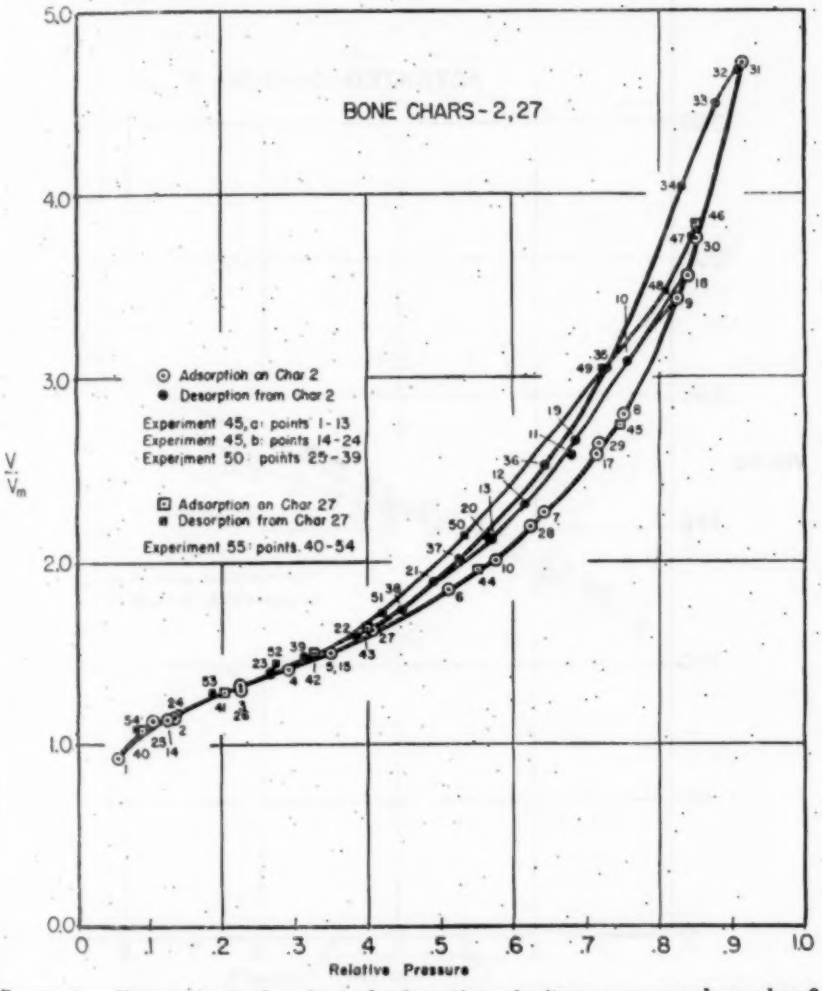

FIGURE 3.—*Hysteresis in the physical adsorption of nitrogen on new bone char-2 and spent bone char-27, both at 77.4° K.*

Ordinates v/v_m represent the ratio of volume adsorbed at equilibrium to volume required to form a monolayer; v_m was computed from the Brunauer, Emmett, and Teller equation. Abscissas represent relative pressures, p/p_0.

tion. The coincidence of the two adsorption and of the two desorption isotherms demonstrates the reproducibility of this particular hysteresis phenomenon. In experiment 50, which is taken to a higher relative pressure, the adsorption points 25 to 31 also fall on the isotherm of experiments 45a and 45b. However, the desorption isotherm defined

by points 31 to 39, lies above the previous desorption isotherm, as is usual in hysteresis phenomena. Although, as previously mentioned, the adsorption isotherm in experiment 55 for the spent bone char-27, points 40 to 46 in squares, coincides with the isotherm of char-2, the desorption isotherm covered by points 46 to 54 is different in that it

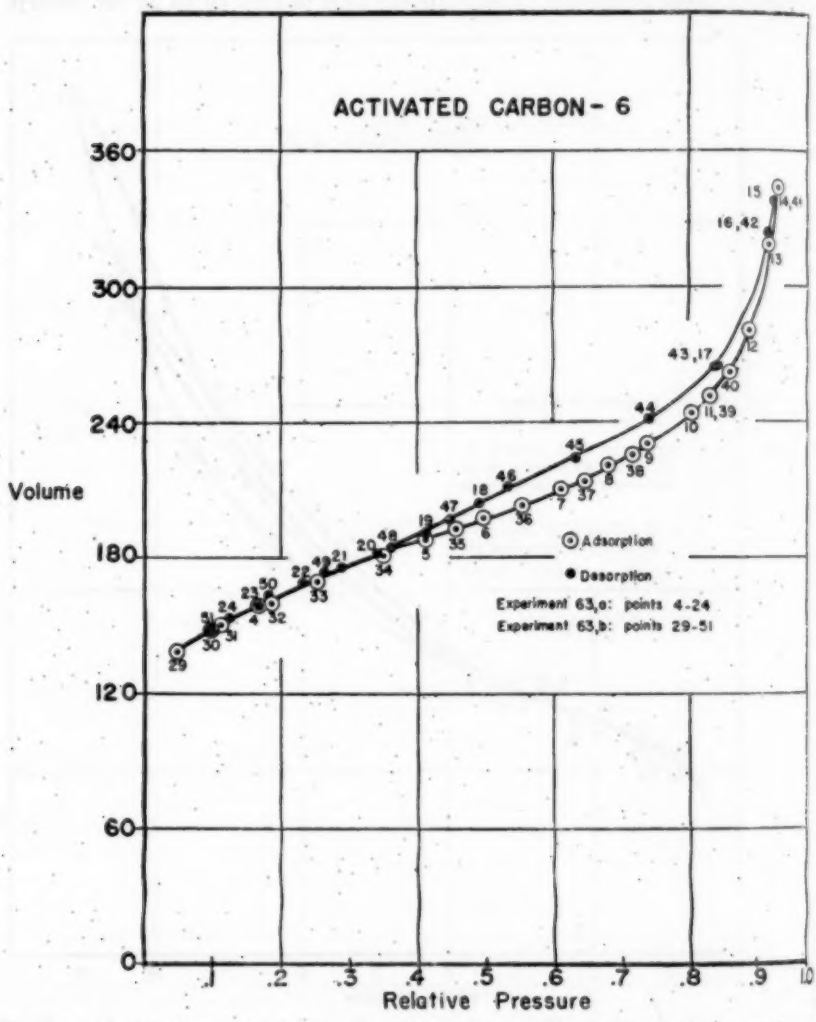

FIGURE 4.—*Hysteresis in the physical adsorption of nitrogen on activated carbon-6 at 77.4° K.*

Ordinates represent volumes, expressed as milliliters at standard temperature and pressure, adsorbed per gram of adsorbent. Abscissas represent relative pressures, p/p_0.

lies above that obtained for the new bone char-2, from which desorption began from an even higher relative pressure.

The isotherms in figure 4 obtained for the activated carbon-6 are also of the S-shaped type, but are much flatter than those for char-2. The spread between the adsorption and desorption isotherms is

smaller on a percentage basis than for the bone chars. Nevertheless, hysteresis is definitely present and, moreover, reproducible. In experiment 63a, points 1 to 14 determine the adsorption isotherm and points 14 to 24 the desorption isotherm. In the subsequent experiment 63b with the same sample of activated carbon-6 the points 29 to 41 fall on the first adsorption isotherm, and as desorption was started from the same relative pressure as in experiment 63a, the points 41 to 51 fall on the desorption isotherm of that experiment.

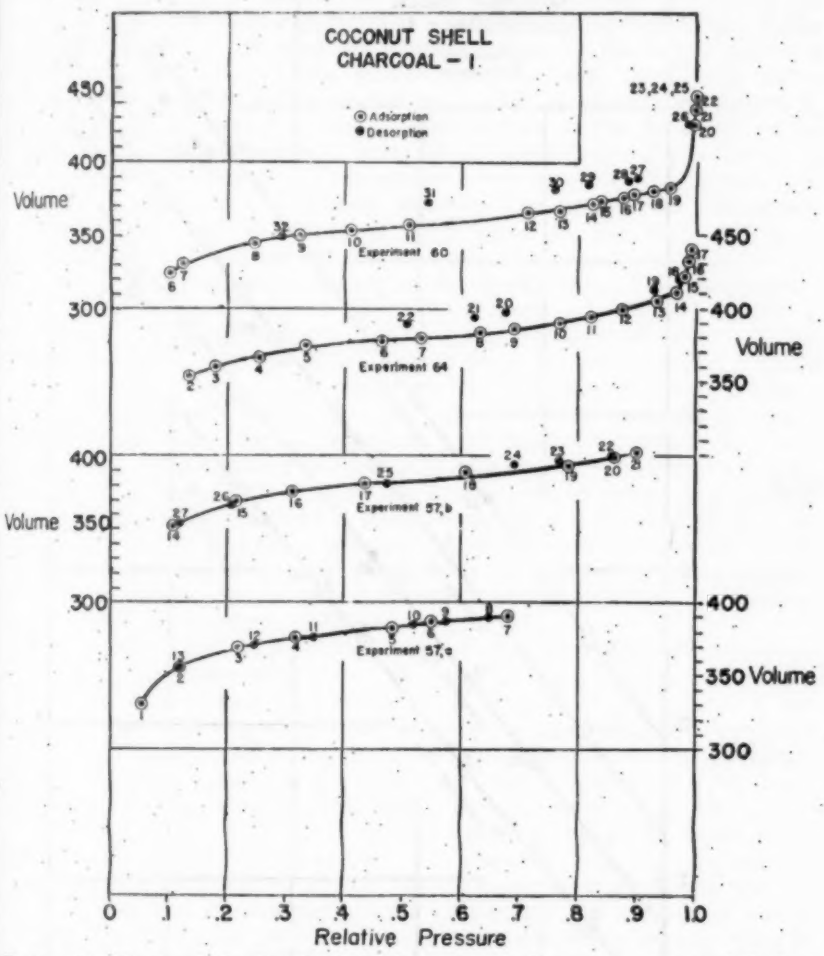

FIGURE 5.—*Hysteresis in the physical adsorption of nitrogen on coconut-shell charcoal-1 at 77.4° K.*

Ordinates represent volumes, expressed as milliliters, at STP, adsorbed per gram of adsorbent. Abscissas represent relative pressures, p/p_0.

The data for coconut-shell charcoal–1 are contained in figure 5. Four experiments are presented, each approaching the saturation pressure of liquid nitrogen to different degrees. In the lowest curve, experiment 57a, the adsorption was determined up to a relative pres-

sure of 0.7. Desorption from this point followed the adsorption isotherm, and all data quite accurately obeyed the Langmuir equation for monomolecular adsorption. In the next-lowest curve of figure 5, experiment 57b, the adsorption was observed up to a relative pressure of 0.9. Desorption from this pressure gave a small but definite indication of the presence of hysteresis, two points being

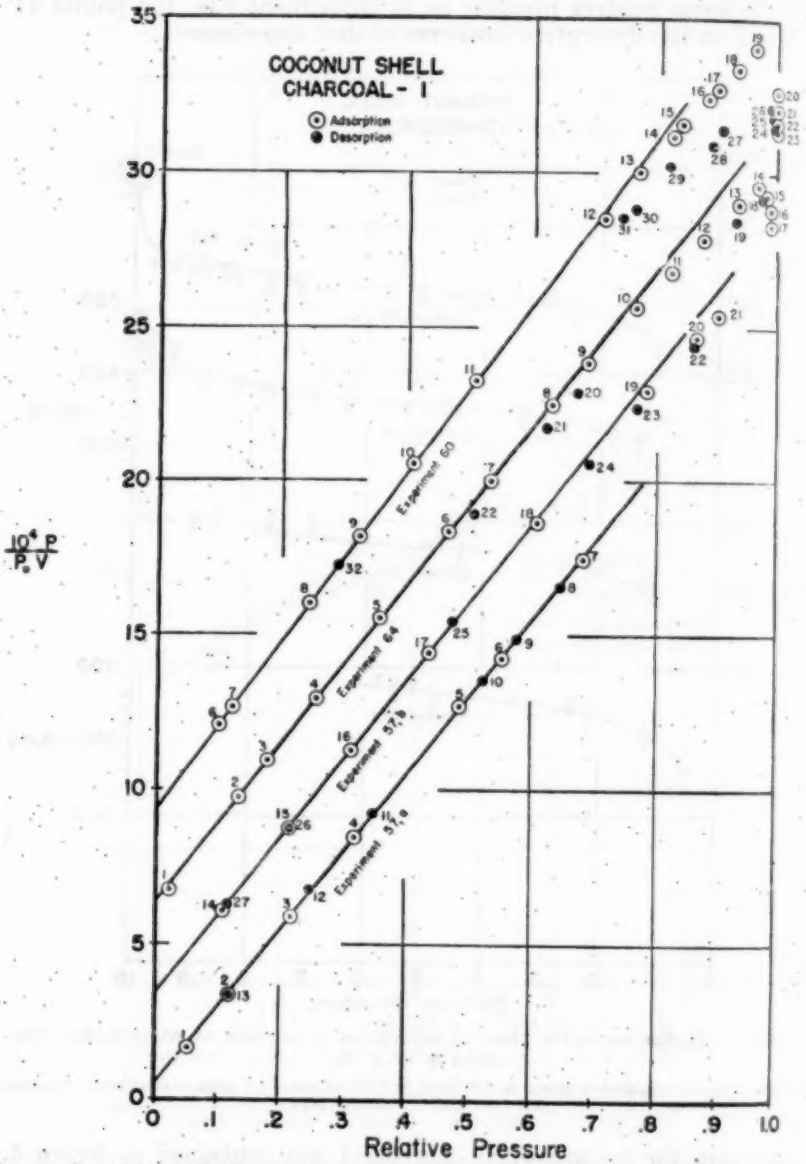

FIGURE 6.—*A test of the Langmuir equation applied to data for adsorption of nitrogen on coconut-shell charcoal-1 at 77.4° K.*

The ordinates $(10^4p)/pv$ of the equation $p/pv=1/Cv_m+p/pv_m$ are displaced upward by 3, 6, and 9 units respectively, for experiments 57b, 64, and 60. Abscissas represent relative pressures, p/p_o.

obtained above the adsorption isotherm. The spread in these data is greater than the relative experimental error in the measurements for a given experiment. However, when compared with either the bone char or the activated carbon–6, it is apparent that there is practically no hysteresis on coconut-shell charcoal if desorption begins at a relative pressure of 0.9.

Several attempts were made to extend the adsorption on the coconut-shell charcoal to pressures in the neighborhood of saturation. The results obtained in experiments 60 and 64 are shown in the upper curves of figure 5. It may be observed that in the range above a relative pressure of 0.8 the points deviate from the linear curve required by the Langmuir equation. This is shown in figure 6, where it may be seen that the deviations are in the direction of increased adsorption, possibly because of multimolecular adsorption at the higher pressures. This excess over unimolecular adsorption is not the result of any known experimental error. In particular, no reasonable error in applying corrections to the ideal gas laws account for this increase in adsorption, when such corrections are applied to the nitrogen remaining in the dead space of the apparatus. Above a relative pressure of about 0.97 there is a sharp increase in adsorption which apparently causes the adsorptive isotherm (fig. 5) to approach the ordinate of saturation pressure tangentially. Upon desorption from these high relative pressures there is evidence of a hysteresis in which the loop closes at a relative pressure between about 0.3 and 0.4. Equilibration at high relative pressures is somewhat slower than at lower pressures, but as shown in the curve for the rate of desorption from coconut-shell charcoal in figure 1, a steady state is apparently obtained. From these data it would appear that hysteresis in the physical adsorption of nitrogen on coconut-shell charcoal is only realized upon desorption from pressures near saturation. The significance of this fact will be apparent when the various theories of hysteresis are reviewed.

Emmett and DeWitt [8] have observed that a leveling off in adsorption takes place beginning at a relative pressure of about 0.80 in the adsorption of nitrogen on porous glass samples at 79° K. In the present research it was also observed to occur at a relative pressure of 0.7 in the adsorption of nitrogen on two samples of silica gel, although at lower relative pressures the contour of these isotherms differ from the shape of the porous glass and nitrogen isotherms. Data are presented in figure 7 for two different samples of commercial silica gels from the same manufacturer. As shown in table 1, the surface area of gel A was found to be 620 square meters per gram and that of gel B 765 square meters per gram. Although the surface of gel B is about 25 percent larger than gel A, it is interesting to note that in the plot of the ratio of V/V_m against relative pressure, the isotherms for the two gels coincide. (Here V is the volume of adsorbed gas, and V_m is the volume of adsorbed gas necessary to cover the surface with a unimolecular layer.) The extent of hysteresis observed for these two samples of silica gel is small, but it is definitely greater than the experimental error.

The evidence for the reality of the hysteresis loops observed in these experiments may be summarized as follows: First, the adsorption branch, starting each time from a freshly outgassed adsorbent, is very satisfactorily reproducible for duplicate runs on a given sample, as for

example experiments 45a and 45b on a single sample of new bone char-2. In the second experiment the adsorption points 1 to 13 (fig. 3) were spaced more widely than in the first experiment, so that the total elapsed time to reach a relative pressure of 0.8, for example, was only about half as long for the second experiment as for the first.

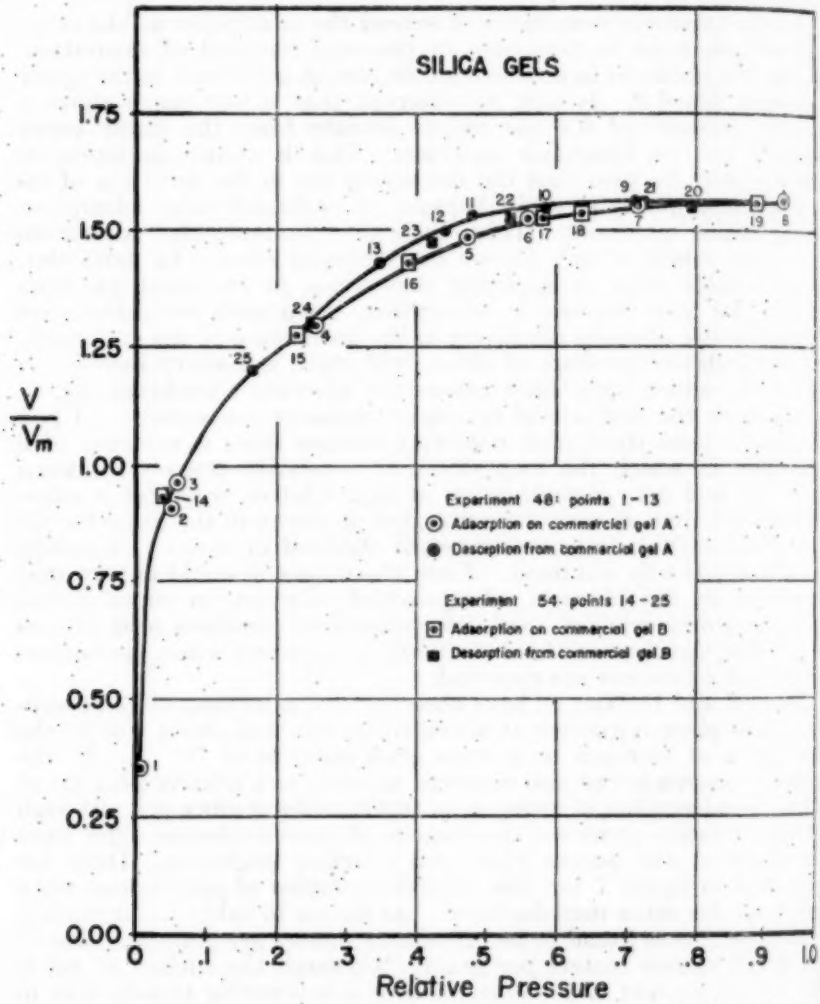

FIGURE 7.—*Hysteresis in the physical adsorption of nitrogen on silica gel at 77.4° K.*

Ordinates v/v_m represent the ratio of volume adsorbed at equilibrium to volume required to form a monolayer; v_m was computed from the Brunauer, Emmett, and Teller equation. Abscissas represent relative pressures, p/p_0.

Nevertheless the two isotherms coincide very well. Second, the desorption isotherms were found to depend upon the maximum adsorptions from which they were begun. In experiment 50 on new bone char-2, shown in figure 3, the points 25 to 39 were carried to a higher relative pressure and a greater total adsorption than in experiments

45a and 45b. It may be seen that the desorption branch obtained by experiment 50 is distinctly above those of the other two isotherms. This behavior is characteristic of hysteresis in systems which, being more conveniently held at constant temperature, have been carefully investigated by many other workers. Third, the hysteresis loops close at the low-pressure end of the isotherms. If both adsorption and desorption always failed to reach their "steady states," there should invariably be a gap at this end of the loop. Concerning the possibility that equilibration may be complete in the region of coincidence of the adsorption and desorption isotherms but incomplete in the region of hysteresis, it may be said that the kinetics of adsorption and desorption appear to be altogether similar in the two regions. These three characteristics of the hysteresis loops constitute impressive evidence that the examples of hysteresis reported in this paper are real.

TABLE 1.—*Constants derived for the physical adsorption of nitrogen on some commercial adsorbents*

[Results of the surface calculations, where v_m is the volume of nitrogen required to form a monomolecular layer on 1 gram of the adsorbent; the surface is in square meters per gram of adsorbent; E_1-E_L is the difference between the average heat of adsorption in the first adsorbed layer and the heat of liquefaction of nitrogen.]

Adsorbent	Experiment No.	v_m	Surface	E_1-E_L
		ml/g	*m²/g*	*cal/mole*
New bone char-2	61	26.4	115	1,000
Do	45a	26.9	117	2,000
Do	45b			
Spent bone char-27	55	4.37	19.3	400
Activated carbon-6	63a	142	623	800
Do	63b			
Coconut-shell charcoal-1	64	385	1,690	700
Do	57a	396	1,740	640
Do	57b	399	1,750	620
Do	60	366	1,610	660
Silica gel A	48	142	620	790
Silica gel B	54	175	765	870

The presence of hysteresis in the adsorption and desorption of nitrogen on charcoals and silica gels is significant because these phenomena do not seem to be obscured by such complications as extensive swelling of the adsorbent, pronounced asymmetry of the adsorbed molecules, and inadequate purification of the adsorbent. The swelling of charcoals during adsorption is so slight [9] that it is unlikely to cause extensive hysteresis of the kind described by Barkas [10]. The nitrogen molecule contains no dipole moment and no other instance of conspicuous asymmetry. The excellent reproducibility of adsorption isotherms on a given sample of char shows that the hysteresis effect cannot be caused by the gradual displacement of a film of adsorbed impurities according to the postulates of Zigmondy.

The surface areas of the adsorbents employed in this investigation, calculated by the method of Brunauer, Emmett, and Teller [2], are summarized in table 1. Hexagonal close-packing in liquid nitrogen was assumed to occur on the adsorbing surface, and an effective area of 4.37 square angstrom units [1] was covered by each milliliter of adsorbed nitrogen at 77° K.

IV. THEORIES OF HYSTERESIS IN PHYSICAL ADSORPTION

1. CAPILLARY CONDENSATION

A comprehensive review of the various theories of hysteresis in physical adsorption has been given recently by Brunauer [12], and recent discussions on the subject have been presented by Rao [11], Emmett and DeWitt [8], and Cohan [14]. An examination of these theories reveals that those that are applicable to well outgassed adsorbents involve the concept of capillary condensation. This concept has not been very successful in interpreting quantitatively the general phenomena of adsorption. However, it seems to offer a partial explanation of hysteresis.

It is recognized on thermodynamic grounds that when a liquid is constrained to present a curved surface, its vapor pressure differs from the vapor pressure of a plane surface of the same liquid. In particular, if the curvature be *concave*, the vapor pressure is reduced and condensation can occur at pressures less than the normal saturation pressure of the liquid. In the case of a spherical meniscus this behavior is quantitatively given by the classical Kelvin equation, which relates the radius of curvature, r, to the ratio of the vapor pressure of the confined liquid, p, to that of the liquid in bulk, p_0, as follows:

$$\ln p/p_0 = \frac{-2\gamma v}{rRT}. \tag{1}$$

Here γ is the surface tension; v is the molar volume of the liquid; R is the gas constant, and T is the absolute temperature.

In applying this relationship to adsorption phenomena, the solid adsorbent is conceived as possessing numerous pores of various shapes and sizes. For mathematical simplicity it is usually assumed that the actual system of pores is equivalent to a hypothetical system of pores having regular geometric forms, such as cylinders. Such a cylindrical capillary will be either completely filled or entirely empty at any particular pressure, as is required by the Kelvin equation. In order to account for the smooth, continuous adsorption isotherms which are found experimentally, it is, therefore, necessary to postulate a continuous distribution of capillaries of gradually increasing radii. Unfortunately, these capillary radii are not subject to independent determination, but are deduced from the adsorption isotherm which they are intended to explain.

It should be possible, nevertheless, to test the self-consistency of the pore-radius distribution for a given adsorbent by evaluating the distribution from an isotherm for a particular vapor, and then by comparing this distribution with others obtained from isotherms of other vapors. Also, the total volumes, as liquids, adsorbed at saturation pressure may be compared for several vapors. In regard to the experimental test of these two conditions, it may be said that they are qualitatively fulfilled. As to the first possibility, Brunauer [12] has examined the available experimental results and has shown the lack of quantitative agreement. Assuming the validity of the unmodified Kelvin equation and using normal values for the surface tension and the molecular volumes of the adsorbed vapors, Brunauer demonstrates that the pore-radius distribution curve for a given adsorbent is not independent of the vapor employed. Apparently the adsorbent can-

not be considered as entirely inert, presenting merely an array of capillaries of various sizes to the adsorbed gas. With regard to the second experimental test, there are a number of cases in which the volume of adsorbed liquid, determined at saturation pressure, has been observed to be constant for various vapors with the same adsorbent. However, there are also a large number of cases in which the adsorption isotherm approaches saturation at a very steep slope. Consequently, it is difficult to estimate the quantity of vapor adsorbed at saturation pressure.

The most useful application of the concept of capillary condensation has been in explaining hysteresis. Theories attempting to explain hysteresis loops of the type presented in figures 2, 3, 4, 5, and 7 have been three in number. The oldest is known as the Zsigmondy theory of partial wetting [12]. This is based on the observation that the angles of contact, θ, between a solid and the liquids that wet it depends upon whether the liquid is advancing over or receding from the solid surface. The difference between the "advancing" and the "receding" angles of contact is often called the hysteresis of the contact angle. When applied to the capillary condensation theory of adsorption, it is assumed that partial wetting occurs in adsorption. This imperfect wetting is attributed to impurities, mostly permanent gases, adsorbed on the walls. The equilibrium pressures are given by the equation

$$\ln p/p_0 = \frac{-2\gamma v \cos \theta}{rRT}. \qquad (2)$$

At saturation pressure a complete wetting of all surfaces takes place. Subsequently the desorption equilibrium takes place from a completely wetted surface, in which $\theta=0$ degrees and, therefore, corresponds to equation 1. As a consequence, the values of p/p_0 calculated for a given radius would be greater in adsorption than in desorption. The serious objection, however, to this explanation of hysteresis is the reproducibility of data in repeated cycles of adsorption and desorption that is obtained with highly evacuated samples. Whereas in some cases it is possible to eliminate hysteresis by drastic evacuation technic, in other cases it is not possible to do so. This rules out the Zsigmondy theory of partial wetting as a general explanation of reproducible hysteresis.

The Kraemer and McBain "bottleneck" theory of capillary condensation assumes the presence of constricted regions in capillaries with one end open. According to this theory, hysteresis results from the following conditions: The narrow neck fills at low relative pressures, but condensation in the body of the capillary takes place only at a higher relative pressure determined by the larger radius; in desorption the pores empty only when the pressure is reduced so that the liquid in the constricted region becomes unstable. This condition of instability is determined by the smaller radius of the neck. Upon being released, the liquid condensed in the larger part of the pores is immediately desorbed. In this way the amount of gas desorbed for a given decrease in pressure is less than the corresponding amount adsorbed until a lower pressure is reached corresponding to the radius of the constriction. Unfortunately, this ingenious explanation of hysteresis is not amenable to quantitative treatment as there is no way of obtaining information concerning the volumes of the various pores and the radii of their wide and narrow parts.

The third explanation of hysteresis, also in terms of capillary condensation, assumes the presence in the adsorbent of cylindrical capillaries without constrictions and with both ends open. If a capillary is open at both ends, L. Cohan [14] has shown that a meniscus cannot form during the adsorption process. Condensation is assumed to occur, however, at a suitable relative pressure on a unimolecular layer already adsorbed to the inner cylindrical surface. This condensation forms an annular ring, or shell, of liquid on the wall. The entire capillary will then fill, as any inner annular ring has a lower vapor pressure than the outermost one. It was shown by Cohan [14] that the relative pressure is given by equation 3, where r_1 is the radius of the annular ring

$$\ln[p/p_0]=\frac{-\gamma v}{r_1 RT} \quad (3)$$

Desorption, on the other hand, occurs from the meniscus formed when the capillary is full, and takes place according to equation 1 with $r=r_1$, assuming complete wetting of the surface. There are two aspects of this theory which are subject to a quantitative test. The theory predicts that the radius at which hysteresis begins, r_h, should be not less than $2D$, where D is the diameter of the adsorbed molecule. Assuming hexagonal close packing in three dimensions for liquid nitrogen at 77.8°K, D=4.33 angstroms. This value corresponds to an average area of 16.22 square angstroms per nitrogen molecule. For this value of D, r_h cannot be less than 8.66 angstroms, which corresponds to a relative pressure of about 0.33, when γ=8.8 and v=34.7. The data obtained for carbon adsorbents and silica gels in this investigation are in agreement with this conclusion. If the capillary condensation is assumed to occur after a unimolecular layer is formed, then D must be measured from the surface of this layer and not from the wall. The second prediction is that for a given volume of gas adsorbed in the region of hysteresis, the relative pressure on the desorption curve should equal the square of the relative pressure on the adsorption curve. This may be seen by combining equations 1 and 2. The data obtained in this investigation are not in agreement with this prediction in any pressure region of the hysteresis loops.

This open-pore theory has the advantage of being subject to certain quantitative tests, but all of these explanations involving capillary condensation suffer the following defects:

(a) The capillary radii are not subject to independent determination, but are deduced from the sorption isotherm which they are supposed to explain.

(b) There is no adequate means of determining: what fraction of the capillary radii are constricted and thus contribute to hysteresis in an indefinite manner; what fraction are open and nontapering and thus contribute to hysteresis in a supposedly definite manner; and what fraction are tapered, or V-shaped, and do not contribute to hysteresis at all.

(c) The many and varied assumptions that have been proposed to modify the capillary condensation theory (specifically the proposed changes in the surface tension, the density of the condensed liquid, the angle of contact between liquid and wall, and the size, shapes, and distribution of pore radii), do not constitute a completely logical

approach to the general phenomena of adsorption in terms of fundamental molecular theory.

(d) The necessity of accounting for at least the first layer of adsorbed gas remains as an independent problem. One does not know whether the capillary condensation is to be considered as being superimposed upon Langmuir adsorption or upon some more complex type of adsorption, which results from the interaction between the unbalanced forces on the surface atoms and the atoms of the adsorbate.

2. MULTIMOLECULAR ADSORPTION

Hysteresis phenomena in adsorption may apparently be divided into two main classes from an experimental point of view. The high-pressure end of the hysteresis loop may close either at a relative pressure definitely below saturation (e. g., $x=0.8$ for the silica gels), or the desorption isotherm may differ from the adsorption isotherms up to pressures very close to saturation without any indication of leveling off. The leveling off of adsorption isotherms is generally interpreted as indicating the stage where the pore structure has been completely filled with adsorbate. Hence where this does not occur, it is difficult to estimate an average pore radius for the adsorbent. Present-day concepts endeavor to classify the various types of hysteresis loops shown by adsorbents in relation to variations in such an average pore radius. For example, Coelingh [13] suggests the following classifications: (1) The very narrow pores of chabasite and some charcoals are too small to exhibit capillary condensation; thus the adsorption and desorption isotherm coincide and no hysteresis is evident, (2) charcoals having wide pores and silica gels having narrow pores, both with pore radii in the neighborhood of 10 angstroms, show hysteresis for small molecules like H_2O and N_2, but no hysteresis for larger molecules, (3) still larger pores show hysteresis for all vapors, and (4) hysteresis in very large pores may extend so close to the saturation pressures that the hysteresis loop cannot be accurately determined. This classification may be overly simplified.

It is now suggested that the concept of hysteresis can be incorporated into the multimolecular theory of adsorption as presented by Brunauer, Deming, Deming, and Teller [15]. These authors have developed a general theory in which the five types of adsorption isotherms may be deducted from a single equation. They attribute the leveling off in the upper portions of certain adsorption isotherms to the increased value for the heat of adsorption of the last layer of molecules, which fill a capillary-like structure. This last adsorbed layer is attracted from either side and, correspondingly, its heat of adsorption (E_L+Q) can be expected to be greater than that of any layer except the very first adsorbed layer. The equation derived by these authors is

$$v=v_m\left[\frac{x}{1-x}\right]+A, \tag{4}$$

where A equals

$$\frac{2(c-1)x+2(c-1)^2x^2+(\bar{n}c^2+\bar{n}h-2\bar{n}c-n^2c^2)x^{\bar{n}}+(2c+\bar{n}^2c^2+2\bar{n}c-c^2[(2+\bar{n})-2h(1+\bar{n})]x^{\bar{n}+1}+(\bar{n}h+2h)x^{\bar{n}+2}}{2[1+2(c-1)x+(c-1)^2x^2+(c^2+h-2c-\bar{n}c^2)x^{\bar{n}}+(\bar{n}c^2+2c-2c^2-2h)x^{\bar{n}+1}+hx^{\bar{n}+2}]}.$$

In equation 4 and in the expression for A, v is the volume of gas adsorbed; v_m is the volume of gas which is required to cover the

surface with a monomolecular layer; x is the relative pressure; $\bar{n}$ is the maximum number of layers that can fit into the capillary; c is a constant related to the increase of the heat of adsorption over the heat of liquefaction (E_L), namely $E_1-E_L=2.303\ RT \log c$, in which E_1 is the heat of adsorption in the first layer, R is the gas constant, and T is the temperature; $h=(\bar{n}c^2-c^2+2c)g$, where g is related to the additional energy, Q, by the expression, $g=e^{Q/RT}$.

Good agreement was found by Brunauer, Deming, Deming, and Teller in applying the above rather formidable equation to the data of Lambert and Clark [16] for the *adsorption* of benzene on a ferric oxide gel. The constants $v_m=0.082$ gram of benzene per gram of gel, $c=27$ (corresponding to $E_1-E_L=2{,}110$ calories), $h=47{,}400$ (corresponding to $Q=1{,}690$ calories), and ($\bar{n}=6$ were used to calculate the lower curve in figure 8. This agrees very favorably with the experimental points in the circles. The agreement is more remarkable when the simplifying assumptions used in developing the theory are considered. In the mathematical derivation of equation 4 it was assumed that the adsorption takes place between plane parallel walls and that all pores throughout the adsorbent are of uniform width.

It is now pointed out that an isotherm agreeing with the desorption data can be calculated to fit the experimental data of Lambert and Clark by changing one constant in the previous calculation. The identical values for V_m, c, and $\bar{n}$ are used as in adsorption, but h is increased to 164,100. This change in h corresponds to increasing Q, by 760 calories, to 2,450 calories. This increase in Q signifies that in the region of hysteresis the heat of desorption is greater than the heat of adsorption. The increment of 760 calories was determined from the data of Lambert and Clark and represents the difference between the average differential heats of desorption and of adsorption calculated by means of the application of the Clapeyron-Clausius equation to the 40° and 60° C isosteres, representing 0.15 to 0.19 gram of benzene adsorbed per gram of gel. In this range the average values of the calculated heats were 8,660 calories for adsorption and 9,420 calories for desorption, the difference being 760 calories. The calculated desorption isotherm, the larger value of Q being used, is shown as the upper curve in figure 8. Agreement with the experimental desorption points is not all that could be desired, but it is certainly all that could be expected. It is remarkable that a change in one particular constant of equation 4 is all that is required to change the isotherm to correspond to the course of the desorption process. It is to be noted that as the hysteresis loop closes, the calculated differential heats of adsorption and of desorption become equal. This may account in part for the deviation between theory and experiment in the lower and upper parts of the desorption branch.

A plausible significance may be attached to the above procedure in that it attributes hysteresis to some fundamental change in the adsorbed layer that takes place at a relative pressure near saturation. A stability of the adsorbed layer to subsequent evaporation results, as evidenced from the increase in the numerical value of Q. A multimolecular layer of adsorbate may be viewed as a physical state whose similarity to the liquid bulk phase must be complete at saturation pressures. Until that similarity is reached there are many inter-

mediate configurations possible in the complex structure of the multimolecular layer. The situation may be analogous to the clusters postulated by J. E. Mayer [17] in his explanation of the phenomena of the critical state by means of a statistical theory of condensing systems. It suggests that molecular clusters of various sizes may

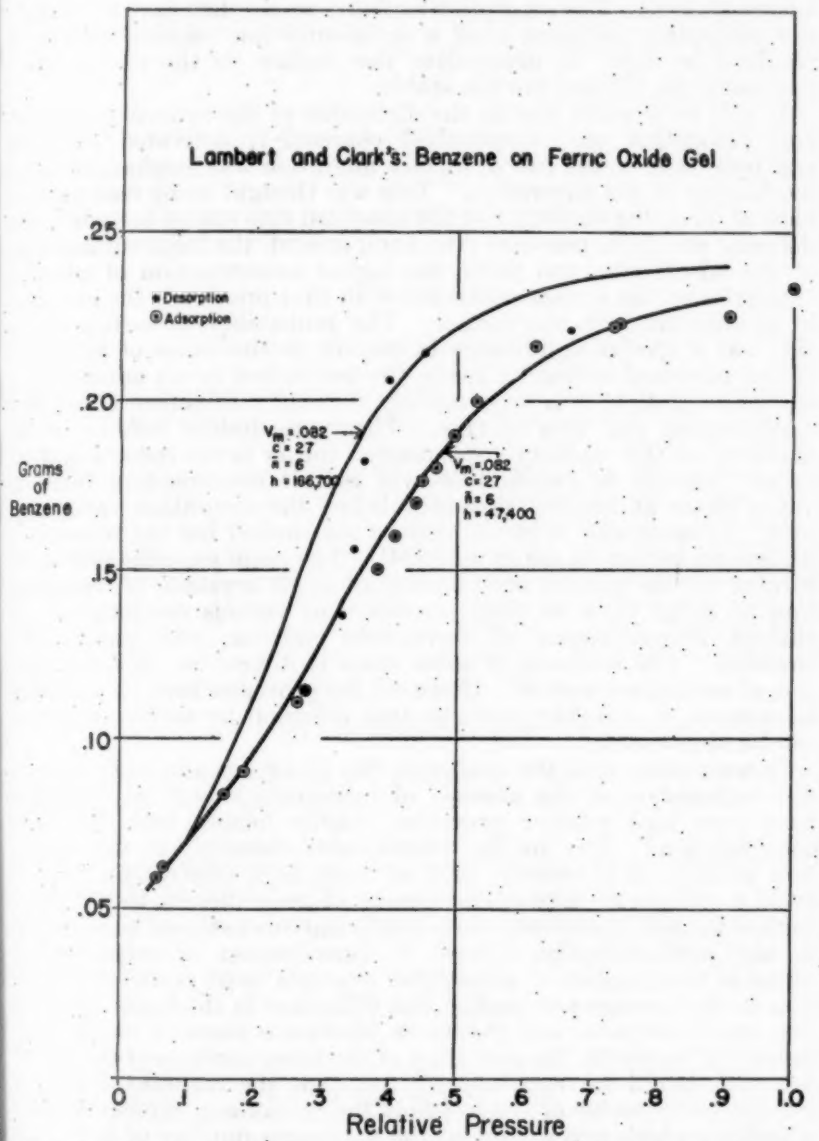

FIGURE 8.—*Calculated isotherms according to the theory of Brunauer, Deming, Deming, and Teller for the data of Lambert and Clark on the adsorption of benzene on a ferric oxide gel.*

Ordinates represent grams of benzene adsorbed per gram of gel and abscissas represent relative pressures, p/p_o.

form gradually at many points on the surface, depending upon the interaction between the adsorbent and the adsorbed layers. These large aggregates may be independent of each other (but in a statistical equilibrium with the vapor) until a certain relative pressure is attained, at which point they are modified by joining together in some fashion. Subsequently, desorption would have to occur from this modified adsorbed layer. The desorption isotherm would then have to lie above the adsorption isotherm until a sufficiently low relative pressure is resumed in order to depopulate the surface to the extent where the molecular clusters are not stable.

It will be recalled that in the discussion of the rates of adsorption and desorption on coconut-shell charcoal–1, activated carbon–6, and bone char–2, the role of surface migration was emphasized in the mechanism of gas adsorption. This was thought to be reasonable in view of, first, the similarity of the observed rate curves for substances differing widely in pore-size structure; second, the large surface areas of the adsorbents; and third, the higher concentration of adsorbed molecules on the surface compared with that present in the gas phase in equilibrium with the surface. The probability of surface migration has a special significance in respect to the cause of hysteresis. If the adsorbed molecules reach the interstices of an adsorbent by surface migration, it is very unlikely that the mechanism of capillary condensation can also operate. This immediately follows, as the mainstay of the capillary condensation theory is the reduction of the vapor pressure to values that will permit condensation from the vapor phase at relative pressures below the saturation vapor pressure. Considerable evidence can be marshalled for the presence of surface migration on many solids [4]. The main experimental proofs involve (1) the growth and solution of single crystals, (2) condensation of metal films on glass, metals, and various crystals, and (3) various measurements of thermionic emission and photoelectric emission. The evidence in some cases is direct, but in other cases it is of an indirect nature. However, for processes involving physical adsorption, it is highly probable that diffusion by surface migration can be appreciable.

In connection with the isotherms (fig. 5) for coconut-shell charcoal, the explanation of the absence of hysteresis, except on desorption from very high relative pressures, readily follows from the above considerations. Due to the unimolecular character of this adsorption process, it is possible only at very high relative pressures to build a sufficiently high concentration of molecules on the adsorbing surface to form the intermediate configurations assumed to be present in the multimolecular layers. A classification of adsorbents in terms of multimolecular adsorption concepts must consider, in addition to the average pore radius, the difference in the heats of adsorption and desorption and the steric hindrance imposed on the polymolecular layers by the geometry of the inner surfaces of the adsorbent. It should be remembered, too, that the constant $\overline{n}$ may be interpreted in terms of the width of the cracks and capillaries of the adsorbent which sets a limit to the maximum number of layers that can be adsorbed even at saturation pressure. At this pressure the limiting value of V/V_m should be equal to $\overline{n}/2$, as layers are building outward from both walls. It may be seen from figure 8 that the limiting value of $V/V_m=3$ for the data of Lambert and Clark is

consistent with the value of $\bar{n}=6$. As Brunauer, Deming, Deming, and Teller point out, this is true only if the value of g is high and that of $\bar{n}$ is low. Elsewhere the experimental value for V/V_m is usually less than $\bar{n}/2$. This is understandable as the multimolecular theory of adsorption has not treated the interaction of each molecule with its neighbor.

Hysteresis in the physical adsorption of gases remains as one of the outstanding problems in the field of adsorption. The phenomenon is recognized to be very complex and to be immediately confronted by the relatively limited progress that has been made in the fundamental study of condensed systems. The investigations based on capillary condensation theories, as pointed out in the first section of this discussion, are of limited application. The multimolecular theory of adsorption, however, may be considered as an alternative approach to the problem with some advantages for the moment in guiding researches in this field.

V. SUMMARY

The physical adsorption and desorption of nitrogen were observed for samples of coconut-shell charcoal, activated carbon, and bone char. It was shown that good approximations to final steady states were obtained in the experiments. No appreciable differences were observed in the time dependency of adsorption or desorption on these adsorbents. From the isotherms for adsorption and desorption it was shown that the magnitude of the hysteresis effect decreased in the order: bone char, activated carbon, silica gel, coconut-shell charcoal. On the last-named substance, hysteresis was shown to occur only if the desorption process was begun very close to saturation pressure—a region in which the Langmuir equation of unimolecular adsorption was not obeyed. The explanations of hysteresis, on the basis of capillary condensation, were reviewed, and an alternative interpretation was suggested in terms of the theory of multimolecular adsorption.

VI. REFERENCES

[1] V. R. Deitz and L. F. Gleysteen, J. Research NBS **29**, 191–225 (1942) RP1496.
[2] S. Brunauer, P. H. Emmett, and E. Teller, J. Am. Chem. Soc. **60**, 309–19 (1938).
[3] V. R. Deitz and L. F. Gleysteen, J. Research NBS **28**, 795–805 (1942) RP1479.
[4] R. M. Barrer, Diffusion in and through solids, 464 pages (Cambridge University Press, England, 1941).
[5] G. Damköhler, Z. physik. Chem. [A] **174**, 222–38 (1935).
[6] R. M. Barrer and E. K. Rideal, Proc. Roy. Soc. [A] **149**, 231–53 (1935).
[7] R. A. Beebe and D. A. Dowden, J. Am. Chem. Soc. **60**, 2912–22 (1938).
[8] P. H. Emmett and T. W. DeWitt, J. Am. Chem. Soc. **65**, 1253–62 (1943).
[9] D. H. Bangham and R. F. Razouk, Proc. Roy. Soc. [A] **166**, 57–86 (1938).
[10] W. W. Barkas, Trans. Faraday Soc. **38**, 447–62 (1942).
[11] K. S. Rao, J. Phys. Chem. **45**, 500–31 (1941).
[12] S. Brunauer, Physical Adsorption, chapter XI, 511 pages (Princeton University Press, Princeton, N. J., 1943).
[13] M. B. Coelingh, Kolloid Z. **87**, 251–72 (1939).
[14] L. Cohan, J. Am. Chem. Soc. **66**, 98–105 (1944).
[15] S. Brunauer, L. S. Deming, W. E. Deming, and E. Teller, J. Am. Chem. Soc. **62**, 1723–32 (1940).
[16] B. Lambert and A. M. Clark, Proc. Roy. Soc. [A] **122**, 497–512 (1929).
[17] J. E. Mayer and M. G. Mayer, Statistical mechanics, page 312, 502 pages (John Wiley & Sons, Inc., New York, N. Y., 1940).

665730—45——5

U. S. Department of Commerce National Bureau of Standards

RESEARCH PAPER RP1675

Part of Journal of Research of the National Bureau of Standards, Volume 35, October 1945

SOME PHYSICAL PROPERTIES OF MICA

By Peter Hidnert and George Dickson

ABSTRACT

This paper gives data on the linear thermal expansion, changes in structure, power factors, and effects of heat treatments on the thickness, opacity, and color of micas (muscovite, phlogopite, biotite, ripidolite, and zinnwaldite) from different domestic and foreign sources. Tremendous linear thermal expansion was noted for some samples of phlogopite and biotite micas in a direction perpendicular to the cleavage plane. The transitions shown in the expansion curves of these samples at elevated temperatures appear to be related to the structural changes indicated in the X-ray diffraction patterns. Heat treatment of two phlogopite micas and two muscovite micas to 600° C, with or without a load, caused considerable increases in the power factors of the former and only slight changes in the latter. Nearly all the muscovite samples showed the greatest increases in thickness (up to 155 percent) after heat treatment at 800° C. The large increases in thickness of nearly all the muscovite samples accompanied changes from clear or translucent to opaque, or from polychrome to metallic color. None of the species of mica can be considered as a substance or material of fixed and reproducible properties. The physical properties of mica depend largely upon the chemical composition, the nature of the crystals, their magnitude and orientation, the presence of impurities, the way in which these enter the structure, the heat treatment, etc. Some of the phlogopite and biotite micas that possess tremendously high thermal expansion in a direction perpendicular to the cleavage plane may be used for high-expanding elements in temperature-responsive devices but may be unsatisfactory for use in devices in which large changes in dimensions with changes in temperature are not desirable.

CONTENTS

	Page
I. Introduction	309
II. Material investigated	311
III. Physical properties	312
1. Thermal expansion	312
2. Changes in structure (by H. C. Vacher)	339
3. Power factors (by E. L. Hall)	342
4. Effects of heat treatments on thickness, opacity, and color	344
IV. Discussion	350
V. Summary and conclusion	351
VI. References	353

I. INTRODUCTION

As an outgrowth of tests made in connection with a military problem, an investigation of the linear thermal expansion of various kinds of micas (muscovite, phlogopite, biotite, ripidolite, and zinnwaldite) was undertaken. The determinations were made in a direction perpendicular to the cleavage plane of the mica. The work was extended to include an investigation of structural changes indi-

cated by Laue X-ray diffraction patterns, power factors, and effects of heat treatments on thickness, opacity, and color.

Mica [1] [1] [2] is one of the most important strategic materials in time of war [3], and is indispensable in some modern applications in

TABLE 1.—*Sources and varieties (or qualities) of mica*

Sample No.	Source	Variety or quality [a]	Submitted by—
	A. MUSCOVITE MICA		
1682	Brazil	White 1441 punch	BG Corporation.
1684	Canada	Amber	Simmonds Aerocessories, Inc.
1685	Brazil	No. 3	Do.
1686	do	No. 5	Do.
1687		Plate mica (processed sheet supplied by New England Mica Co).	Do.
1689	Los Volcansillos Mine, Guatemala	Verde claro	Office of Economic Warfare.[b]
1690	do	Verde oscuro	Do.
1691	Durania Section, Colombia	Black stained [c]	Do.
1692	do	Stained [d] or good stained [e]	Do.
1693	El Mico Prospect, San José de la Montaña Mica District, Colombia.		Do.
1694	Near Camana, Peru		Do.
1695	Near Camana, Ferreyros, Peru		Do.
1696	Amber Mine, Concepcion Area, Depto. Santa Cruz, Bolivia.		Do.
1697	La Negra Mine, Concepcion Area, Depto. Santa Cruz, Bolivia.		Do,
1698	San Juan Mine, Concepcion Area, Depto. Santa Cruz, Bolivia.		Do.
1699	New Hampshire	First quality	Colonial Mica Corporation.
1700	do	Second quality	Do.
1701	Old Mike Mine, 4½ miles north of Custer, S. Dak.	First quality	Do.
1702	do	Second quality	Do.
1703	Mill Race Mine, Avery County, N. C.	Green, first quality	Do.
1704	do	Green, second quality	Do.
1705	Sink Hole Mine, near Bandana, Mitchell County, N. C.	Ruby, first quality	Do.
1706	Hawkins Mine, Stokes County, N. C.	Ruby, second quality	Do.
1707	Petaca Area, N. Mex	First quality	Do.
1708	do	Second quality	Do.
1729	Purdy Mine, Mattawan Twp., Ontario, Canada.	Clear,[f] No. 1 quality	Bureau of Mines, Canada.
1731	Simard Mine, Bergeronnes Twp., Saguenay Co., Québec, Canada.	Ruby	Do.
1741	San Jorge Mine, Concepcion Area, Depto. Santa Cruz, Bolivia.		Office of Economic Warfare.[b]
1742	Cordoba, Argentina	Semi clear	Do.
1743	do	Semi stained	Do.
1744	do	Stained [d]	Do.
1745	do	Light green	Do.
1746	Catamarca, Argentina	Clear [f]	Do.
1747	do	Semi clear	Do.
1748	San Luis, Argentina	do	Do.
1749	Hibbs Mine, Hebron, Maine		H. W. Bearce, National Bureau of Standards.

[a] For classification of quality of mica, see ASTM designation: D351-38, ASTM Standards, Part III, Nonmetallic Materials, p. 391 (1942) (Am. Soc. Testing Materials, Philadelphia, Pa.).

[b] Now Foreign Economic Administration.

[c] *Black stained:* Apt to contain some mineral inclusions consisting of magnetite (black).

[d] *Stained:* Free of mineral inclusions and cracks, but may contain considerable clay and vegetable stains and may be more wavy and softer than the better qualities.

[e] *Good stained:* Free of mineral inclusions and cracks but contains air inclusions, some vegetable inclusions, and may be somewhat wavy.

[f] *Clear:* Free of all mineral and vegetable inclusions, stains, air inclusions, waves, or buckles. Hard transparent sheets.

[1] The designation "mica" has been traced back to a publication by Agricola in 1546.

[2] Figures in brackets indicate the literature references at the end of this paper.

[3] It has been stated in the public press that mica is probably the most important single war material for without it "there would be no radar, no radio, no electric gun controls, and no detector devices."

TABLE 1.—*Sources and varieties (or qualities) of mica*—Continued

Sample No.	Source	Variety or quality [a]	Submitted by—
		B. PHLOGOPITE MICA	
1681	Madagascar	Black, No. 995	BG Corporation.
1683	do		Simmonds Aerocessories, Inc.
1688	Mozambique, Africa		Office of Economic Warfare.[b]
1709	do		Do.
1710	do	Silver	Do.
1711	Burgess, Canada	National Museum specimen No. 78218.	National Museum.
1712	St. Lawrence County, N. Y.	National Museum specimen No. C3681.	Do.
1732	St. Lawrence Mica Co. Mine, Petit Pré., Quebec, Canada.	Spark plug grade	Bureau of Mines, Canada.
		C. BIOTITE MICA	
1713	E. Blake Mine, Newdale, N. C.	National Museum specimen No. 90467.	National Museum.
1730	Faraday Twp., Hastings Co., Ontario, Canada.		Bureau of Mines, Canada.
1733	Ledford Cove Mica Mine, Macon County, N. C.		Geological Survey.
1734	Saunders Quarry, Oxford County, Maine.		Do.
		D. RIPIDOLITE MICA	
1714	Three miles south of Westchester, Pa.	National Museum specimen No. 79023.	National Museum.
		E. ZINNWALDITE MICA	
1735	Morefield Mine, Amelia, Va.		Geological Survey.

time of peace. It is used in many products, such as condensers, electric generating and motive equipment, radio tubes, airplane spark plugs, electric-light bulbs and sockets, X-ray apparatus, heating elements, and so forth.

Samples of mica were obtained from the corporations and Government agencies indicated in table 1.

II. MATERIAL INVESTIGATED

Fifty samples consisting of five types of mica were investigated for three or more of the following physical properties: Thermal expansion; changes in structure; power factors; and effects of heat treatments on thickness, opacity, and color. Available information about the sources and the varieties (or qualities) of these samples is indicated in table 1.

No chemical analyses were made on the samples of mica used in this investigation. The chemical composition of muscovite [4] mica may be represented approximately by $[Al_2]\ (AlSi_3)O_{10}(OH, F)_2\ K$. Aluminum, $[Al_2]$, is replaced by magnesium in phlogopite [5] mica,

[4] The name *muscovite* for potash mica was reported by De Boot [2] to be derived from the locality Muskovia in Russia, where this mica was found.

[5] Phlogopite mica has a pearly to submetallic luster on cleavage surfaces, with a coppery reflection, which gave rise to its name, derived from the Greek word "phlogopos," firelike [1].

$[Mg_3]$ $(AlSi_3)O_{10}$ $(OH, F)_2$ K, and by magnesium, lithium, titanium, ferric and ferrous iron in other micas. Additional information about the chemical composition of different micas may be obtained from publications by Horton [3], Hendricks and Jefferson [4], Pauling [5], Mohr [6], and Mellor [7]. Mica contains chemically combined water. The most common impurities in mica are iron oxides, silica, and clay. The spotting or staining of mica has been ascribed to the inclusion of thin scales or streaks of dark minerals, most frequently iron oxides.

Hendricks and Jefferson [4] stated that moscovite mica has a unique structure because of its distorted layer, whereas the biotite micas have variable structures because their layers are symmetrical. The distortion of the layer in muscovite mica is a result of incomplete filling of the octahedral positions, so that some octahedral edges will be differently surrounded than others. All octahedral positions in the biotite micas are filled and the octahedral edges are equivalent.

Hendricks and Jefferson [4] assumed that many elements of a mosaic in a mica crystal showing a well-developed structure are perfectly regular, and any diffuse scattering is due to random shifts in a limited number of the mosaic elements.

III. PHYSICAL PROPERTIES

1. THERMAL EXPANSION

The fused-quartz-tube expansion apparatus described by Hidnert and Sweeney [8] was modified so that short samples of mica could be used. With two exceptions,[6] each sample consisted of 20 to 105 disks of mica, approximately 16 mm in diameter. The disks of various thicknesses were stacked to form a cylindrical sample 16 to 23 mm in height (see footnote 6), in order to determine the linear thermal expansion in a direction[7] perpendicular to the cleavage plane. The sample rested on a flat disk of fused quartz, which was placed at the bottom of the fused-quartz tube in order to avoid bending the disks of mica by the curvature of the bottom surface of the tube. Similarly, a flat disk of fused quartz was placed on top of the sample. A 45-cm movable fused-quartz rod rested on the upper flat disk of fused quartz and extended above the open end of the fused-quartz tube. This rod is hollow but closed at the ends. The bottom of the rod is concave and the top is flat. A bar of steel (about 38 cm long) with a weight at each end was placed horizontally at the top of the 45-cm movable fused-quartz rod, so that the center of gravity of the steel bar and weights was at a point on the vertical axis of the fused-quartz rod. The foot of a dial indicator graduated to 0.01 mm rested on top of the steel bar. One junction of a Chromel-Alumel thermocouple was attached to the side of the upper flat disk of fused quartz above the sample of mica. An electric furnace surrounding the tube containing the sample was used to control temperature during heating and cooling.

Each sample of mica was subjected to a load represented by the sum of the weights of the upper fused-quartz disk, the movable

[6] Sample 1681A consisted of 1 disk 0.3 mm in height (thickness). Sample 1709 consisted of 10 disks and was 3 mm in height.

[7] The axis of the cylindrical sample represented the direction perpendicular to the cleavage plane of the mica.

fused-quartz rod, the steel bar and weights, and the force exerted by the foot of the dial indicator. In most of the expansion determinations, the load on the sample was 30 lb/in.^{2} (2.11 kg/cm^2). In nine determinations the load [8] was 1 lb/in.^{2} (0.07 kg/cm^2) and in one determination the load was 10 lb/in.^{2} (0.70 kg/cm^2).

The dial indicator fastened near the top of the fused-quartz tube indicated the differential expansion between the sample and an equivalent length of fused quartz. A correction for the small expansion [9] of fused quartz was applied. When enormous expansion beyond the range (13 mm) of the dial indicator was about to occur, the dial indicator was removed from the fused-quartz tube, and measurements of the displacements of the upper surface of the movable fused-quartz rod above the upper end of the fused-quartz tube were made with calipers and a steel scale graduated in millimeters. When the sample had contracted sufficiently during cooling so that it was again possible to make observations within the range of the dial indicator, the indicator was replaced on the fused-quartz tube.

Figures 1 and 2 of the publication by Hidnert and Sweeney [8] show photographs of the fused-quartz-tube apparatus and auxiliary equipment before the modifications indicated in the present paper were made. Prints showing details of the original apparatus are available for persons interested in constructing this equipment.

Figures 1 to 21, inclusive, indicate the results obtained on the linear thermal expansion of 30 samples of mica (muscovite, phlogopite, biotite, ripidolite, and zinnwaldite) in a direction perpendicular to the cleavage plane when subjected to a load. In most cases, the load was 30 lb/in.^{2}

The results obtained on the linear thermal expansion of 14 samples of moscovite mica in a direction perpendicular to the cleavage plane when subjected to a load of 30 lb/in.^{2} are shown in figures 1 to 5, inclusive. The samples of muscovite mica were maintained at room temperature in the thermal-expansion apparatus under the load indicated for 17 to 23 hours before they were heated. During this interval of time the shrinkage of the samples varied from 0.1 to 0.3 percent. Most of the shrinkage at the initial temperature occurred during the first few (1 to 7) hours. During the first heating, a slight shrinkage was noted for most of the samples when they were maintained for approximately 1 hour at 100°, 150°, 200°, and 250° C, respectively. Slight additional shrinkage was observed when the samples were held overnight at approximately 250° C. Most of the samples contracted in an irregular manner during the first heating from room temperature to 600° C. This contraction for the entire range was less than 2 percent for all except three samples. In one sample (1687, fig. 2), the contraction during heating between room temperature and 600° C was 4.1 percent. In two samples (1682 and 1696, figs. 1 and 4), an expansion of 0.4 percent occurred on the first heating from room temperature to 600° C. Smooth contraction curves were obtained for all samples except 1684 (fig. 1) and 1687 (fig. 2), when they were cooled from 600° C to room temperature. Most of the curves obtained on heating and cooling in the second test are close to the corresponding curves obtained on cooling in the first test. The authors are of the opinion that the shrinkages that occurred in the samples of muscovite micas at room temperature prior

[8] When the load was 1 lb/in.^{2}, the steel rod and weights were not used.

to heating and at higher temperatures on the first heating resulted principally from the load on the samples which forced the laminas, or layers, of the micas closer together. It is probable that evolution of moisture was also a factor in the shrinkages of these micas on the first heating.

The results obtained on the linear thermal expansion of 10 samples of phlogopite mica in a direction perpendicular to the cleavage plane

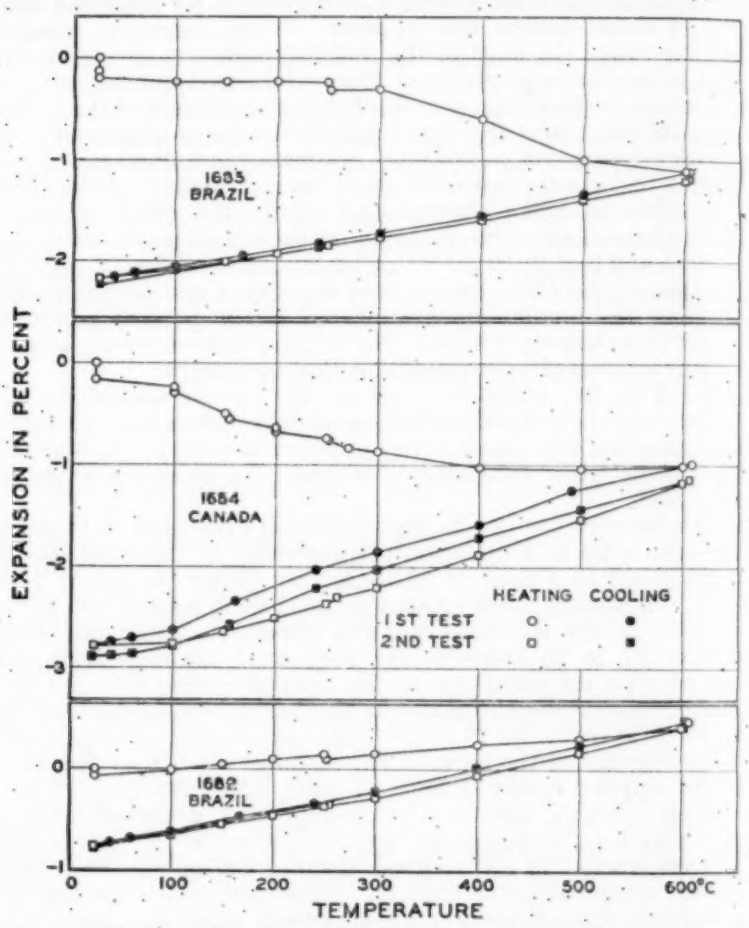

FIGURE 1.—*Linear thermal expansion of three samples of muscovite mica from Brazil and Canada in a direction perpendicular to the cleavage plane when subjected to a load of 30 lb/in.*[2]

when subjected to a load are shown in figures 6 to 15, inclusive. From the curves it can be seen that the linear thermal expansion of some of the samples is tremendous. In fact, this expansion is many times that of any other known solid material.

Five of the samples of phlogopite mica were maintained at room temperature in the thermal-expansion apparatus under a load of 30 lb/in.^{2} from 16 to 21 hours before heating. During this interval the shrinkage varied from 0.0 to 0.2 percent, slightly less than for

the muscovite samples tested. Samples 1681A (fig. 7) and 1709 (fig. 10), on which no shrinkage was detected at room temperature, were made up of 1 and 10 disks, respectively, whereas the other three samples of phlogopite mica contained 55 or 80 disks.

Four samples of phlogopite mica (1681, 1681A, 1688, and 1711, figs. 6, 7, 9, and 12) expanded from 50 to 166 percent when heated from room temperature to 600° C under a load of 30 lb/in^2. The

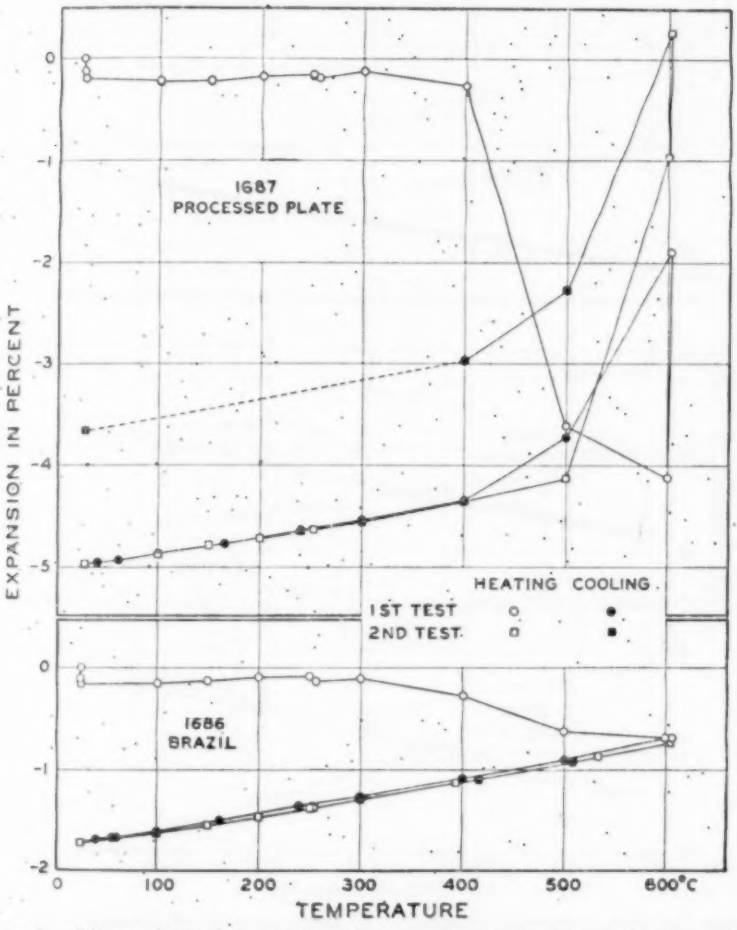

FIGURE 2.—*Linear thermal expansion of a sample of muscovite mica from Brazil and of a processed plate of muscovite mica (sample 1687) in a direction perpendicular to the cleavage plane when subjected to a load of 30 lb/in.*[2]

expansion curves of these four samples show that the rate of expansion is comparatively low between room temperature and 100° C but very high for a short interval [9] between 100° and 250° C. Above 250° C the rate of expansion is lower, although it remains high up to 600° C. The expansion curves of these samples of phlogopite are irreversible.

[9] During the first heating of samples 1681 and 1688, evolution of moisture was noted between 150° and 200° C.

In general, the cooling curve lies above the heating curve, and on cooling, the rapid contraction takes place at a lower temperature than does the rapid expansion on heating. When the heating and cooling cycle was repeated the curves on heating and cooling were closer together, and the total expansion was less on each successive cycle. The first run on sample 1681A is unusual in that the curve obtained on cooling from 600° to about 200° C lies below the curve obtained on

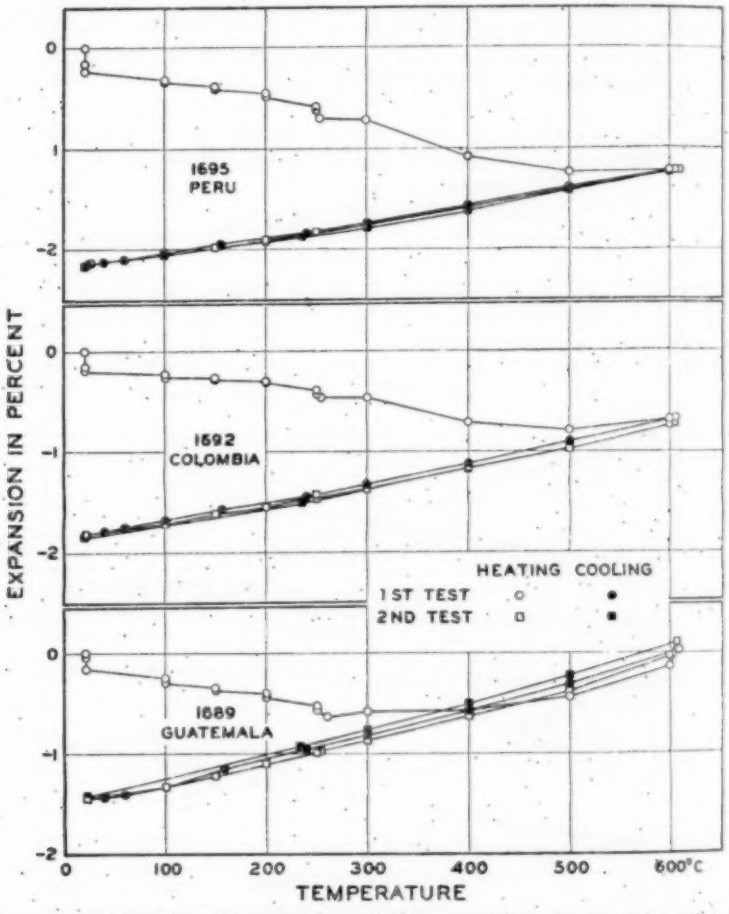

FIGURE 3.—*Linear thermal expansion of three samples of muscovite mica from Guatemala, Colombia, and Peru in a direction perpendicular to the cleavage plane when subjected to a load of 30 lb/in.*^{2}

heating from about 200° to 600° C. The curves on heating and cooling between 100° and 600° C for the fourth test of sample 1711 are nearly reversible. All four of these samples of phlogopite mica returned to within 2 percent of their original lengths after they were heated to 600° C and cooled to room temperature under a load of 30 lb/in^2.

Phlogopite samples 1681 (fig. 6) and 1681A (fig. 7) were from the same source and supposedly were of identical material, the only

apparent difference in the samples being that 1681 was made up of 80 disks to form a stack 17.2 mm high, whereas 1681A consisted of 1 disk 0.28 mm thick. The great difference in the expansion seems to indicate that this phlogopite mica is not uniform.

Phlogopite sample 1711 (fig. 12) was heated three times under a load of 1 lb/in². Under this load the expansion from room temperature

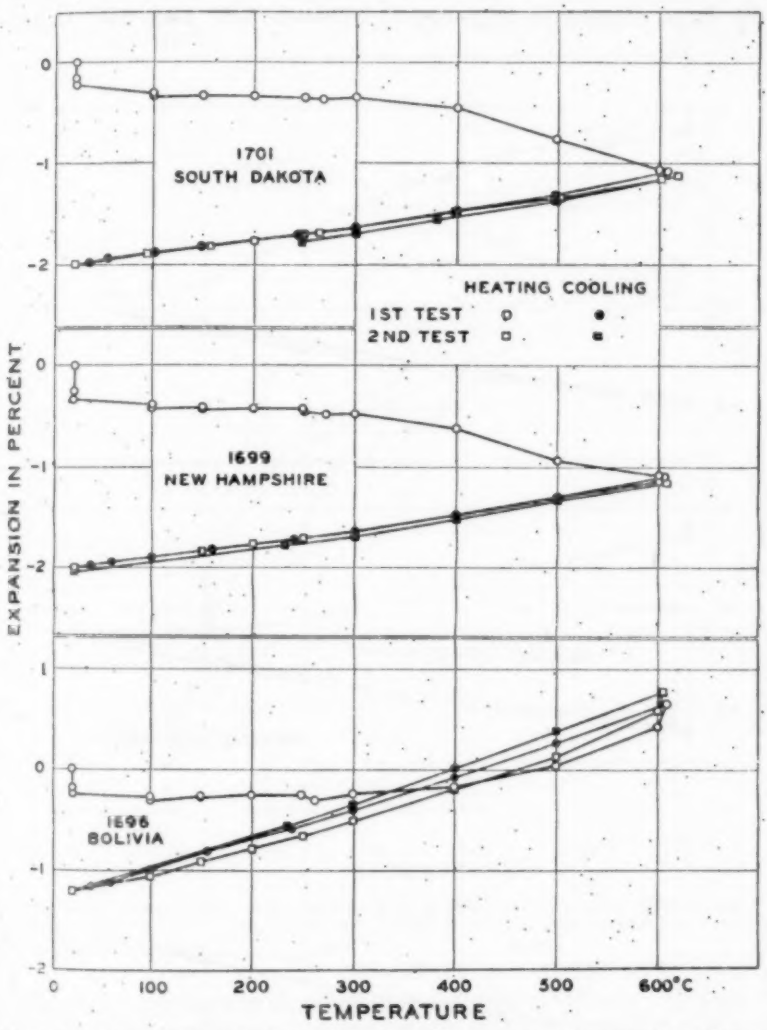

FIGURE 4.—*Linear thermal expansion of three samples of muscovite mica from Bolivia, New Hampshire, and South Dakota in a direction perpendicular to the cleavage plane when subjected to a load of 30 lb/in.*²

to 600° C was the highest of any mica measured, varying from about 300 percent for the first heating to about 240 percent for the third heating. The fourth run on this sample was made with a 30 lb/in². load, which reduced the total expansion to 50 percent.

Phlogopite samples 1683, 1712, and 1732 (figs. 8, 13, and 15) when subjected to a load of 30 lb/in^2. expanded much less (all below 15 percent) than the four samples of phlogopite mica discussed above, but there is a similarity in the shapes of the expansion curves. The similarity is more apparent after the first heating. During the first heating, samples 1712 and 1732 indicated shrinkage up to 200° C and 150° C, respectively. The former sample also indicated comparatively large expansion (4 percent) between 500° and 650° C and a

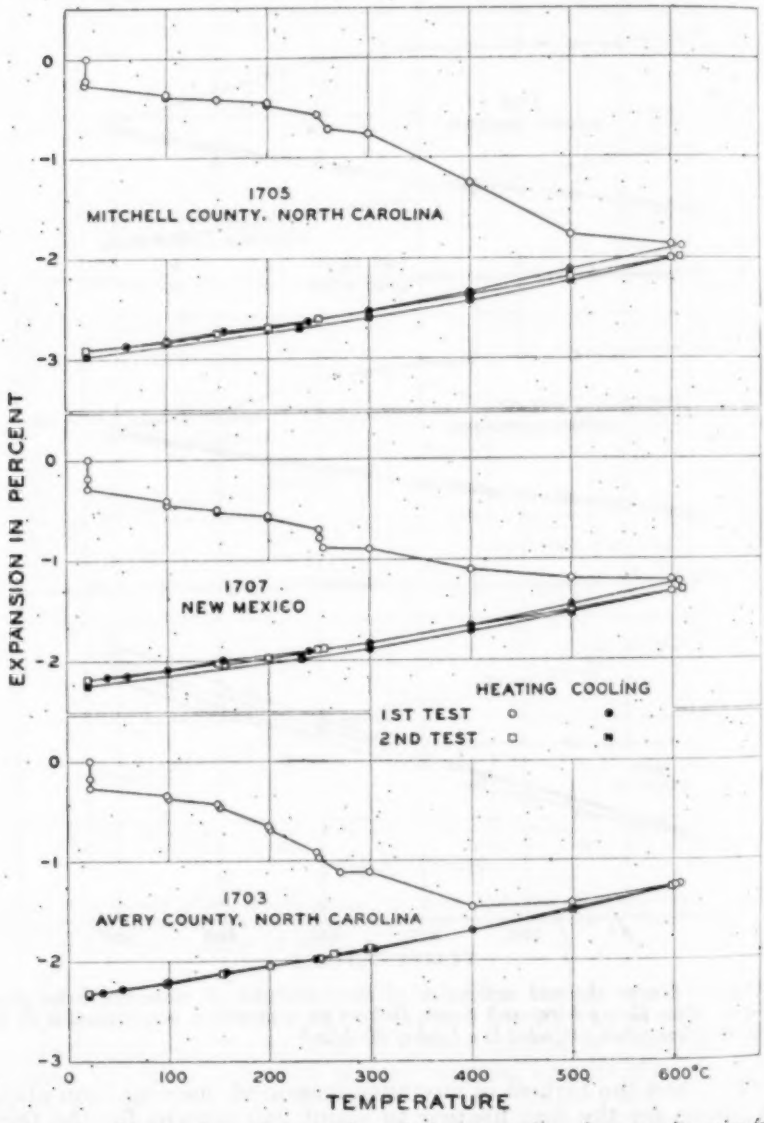

FIGURE 5.—*Linear thermal expansion of three samples of muscovite mica from North Carolina and New Mexico in a direction perpendicular to the cleavage plane when subjected to a load of 30 lb/in.*^{2}

shrinkage of 3 percent during further heating from 650° to 700° C. A duplicate of sample 1712 (fig. 14) under a load of 1 lb/in.² showed practically no shrinkage when heated from room temperature to 200° C and a much larger expansion (17 percent) between 500° and 600° C. Repeated heating under a 10 lb/in². or 1-lb/in². load eliminated the high expansion or shrinkage between 500° and 700° C on samples 1712 and 1712A (figs. 13 and 14).

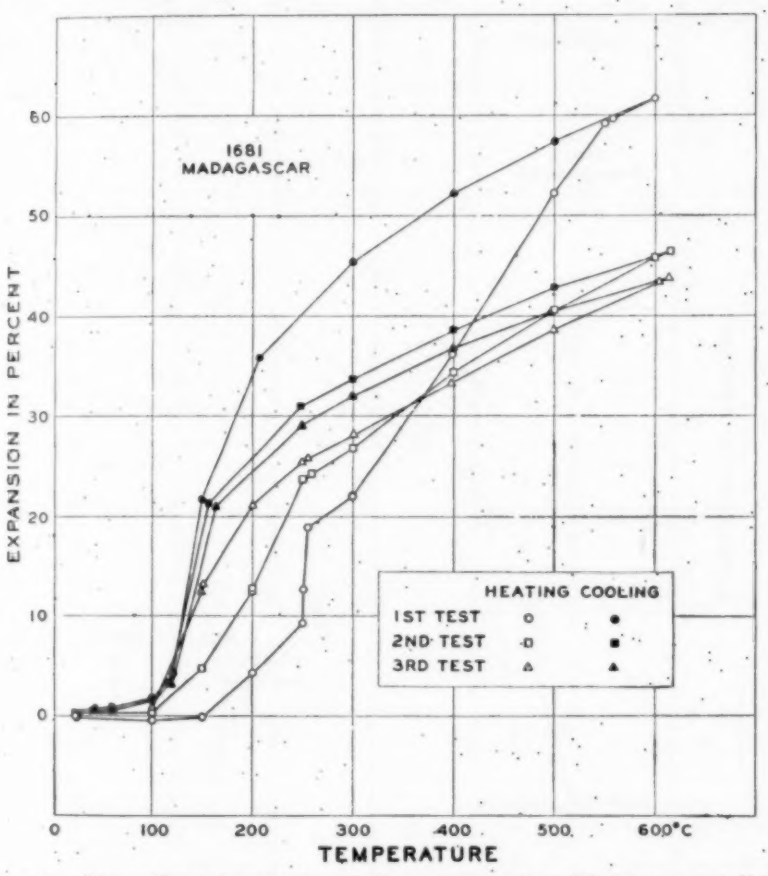

FIGURE 6.—*Linear thermal expansion of phlogopite mica from Madagascar (80 disks, sample 1681) in a direction perpendicular to the cleavage plane when subjected to a load of 30 lb/in.²*

The expansion curves of phlogopite samples 1709 (fig. 10) and 1710 (fig. 11) do not resemble the curves for any of the other phlogopite micas. Both samples exhibited large shrinkage when heated above 500° or 600° C during the first heating under a load of 30 lb/in².

The expansion curves of four samples of biotite micas are shown in figures 16 to 19, inclusive. These curves are irreversible on the heating and cooling cycles.

A shrinkage of 0.4 percent occurred when the biotite sample 1713 from Newdale, N. C. (fig. 16) was maintained in the thermal-expansion

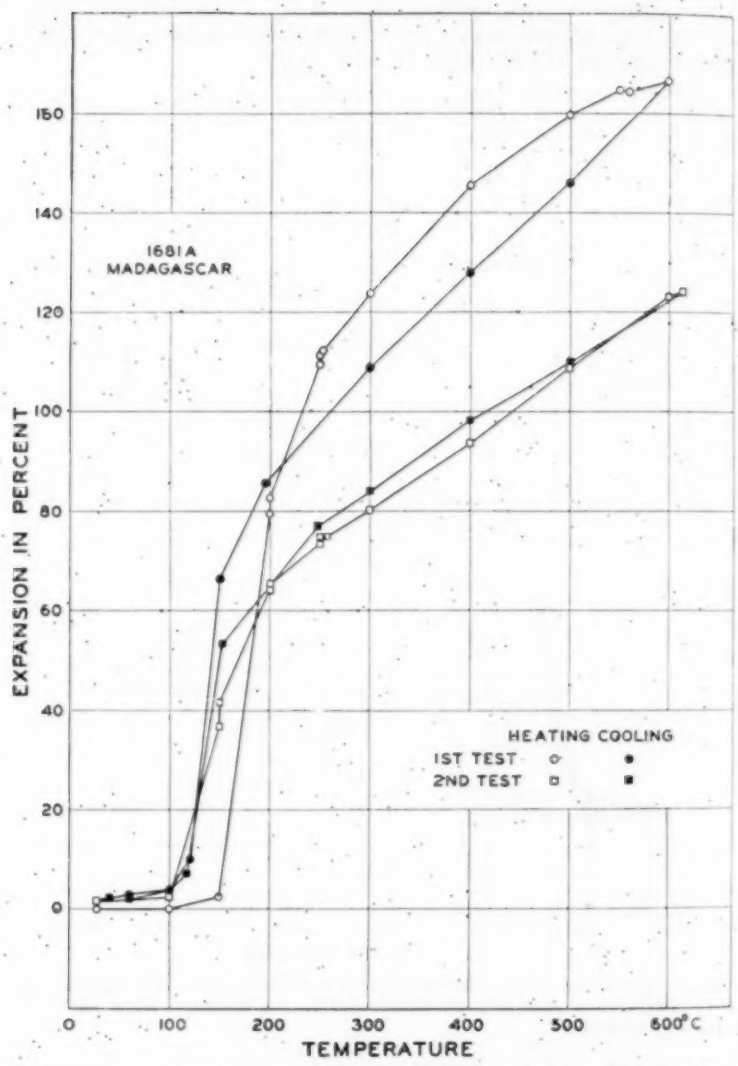

FIGURE 7.—*Linear thermal expansion of phlogopite mica from Madagascar (one disk, sample 1681A from same lot as sample 1681, fig. 6) in a direction perpendicular to the cleavage plane when subjected to a load of 30 lb/in.²*

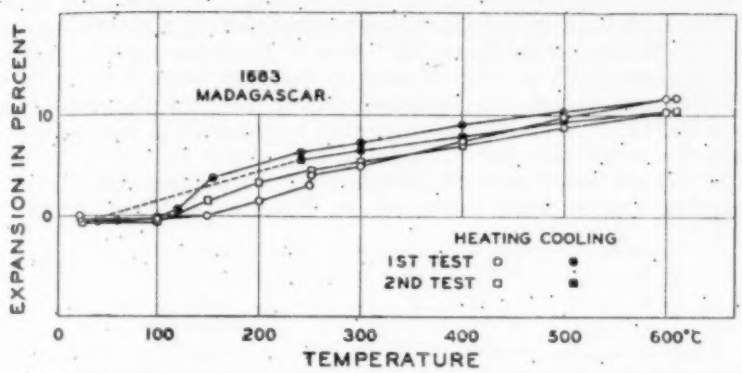

FIGURE 8.—*Linear thermal expansion of a sample of phlogopite mica from Madagascar in a direction perpendicular to the cleavage plane when subjected to a load of 30 lb/in.*[2]

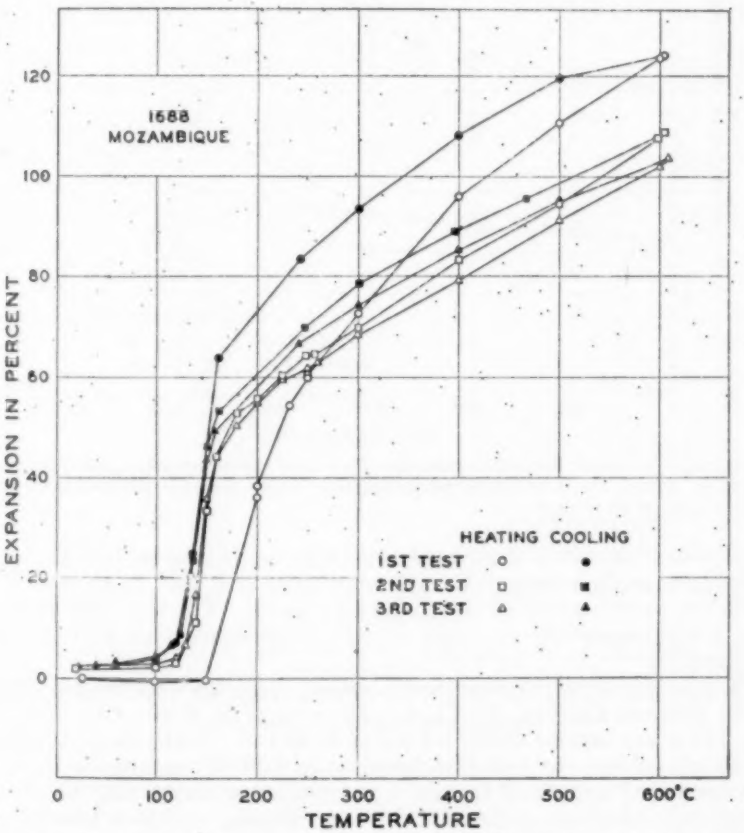

FIGURE 9.—*Linear thermal expansion of a sample of phlogopite mica from Mozambique, Africa, in a direction perpendicular to the cleavage plane when subjected to a load of 30 lb/in.*[2]

apparatus at room temperature under a load of 30 lb/in.^{2} for 22 hours. Further shrinkage of 0.4 percent occurred during the first heating to 150° C. When heated from 150° to 600° C, the sample expanded 11 percent from 150° to 500° C and 41 percent from 500° to 600° C. Moisture was noted on the fused-quartz tube of the apparatus at about 600° C.[10] The curve for cooling below 500° C lies considerably above the expansion curve. At the end of the first test, the length of the sample was 3 percent greater than its original length. Similar expansion curves were obtained on repeated heating, except that

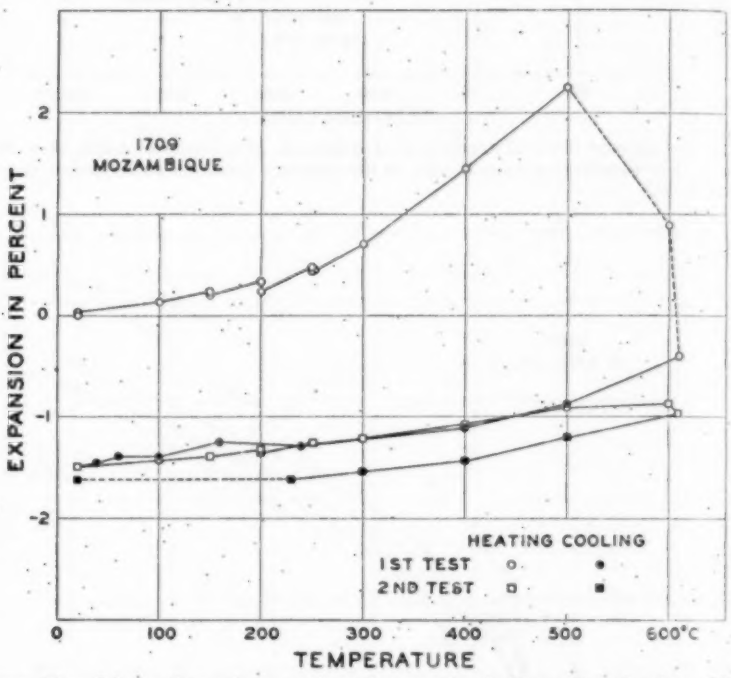

FIGURE 10.—*Linear thermal expansion of a sample of phlogopite mica from Mozambique, Africa, in a direction perpendicular to the cleavage plane when subjected to a load of 30 lb/in.*^{2}

expansion instead of shrinkage occurred on heating to 150° C, and the total expansion between room temperature and 600° C decreased with each successive cycle of heating and cooling. On the sixth heating,[11] the total expansion between room temperature and 600° C was 6 percent.

Somewhat similar curves were obtained for the two biotite samples, 1733 (Macon County, N. C., fig. 18) and 1734 (Oxford County, Me., fig. 19) when heated under a load of 30 lb/in.^{2} Both samples indicated small shrinkage for the first heating to 200° C, moderate expansion between 200° and 550° C, and high expansion above 550° C. Sample 1734 expanded more than 60 percent during the first heating from

[10] Moisture was also noted at higher temperatures during the sixth heating.

[11] After the sixth test, the color of some of the biotite mica disks of sample 1713 was found to have changed from black to a golden copper color.

550° to about 665° C. A shrinkage amounting to more than 20 percent occurred during further heating of this sample from 665° to 700° C. The length of sample 1734 after the first heating and cooling cycle was 6 percent greater than the original length. The maximum expansion of each sample during the second heating was less than that observed in the first heating.

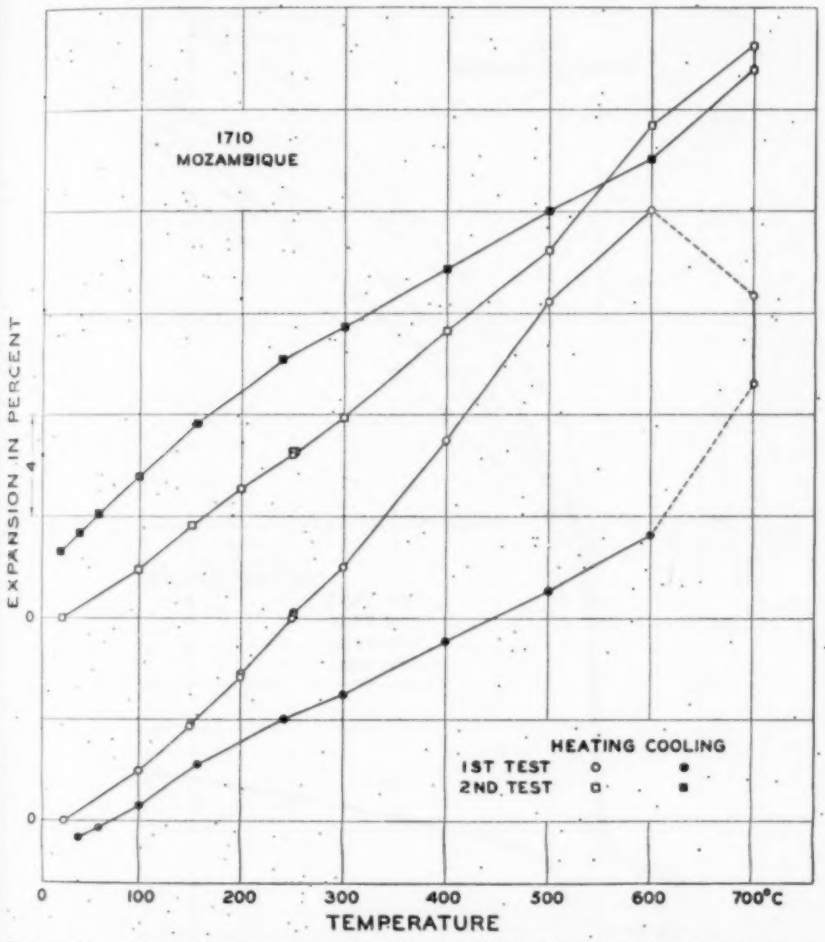

FIGURE 11.—*Linear thermal expansion of a sample of phlogopite mica from Mozambique, Africa, in a direction perpendicular to the cleavage plane when subjected to a load of 30 lb/in.² during the first test and 1 lb/in.² during the second test.*

The tests were plotted from different origins.

The expansion curve of biotite sample 1730 from Ontario, Canada (fig. 17) is different from the curves for the three biotite samples of the United States. A shrinkage of 0.4 percent occurred during the first heating to 250° C with a load of 30 lb/in.², and then an expansion of only 0.8 percent when heated from 250° to 700° C. When cooled from 700° C to room temperature the sample contracted 1.7 percent.

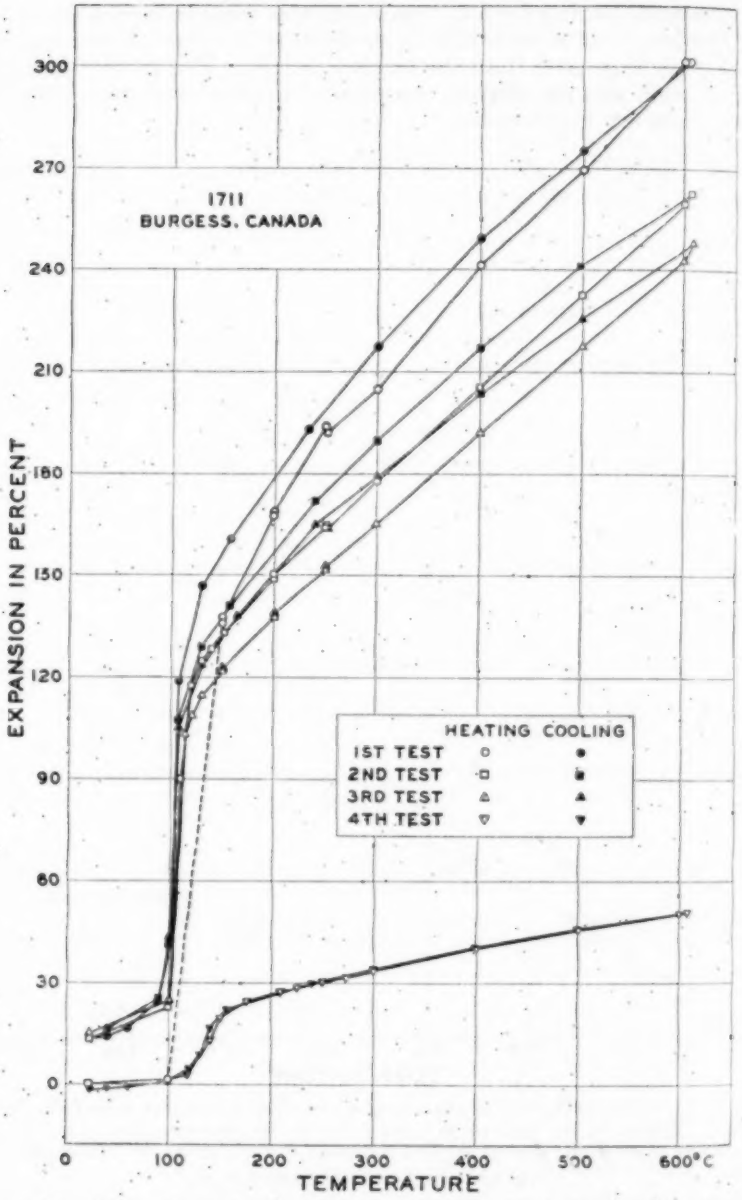

FIGURE 12.—*Linear thermal expansion of a sample of phlogopite mica from Burgess, Canada, in a direction perpendicular to the cleavage plane when subjected to a load of 1 lb/in.² during the first, second, and third tests and 30 lb/in.² during the fourth test.*

The fourth test was plotted from the same origin as the first test.

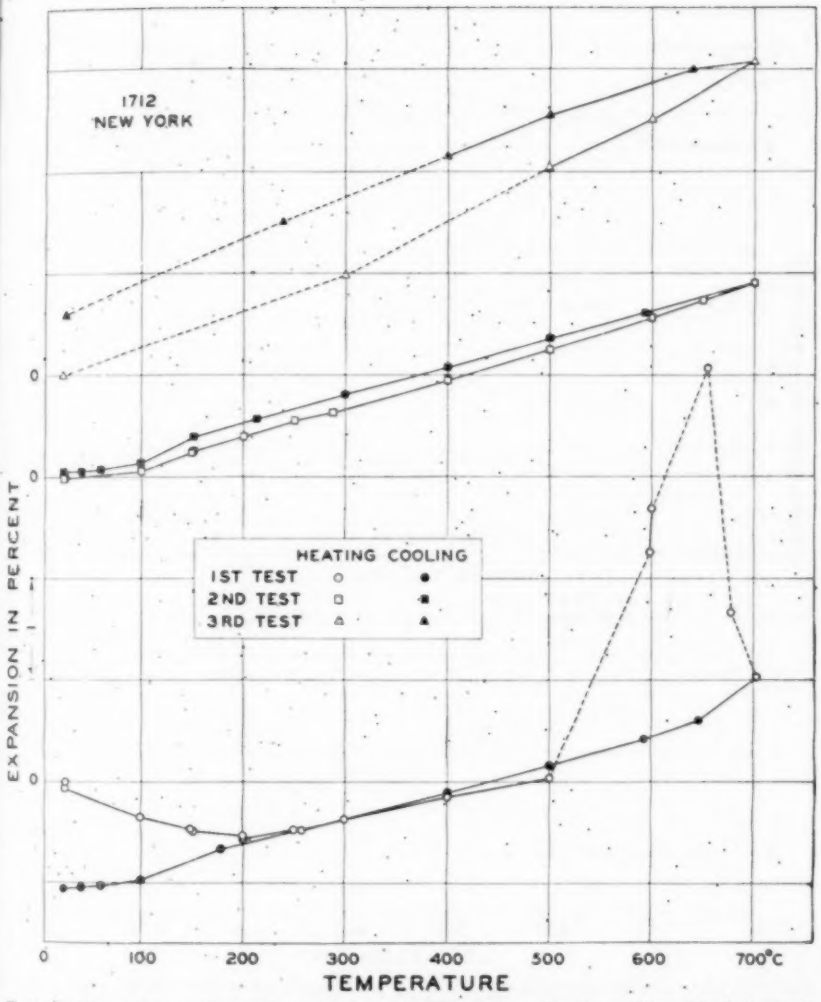

FIGURE 13.—*Linear thermal expansion of phlogopite mica from New York (sample 1712) in a direction perpendicular to the cleavage plane when subjected to loads of 30, 10, and 1 lb/in². during the first, second, and third tests, respectively.*

The tests were plotted from different origins.

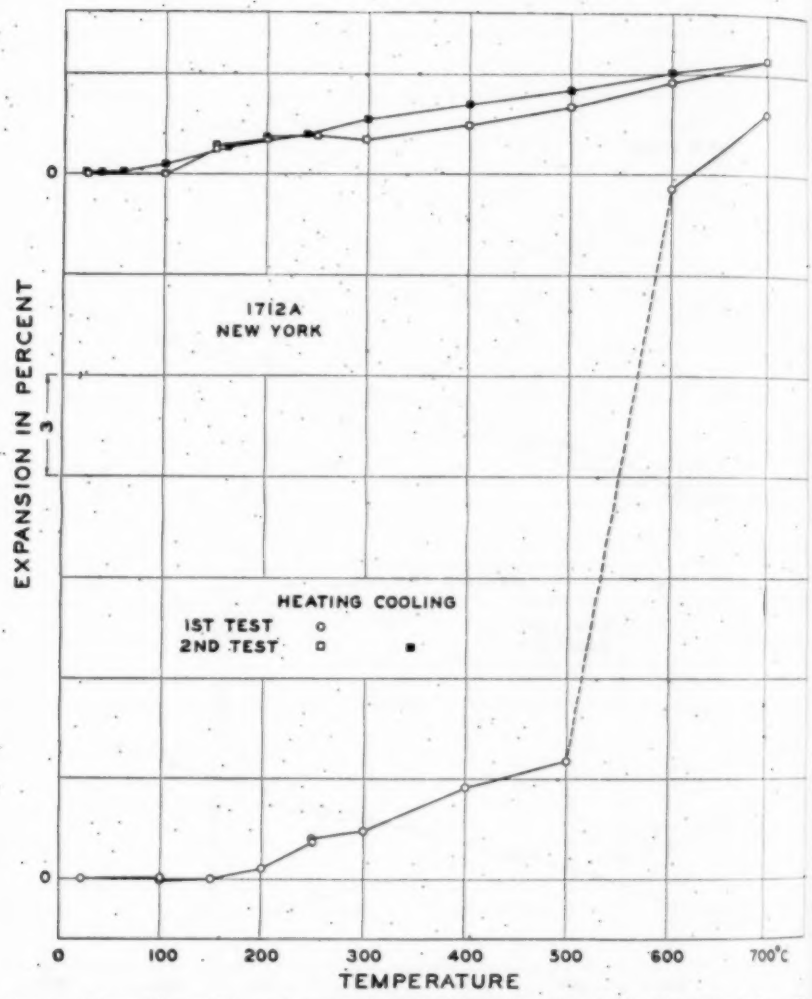

FIGURE 14.—*Linear thermal expansion of phlogopite mica from New York (sample 1712A, from same lot as sample 1712, fig. 13) in a direction perpendicular to the cleavage plane when subjected to a load of 1 lb/in². during the first and second tests.*

The tests were plotted from different origins.

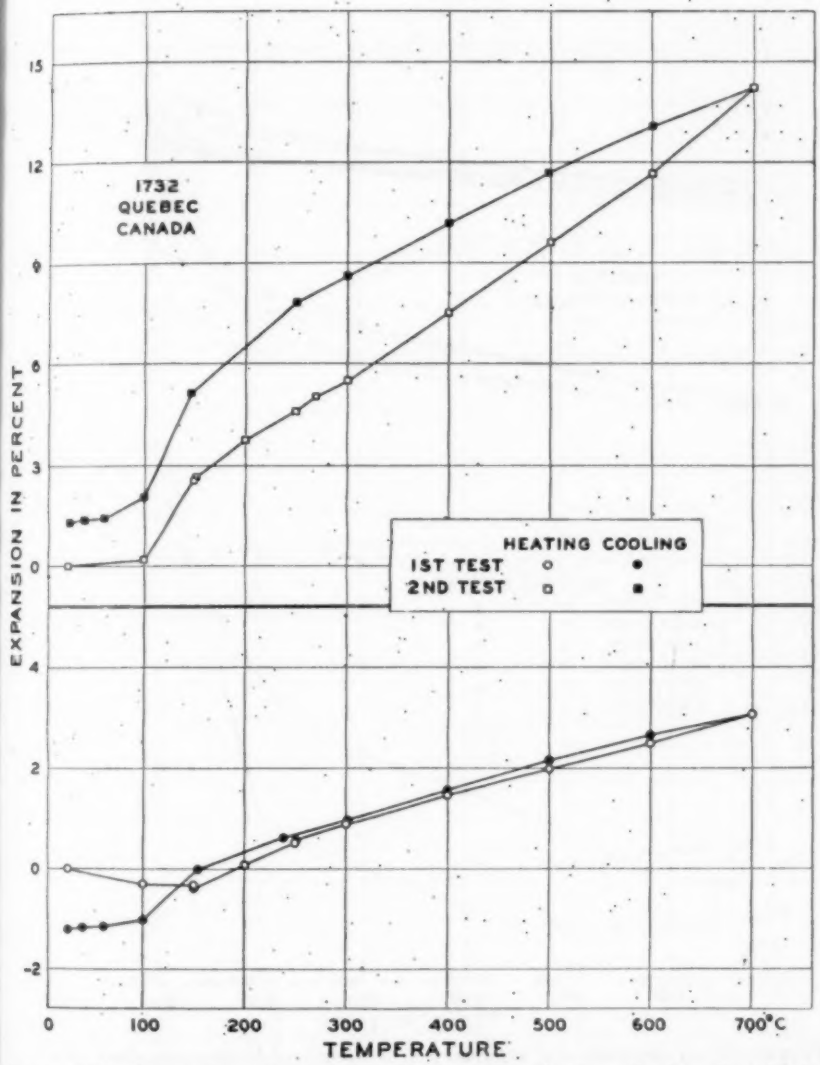

FIGURE 15.—*Linear thermal expansion of phlogopite mica from Quebec, Canada, in a direction perpendicular to the cleavage plane when subjected to loads of 30 and 1 lb/in², during the first and second tests, respectively.*

The tests were plotted from different origins.

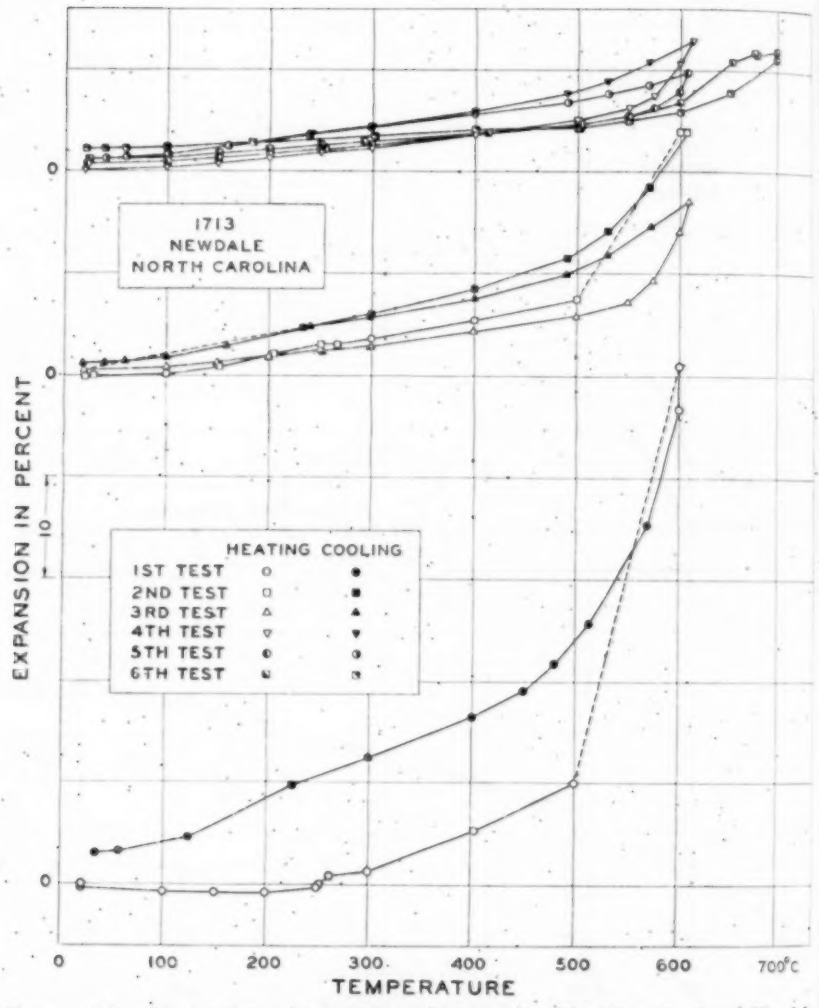

FIGURE 16.—*Linear thermal expansion of a sample of biotite mica from Newdale, North Carolina, in a direction perpendicular to the cleavage plane when subjected to a load of 30 lb/in².*

Tests 1, 2, and 4 were plotted from different origins.

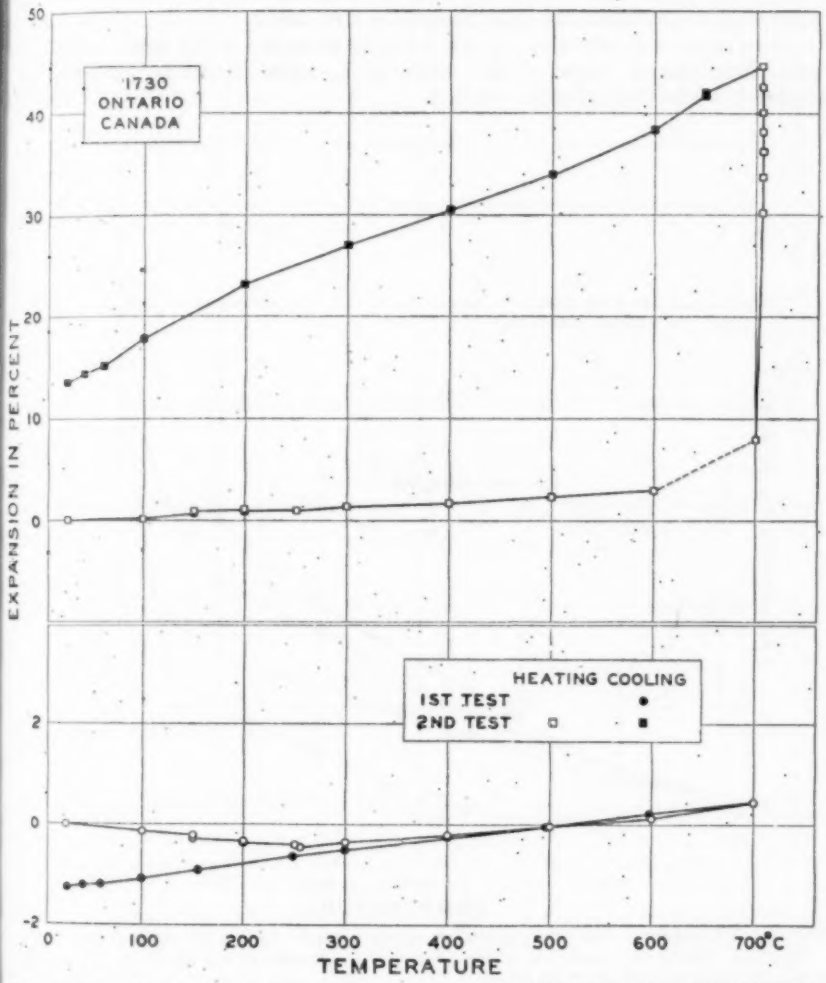

FIGURE 17.—*Linear thermal expansion of a sample of biotite mica from Ontario, Canada, in a direction perpendicular to the cleavage plane when subjected to loads of 30 and 1 lb/in². during the first and second tests, respectively.*

The tests were plotted from different origins.

During the second heating and cooling cycle, the sample was subjected to a load of only 1 lb/in.^{2} The expansion was 3 percent from 20° to 600° C. At about 700° C, the sample expanded considerably (about 36 percent). The curve obtained during cooling lies considerably above the expansion curve. The length after the second test was 14 percent greater than the length before this test.

After the expansion tests on biotite samples 1733 and 1730, the outer laminas of some of the mica disks were found to be partially separated and wrinkled or curled.

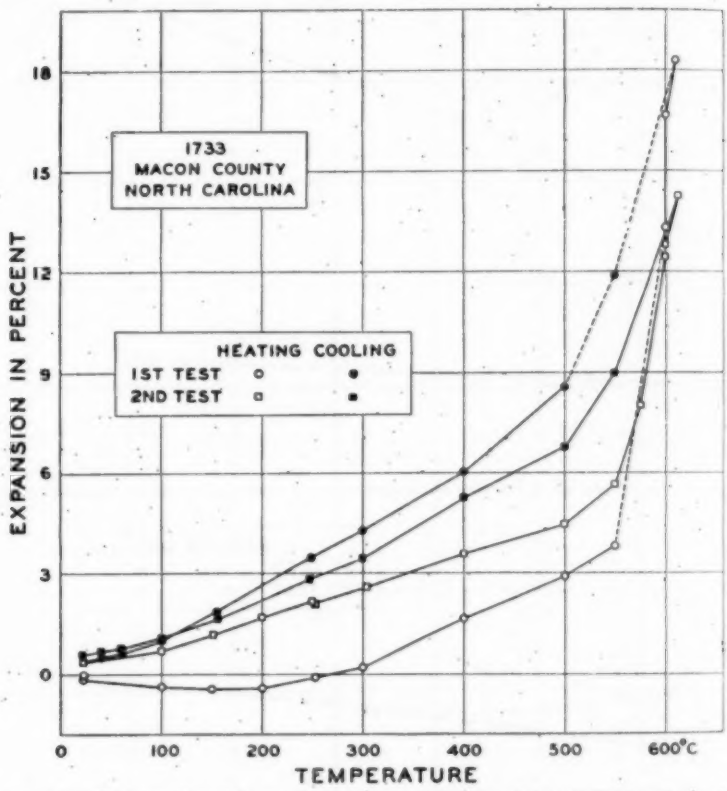

FIGURE 18.—*Linear thermal expansion of a sample of biotite mica from Macon County, North Carolina, in a direction perpendicular to the cleavage plane when subjected to a load of 30 lb/in^2.*

Figure 20 shows the results obtained on a sample of ripidolite mica from Pennsylvania that was subjected to a load of 30 lb/in.^{2} during two cycles of heating and cooling. The sample indicated shrinkage during the first heating from 20° to 700° C. At 100°, 150°, 200°, and 250° C, shrinkage was noted when the sample was held at constant temperature for one-half hour or longer. The large shrinkage indicated on the curve at about 250° C occurred during a period of 17 hours. The shrinkage of the sample when heated from 20° to 700° C was 5 percent. When cooled from 700° to 20° C the sample contracted regularly. The total contraction for this temperature

range was 0.8 percent. During the second heating and cooling cycle, the sample expanded and contracted, respectively, in a regular manner. The expansion for the second heating from 20° to 700° C was only 0.5 percent.

The results obtained on a sample of zinnwaldite mica subjected to a load of 30 lb/in.[2] during two cycles of heating and cooling are shown in figure 21. Shrinkage was noted when the sample was heated to 250° C. A slight shrinkage occurred at 250° C when the sample was kept at constant temperature for 17 hours. When heated from 250°

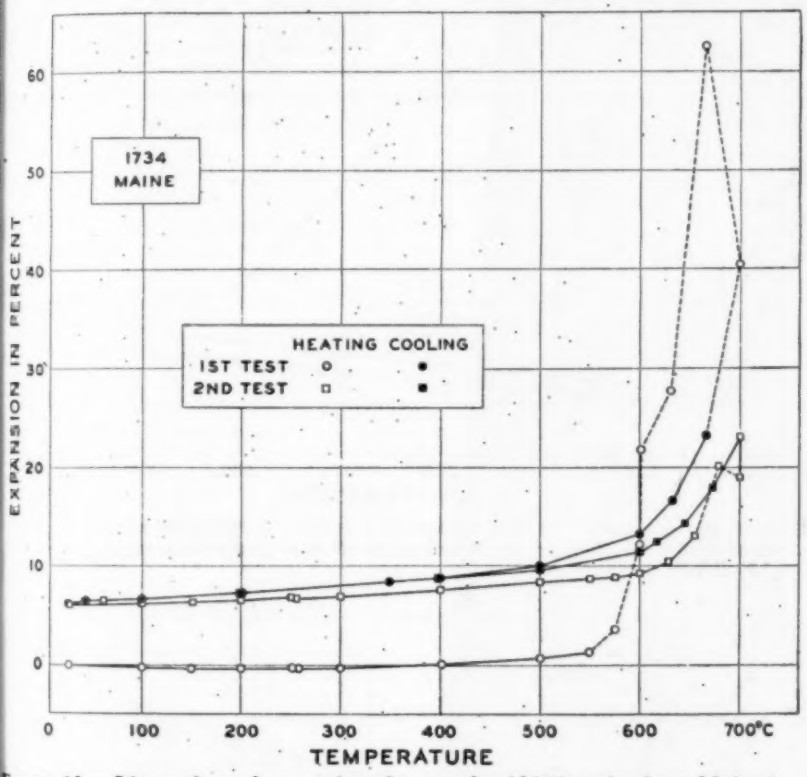

FIGURE 19.—*Linear thermal expansion of a sample of biotite mica from Maine in a direction perpendicular to the cleavage plane when subjected to a load of 30 lb/in*[2].

to 700° C, the sample expanded 1.1 percent. An increase in the rate of expansion was noted between 600° and 700° C. The contraction during cooling from 700° to 20° C was 1.8 percent. Expansion occurred throughout the range during the second heating from 20° to 700° C. An increase in the rate of expansion also occurred between 600° and 700° C. An expansion of 0.1 percent was noted when the sample was maintained at 700° C for 10 minutes. The latter observation, and the fact that the rate of expansion increased between 600° and 700° C, indicate the probable existence of a transition in the neighborhood of 700° C[12].

[12] Expansion measurements were terminated at 700° C in order to avoid the danger of the mica disks fusing to the fused-quartz parts of the apparatus.

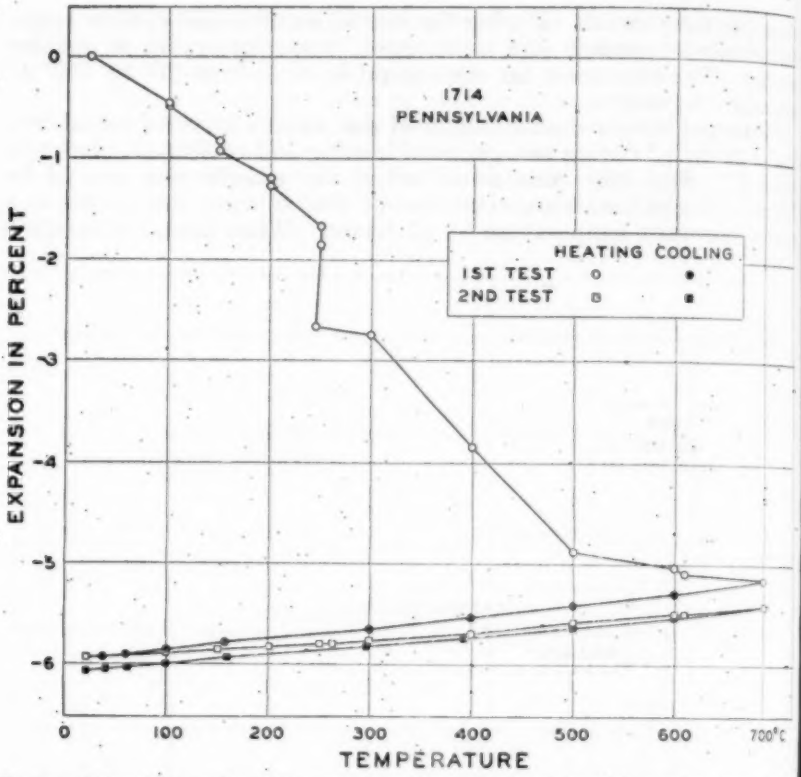

FIGURE 20.—*Linear thermal expansion of a sample of ripidolite mica from Pennsylvania in a direction perpendicular to the cleavage plane when subjected to a load of 30 lb/in².*

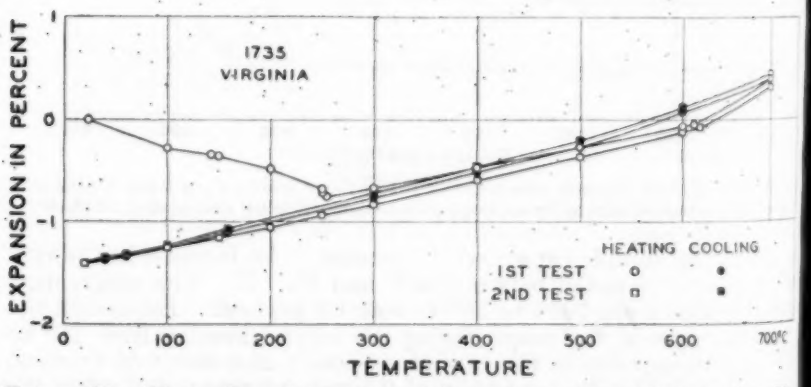

FIGURE 21.—*Linear thermal expansion of a sample of zinnwaldite mica from Virginia in a direction perpendicular to the cleavage plane when subjected to a load of 30 lb/in².*

Table 2 gives average coefficients of expansion and coefficients of contraction of the samples of mica that were computed from the data plotted in figures 1 to 21, inclusive. The table also shows the changes in length of the samples after they were heated and cooled. Most of the coefficients of the samples of phlogopite and biotite micas are extraordinarily high. The maximum coefficients of expansion of these two types of mica are 0.0552 and 0.00411 per degree centigrade, respectively. The coefficients of expansion of the samples of muscovite, ripidolite, and zinnwaldite micas are comparatively low. The maximum coefficient of expansion of these three types of mica is 0.000036 per degree centigrade. In most cases when the load perpendicular to the cleavage plane of samples of phlogopite and biotite micas was decreased, the coefficients of expansion and contraction increased. Conversely, by applying heavier loads to these micas, it is possible to reduce the expansion.

TABLE 2.—*Coefficients of expansion[a] of mica in a direction perpendicular to cleavage plane*

Sample No.	Source	Test	Load perpendicular to cleavage plane of sample	Average coefficients of expansion per degree centigrade		Average coefficients of contraction per degree centigrade		Change in length after heating and cooling[b]
				20° to 300° C	300° to 600° C	600° to 300° C	300° to 20° C	
A. MUSCOVITE MICA								
			lb/in.²	$\times 10^{-6}$	$\times 10^{-6}$	$\times 10^{-6}$	$\times 10^{-6}$	*Percent*
1682	Brazil	1	30	8	9	23	20	−0.8
		2	30	17	24	23	20	−.0
1684	Canada	1	30	(c)	(c)	28	33	−2.8
		2	30	21	34	29	31	−.1
1685	Brazil	1	30	(c)	(c)	20	16	−2.2
		2	30	15	18	19	16	−.0
1686	do	1	30	(c)	(c)	19	16	−1.7
		2	30	15	18	(d)	(d)	−.0
1687	Plate mica (processed sheet supplied by New England Mica Co.).	1	30	(c)	(c)	(c)	16	−5.0
		2	30	15	(f)	(e)		+1.3
1689	Los Volcansillos Mine, Guatemala	1	30	(c)	15	27	23	−1.4
		2	30	21	28	28	24	+.0
1692	Durania Section, Colombia	1	30	(c)	(b)	21	18	−1.8
		2	30	16	21	22	17	−.0
1695	Near Camana, Ferreyros, Peru	1	30	(c)	(c)	17	15	−2.1
		2	30	14	17	18	13	−.0
1696	Amber Mine, Concepcion Area, Depto. Santa Cruz, Bolivia.	1	30	(c)	22	34	29	−1.2
		2	30	25	36	37	31	+.0
1699	New Hampshire	1	30	(c)	(c)	18	13	−2.0
		2	30	13	16	17	13	−.0
1701	Old Mike Mine, 4½ miles north of Custer, S. Dak.	1	30	(c)	(c)	18	13	−2.0
		2	30	13	16	18		
1703	Mill Race Mine, Avery County, N. C.	1	30	(c)	(c)	21	15	−2.3
		2	30	16	20	21	17	−.0
1705	Sink Hole Mine, near Bandana, Mitchell County, N. C.	1	30	(c)	(c)	21	13	−2.9
		2	30	13	18	20	13	−.1
1707	Petaca Area, N. Mex	1	30	(c)	(c)	19	13	−2.2
		2	30	13	17	18	13	−.1

See footnotes at end of table.

TABLE 2.—*Coefficients of expansion[a] of mica in a direction perpendicular to cleavage plane*—Continued

Sample No.	Source	Test	Load perpendicular to cleavage plane of sample	Temperature range	Average coefficient of expansion per degree centigrade	Average coefficient of contraction per degree centigrade	Change in length after heating and cooling[b]
					B. PHLOGOPITE MICA		
			lb/in.²	*° C*			*Percent*
				150 to 255	0.00182		
				300 to 550	.00149		
		1	30	600 to 300		0.000546	+0.1
				207 to 122		.00372	
				100 to 24		.000164	
				22 to 100	.000026		
				100 to 250	.00153		
				300 to 600	.000632		
1681	Madagascar	2	30	615 to 300		.000404	+.2
				300 to 157		.000864	
				157 to 117		.00462	
				100 to 22		.000138	
				22 to 100	.000051		
				100 to 200	.00202		
				200 to 302	.000688		
		3	30	302 to 604	.000504		−.1
				614 to 299		.000375	
				299 to 163		.000810	
				163 to 120		.00414	
				100 to 22		.000121	
				27 to 100	.000001		
				150 to 200	.0157		
				200 to 300	.00426		
		1	30	300 to 500	.00180		+1.8
				600 to 300		.00192	
				300 to 195		.00223	
				150 to 121		.0198	
1681A	Madagascar			100 to 26		.000289	
				26 to 100	.000097		
				100 to 150	.00729		
				200 to 300	.00152		
		2	30	300 to 600	.00143		.0
				614 to 300		.00128	
				300 to 153		.00207	
				153 to 117		.0130	
				100 to 29		.000299	
				100 to 200	.000178		
				300 to 600	.000223		
		1	30	611 to 300		.000141	−.1
				300 to 155		.000248	
				155 to 120		.000870	
1683	Madagascar			100 to 25		.000067	
				25 to 100	.000020		
		2	30	100 to 300	.000293		−.1
				300 to 600	.000166		
				611 to 300		.000127	
				150 to 200	.00752		
				200 to 300	.00343		
		1	30	300 to 600	.00170		+1.9
				605 to 300		.00100	
				162 to 120		.0136	
				100 to 25		.000261	
				22 to 100	.000059		
				120 to 180	.00834		
				200 to 300	.00143		
1688	Mozambique, Africa	2	30	300 to 598	.00126		+.1
				606 to 301		.000995	
				301 to 162		.00182	
				162 to 125		.0120	
				100 to 23		.000222	
				23 to 100	.000092		
				120 to 160	.00995		
				200 to 300	.00135		
		3	30	300 to 600	.00112		+.1
				609 to 300		.000941	
				300 to 159		.00178	
				159 to 125		.0119	
				100 to 21		.000224	

See footnotes at end of table.

TABLE 2.—*Coefficients of expansion[a] of mica in a direction perpendicular to cleavage plane*—Continued

Sample No.	Source	Test	Load perpendicular to cleavage plane of sample	Temperature range	Average coefficient of expansion per degree centigrade	Average coefficient of contraction per degree centigrade	Change in length after heating and cooling[b]
	B. PHLOGOPITE MICA—Continued						
			lb/in.²	*° C*			*Percent*
1709	Mozambique, Africa	1	30	19 to 99	0.000013		−1.5
				300 to 500	.000077		
				611 to 300		.000026	
		2	30	20 to 300	.000010		−.1
				300 to 600	.000012		
				609 to 300		.000019	
				300 to 20		.000003	
1710	Mozambique, Africa	1	30	24 to 300	.000362		−1.1
				300 to 600	.000468		
				600 to 300		.000210	
				300 to 40		.000217	
		2	1	22 to 300	.000283		+2.6
				300 to 600	.000384		
				600 to 300		.000220	
				300 to 21		.000318	
1711	Burgess, Canada	1	1	22 to 100	.000167		+13.3
				100 to 150	.0272		
				300 to 600	.00322		
				607 to 300		.00275	
				300 to 158		.00397	
				107 to 90		.0548	
				90 to 22		.00165	
		2	1	22 to 100	.00121		+1.3
				100 to 120	.0478		
				200 to 300	.00276		
				300 to 600	.00273		
				608 to 300		.00237	
				300 to 157		.00341	
				107 to 90		.0476	
				90 to 22		.00154	
		3	1	22 to 100	.00127		+.2
				100 to 114	.0552		
				300 to 600	.00259		
				610 to 300		.00222	
				300 to 164		.00300	
				108 to 90		.0457	
				90 to 22		.00157	
		4	30	22 to 100	.000179		−1.6
				119 to 151	.00522		
				210 to 300	.000666		
				300 to 600	.000570		
				608 to 300		.000543	
				300 to 157		.000830	
				140 to 120		.00614	
				100 to 22		.000337	
1712	St. Lawrence County, N. Y.	1	30	200 to 300	.000048		−1.1
				300 to 500	.000020		
				593 to 300		.000027	
				100 to 22		.000012	
		2	10	21 to 288	.000024		+.1
				288 to 600	.000030		
				593 to 300		.000027	
				300 to 21		.000027	
		3	1	21 to 300	.000035		+.6
				300 to 600	.000051		
				500 to 23		.000041	
1712A	St. Lawrence County, N. Y.	1	1	300 to 500	.000104		
		2	1	23 to 100	−.000002		+.1
				298 to 600	+.000057		
				600 to 300		.000046	
				300 to 23		.000057	
1732	St. Lawrence Mica Co. Mine, Petit Pré., Quebec, Canada.	1	30	150 to 300	.000083		−1.2
				300 to 600	.000054		
				600 to 301		.000057	
				100 to 22		.000025	
		2	1	22 to 100	.000023		+1.3
				200 to 301	.000176		
				301 to 601	.000206		
				600 to 300		.000149	
				100 to 23		.000098	

See footnotes at end of table.

TABLE 2.—*Coefficients of expansion[a] of mica in a direction perpendicular to cleavage plane*—Continued

Sample No.	Source	Test	Load perpendicular to cleavage plane of sample	Temperature range	Average coefficient of expansion per degree centigrade	Average coefficient of contraction per degree centigrade	Change in length after heating and cooling[b]
				C. BIOTITE MICA			
			lb/in.[2]	*°C*			*Percent*
		1	30	100 to 200	0.000000		
				300 to 500	.000434		
				500 to 600	.00411		
				600 to 450		0.00184	+2.0
				450 to 300		.000441	
				300 to 34		.000357	
		2	30	21 to 300	.000130		
				300 to 500	.000198		
				500 to 600	.00164		
				608 to 490		.00105	+.6
				490 to 300		.000293	
				300 to 20		.000195	
		3	30	20 to 300	.000081		
				300 to 500	.000153		
				500 to 600	.000830		
				609 to 490		.000609	+.6
				490 to 299		.000225	
1713	E. Blake Mine, Newdale, N. C.			299 to 19		.000161	
		4	30	19 to 300	.000079		
				300 to 500	.000136		
				500 to 600	.000567		
				613 to 490		.000427	+.7
				490 to 300		.000171	
				300 to 22		.000131	
		5	30	22 to 300	.000064		
				300 to 504	.000103		
				504 to 600	.000337		
				608 to 490		.000251	+.3
				490 to 300		.000131	
				300 to 21		.000111	
		6	30	22 to 293	.000063		
				293 to 500	.000086		
				500 to 600	.000220		
				600 to 700	.000511		
				700 to 600		.000534	+1.0
				600 to 500		.000135	
				500 to 300		.000055	
				300 to 21		.000044	
		1	30	300 to 600	.000016		
				600 to 700	.000032		
				700 to 300		.000024	−1.3
1730	Faraday Twp., Hastings Co., Ontario, Canada.			300 to 23		.000027	
		2	1	22 to 300	.000049		
				300 to 600	.000055		
				600 to 700	.000496		+11.1
				706 to 301		.000435	
				301 to 22		.000485	
		1	30	200 to 300	.000063		
				300 to 550	.000144		
				550 to 610	.00244		
				610 to 550		.00107	+.6
				550 to 500		.000669	
				500 to 300		.000215	
1733	Ledford Cove Mica Mine, Macon County, N. C.			300 to 22		.000141	
		2	30	22 to 304	.000079		
				304 to 500	.000095		
				500 to 550	.000238		
				550 to 613	.00136		
				613 to 550		.000830	+.2
				550 to 500		.000446	
				500 to 300		.000166	
				300 to 22		.000102	
		1	30	22 to 300	−.000008		
				300 to 550	+.000061		
				550 to 601	.00403		+6.1
				600 to 348		.000190	
1734	Saunders Quarry, Oxford County, Maine.			348 to 23		.000071	
		2	30	23 to 300	.000030		
				300 to 600	.000078		
				600 to 399		.000133	+.2
				399 to 198		.000065	
				198 to 20		.000062	

See footnotes at end of table.

TABLE 2.—*Coefficients of expansion[a] of mica in a direction perpendicular to cleavage plane*—Continued

Sample No.	Source	Test	Load perpendicular to cleavage plane of sample	Temperature range	Average coefficient of expansion per degree centigrade	Average coefficient of contraction per degree centigrade	Change in length after heating and cooling[b]
			lb/in.[2]	°C	×10⁻⁶	×10⁻⁶	*Percent*
	D. RIPIDOLITE MICA						
1714	Three miles south of Westchester, Pa.	1	30	700 to 300		12	−5.9
				300 to 21		11	
		2	30	21 to 300	6		−.1
				300 to 700	9		
				700 to 296		10	
				296 to 22		9	
	E. ZINNWALDITE MICA						
1735	Morefield Mine, Amelia, Va.	1	30	300 to 600	20		−1.4
				700 to 300		29	
				300 to 21		23	
		2	30	21 to 300	21		+.0
				300 to 600	23		
				700 to 300		29	
				300 to 22		24	

[a] In parts A, D, and E of the table, each coefficient of expansion is expressed in the usual way as a whole number multiplied by 10^{-6}. However, in parts B and C, where most of the coefficients are extremely large, they are expressed as decimal fractions. The first coefficient in part B is 0.00182. If written as in part A, it is 1820×10^{-6}.

[b] Determined from the heating and cooling curves in figures 1 to 21. The plus sign indicates an increase in length and the minus sign a decrease in length.

[c] Sample indicated shrinkage when heated during this temperature range.

[d] Average coefficient of contraction from 600° to 20° C, 18×10^{-6} per degree centigrade.

[e] Average coefficients of contraction from 600° to 500° C and from 500° to 300° C, 177×10^{-6} and 41×10^{-6} per degree centigrade, respectively.

[f] Average coefficients of expansion from 300° to 500° C and from 500° to 600° C, 22×10^{-6} and 316×10^{-6} per degree centigrade, respectively.

[g] Average coefficient of contraction from 600° to 500° C, 248×10^{-6} per degree centigrade.

[h] Sample indicated shrinkage when heated to 500° C; coefficient of expansion from 500° to 600° C, 10×10^{-6} per degree centigrade.

[i] Sample indicated shrinkage when heated to 400° C; coefficient of expansion from 400° to 600° C, 10×10^{-6} per degree centigrade.

Megaw [10] and Wood [11] reported data on the linear thermal expansion of mica in a direction perpendicular to the cleavage plane. Their results and those given by other observers on the linear thermal expansion of mica in a direction parallel to the cleavage plane are given in table 3. This table also includes data on the linear thermal expansion of pulverized mica, rods prepared from pulverized mica, and of micanite.

From his X-ray examination of the phlogopite mica specimens used in his determinations of their thermal expansion, Wood [11] found that, in contrast with the usual effect of annealing, the heat treatment of mica may bring about a pronounced mosaic formation without apparent change in external appearance; that this structure is not necessarily stable but may revert appreciably to the initial state during cooling; and that these particular thermal and structural characteristics are interdependent. He concluded that measurements of thermal expansion of the lattice constant perpendicular to the cleavage plane indicate that the transition to the mosaic structure does not,

TABLE 3.—*Coefficients of linear thermal expansion of mica by previous observers*

Observer	Date	Material	Direction in which linear expansion was determined	Temperature range	Average coefficient of expansion per degree centigrade	Remarks
				°C	$\times 10^{-6}$	
Braesco [12, 13]	1913 & 1920	Rod of pulverized mica agglomerated with sodium silicate and water.	Along axis of rod			Observed regular expansion up to about 900°C. No quantitative data were reported.
Souder and Sweeney [14]	1925	Micanite (layers of mica stuck together with shellac. About 5 percent of the weight of the material was shellac.)	Parallel to cleavage plane	18 to 80	8.9	
Ebert [15]	1927	Mica	do	−253 to −190	2.4	Coefficients of expansion computed by Hidnert and Dickson from data by Ebert.
				−190 to 0	6.3	
				0 to +100	9.0	
				+100 to 250	9.0	
				250 to 500	11.0	
Ebert [16]	1928	Mica, ruby	do	−253 to −190	2.4	Coefficients of expansion computed by Hidnert and Dickson from data by Ebert who stated that his values are accurate to about 5 percent.
				−190 to 0	6.3	
				0 to +100	9.0	
				+100 to 250	9.5	
				250 to 500	11.3	
Heindl [17]	1932	Pulverized muscovite mica heated to 1,225°C.	No definite direction	20 to 100	7.0	Three small tetrahedra were used for the sample of material for determination of linear expansion by interference method. The coefficient of expansion from 20° to 100°C was obtained from unpublished data.
				20 to 900	8.3	
Megaw [10]	1933	Flake of phlogopite mica from Ceylon.	Perpendicular to cleavage plane.	20 to 100	14.9	Used X-ray method. Probable error of coefficient of expansion, $\pm 1.5 \times 10^{-6}$.
Ebert [18]	1935	Phlogopite mica	Parallel to cleavage plane	0 to 100	13.5	Coefficients of expansion computed by Hidnert and Dickson from data by Ebert who stated that the accuracy of his values is 1 to 2 percent.
				100 to 200	13.5	
				200 to 300	14.5	
				300 to 400	14.5	
				400 to 500	13.0	
		Muscovite mica	do	0 to 100	8.5	
				100 to 200	8.0	
				200 to 300	10.0	
				300 to 400	12.0	
				400 to 500	12.0	
Wood [11]	1937	Four specimens of Canadian phlogopite mica (dark, medium, and light).	Perpendicular to cleavage plane.	20 to 400	16.2 to 18.3	Used X-ray method. Expansion curves between room temperature and 400°C are smooth, and the points obtained in the rising and falling halves of the cycle lie on the same curve.
Hicks and Fan-Yi Wei [19]	1939	Rod prepared from pulverized muscovite mica.	Along axis of rod	100 to 600	12	Derived from expansion curve published by Hicks and Fan-Yi Wei. They reported a contraction from about 600° to 680°C.
				600 to 880	35	

however, affect the perfection of atomic arrangement in the individual crystallites and that no chemical changes are involved.

The term "thermal expansion" as used by the present authors for the micas they investigated represents the thermal expansion of the laminas of one or more disks of mica in a direction perpendicular to the cleavage plane plus the displacements or separations between the laminas during heating or cooling.

2. CHANGES IN STRUCTURE

By H. C. Vacher [13]

The expansion and contraction curves of some phlogopite micas (figs. 6, 7, 9, and 12) suggested that changes in structure occurred between 100° and 250° C. No such change in this temperature range was indicated for the muscovite micas or for the biotite micas. The curves for the first heating-cooling cycle for biotite micas from North Carolina and Maine (figs. 16, 18, and 19) are very steep between 500° and 600° C (or 700° C), but for successive cycles the steep portion is less pronounced. This indicated that a change in the structure of these biotite micas was initiated between 500° and 600° C, which became more complete after each cycle.

In determining the coefficient of thermal expansion for the crystal lattice of Canadian phlogopite with an X-ray spectrometer, Wood [11] found that the lattice expansion and contraction perpendicular to the cleavage plane was uniform and followed the same curve between 18° and 400° C. He showed, however, that the diffraction lines obtained from some samples were considerably more diffuse and broken in the range from 200° to 400° C than in the range from 18° to 200° C. It was concluded that some phlogopite micas form a macromosaic structure when heated above 200° C that incompletely reverts to the initial condition when cooled below 200° C. It is very probable that a change in structure of this nature would be registered on thermal-expansion and contraction curves. In order to determine if this is true for some micas used in the present investigation, Laue diffraction patterns were obtained on some samples (see table 4) at room temperature and at elevated temperatures.

A sketch of the furnace used in obtaining the Laue patterns is shown in figure 22. The furnace was constructed by winding Nichrome wire, 0.020-in. diameter, around asbestos board (⅛ by 1⅜ by 2¾ in.) containing a channel 1/16 in. deep by 1 1/16 in. wide. The mica-disk specimen (⅝-in. diameter) was sandwiched between two aluminum strips (0.045-in. and 0.010-in. thickness) and slid along the channel until it was opposite the pinhole collimator. The primary and diffracted beams passed through holes (⅛-in. and ¼-in. diameter, respectively) in the specimen holder. Aluminum foil (0.002-in. thickness) covered the ¼-in. diameter hole to reduce the temperature gradient. Diffracted beams from crystals in the aluminum foil were registered on the film, but they were easily distinguished by their small size from those diffracted from the mica specimen. The furnace was fastened to the pinhole collimator by means of a flange and aluminum strip. In this position the collimated beam was perpendicular to the cleavage plane of the specimen. The temperature was

[13] Division of Metallurgy, National Bureau of Standards.

determined with a Chromel-Alumel thermocouple that had been previously calibrated to correspond to a thermocouple located adjacent to the specimen and in the path of the collimated beam. Unfiltered radiation from a molybdenum target was used in obtaining the Laue patterns. A pattern was obtained at room temperature, and then the temperature was increased to 100° C and maintained constant to within 15° C. After exposing the film for 4 hours, the temperature was increased to 150° C and another film was exposed for 4 hours. The furnace was cooled after each 4-hour exposure period unless there was sufficient time to obtain a 4-hour exposure at a different temperature during the same day. Table 4 shows the heating-cooling cycles and the temperatures at which patterns were obtained for each specimen of mica.

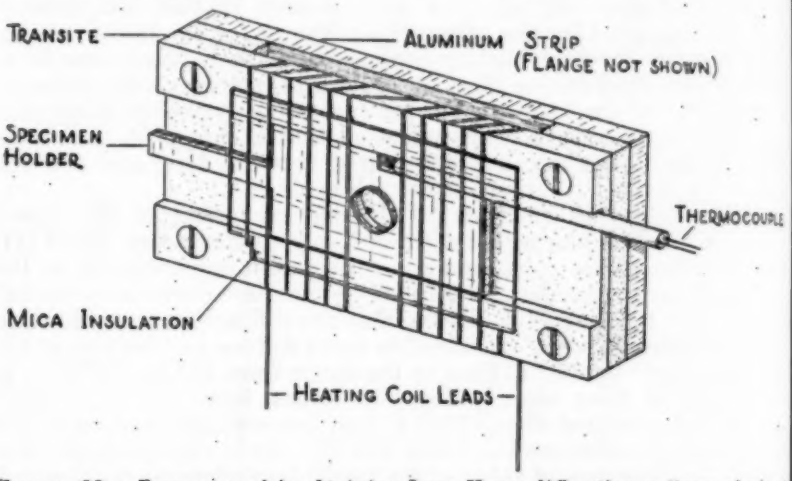

FIGURE 22.—*Furnace used in obtaining Laue X-ray diffraction patterns of mica at elevated temperatures.*

Different micas differed characteristically within the range of temperatures investigated. Figure 23 illustrates the change that occurred in muscovite mica (sample 1682) between 100° and 145° C. The type of pattern (fig. 23, A) obtained at room temperature before and after the heating-cooling cycles, consisted of single diffraction spots, whereas at 145°, 190°, 240°, and 285° C some of the spots were doubled (fig. 23, *B*). The doubling of spots at elevated temperatures cannot always be considered as reversible, for patterns of the type shown in figure 23, *B*, were obtained from other muscovite mica samples in the "as received" condition. Double spots indicate that diffractions were registered from two crystals differing slightly in orientation. It is noteworthy that the double spots are symmetrical to the line of symmetry (*Y*, fig. 23). The thermal-expansion and contraction curves (sample 1682, fig. 1) show no evidence of a transition to correspond to the change in structure that occurred between 100° and 145° C.

Patterns typical of the changes that occurred in some phlogopite micas (samples 1681, 1681A, and 1688) when heated to elevated temperatures are shown in figure 24. Inspection shows that spots in three zone lines (marked *X*, *Y*, and *Z* in fig. 24) intersecting at approx-

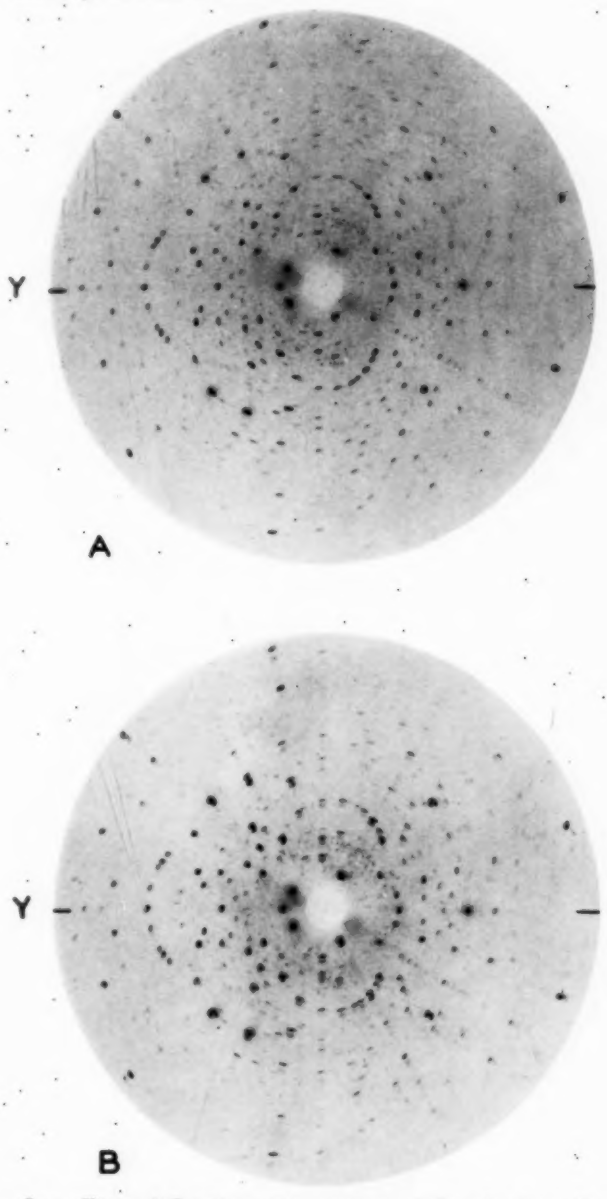

FIGURE 23.—*Laue X-ray diffraction patterns of muscovite mica from Brazil (sample 1682).*

A, Typical of patterns obtained at and below 100° C; *B*, typical of patterns obtained at 145°, 190°, 240°, and 285° C. Double spots are the result of diffractions by two crystals of slightly different orientations. Molybdenum target, distance from specimen to film, 4 cm. Reduced ¼.

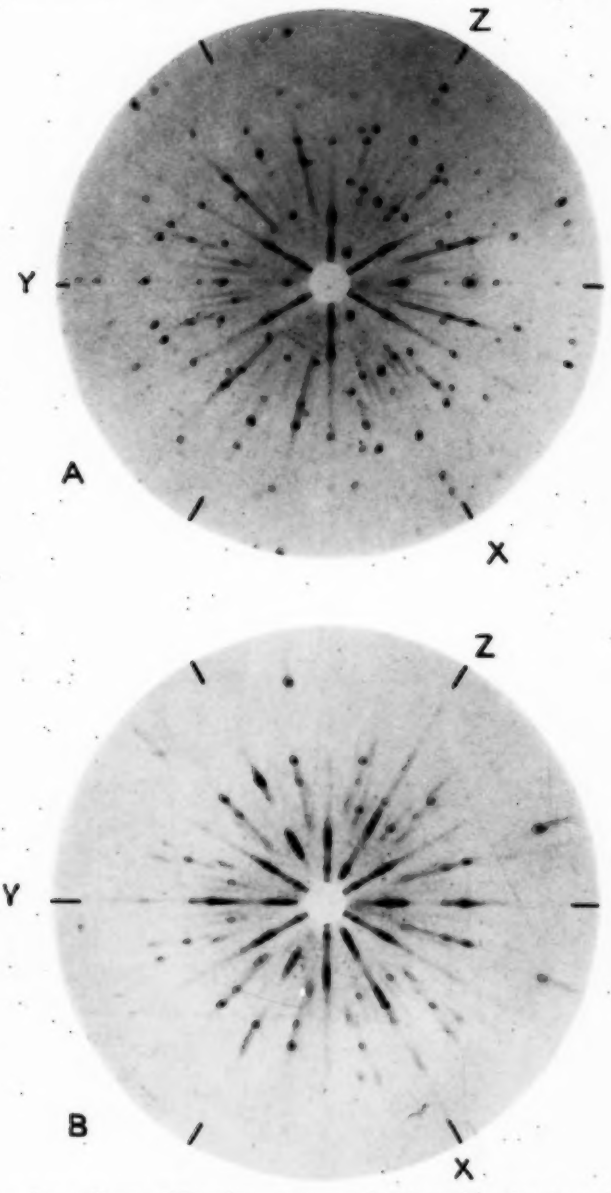

FIGURE 24.—*Laue X-ray diffraction patterns of phlogopite mica from Madagascar and Mozambique (samples 1681, 1681A and 1688).*

A, Typical of patterns obtained at temperatures below the transition temperature. The transition temperature was found to be different for different samples of phlogopite mica; *B*, typical of patterns obtained at temperatures above the transition temperature. The increase in asterism is thought to be the result of buckling of very thin layers parallel to the cleavage plane. Molybdenum target, distance from specimen to film, 4 cm. Reduced ¼.

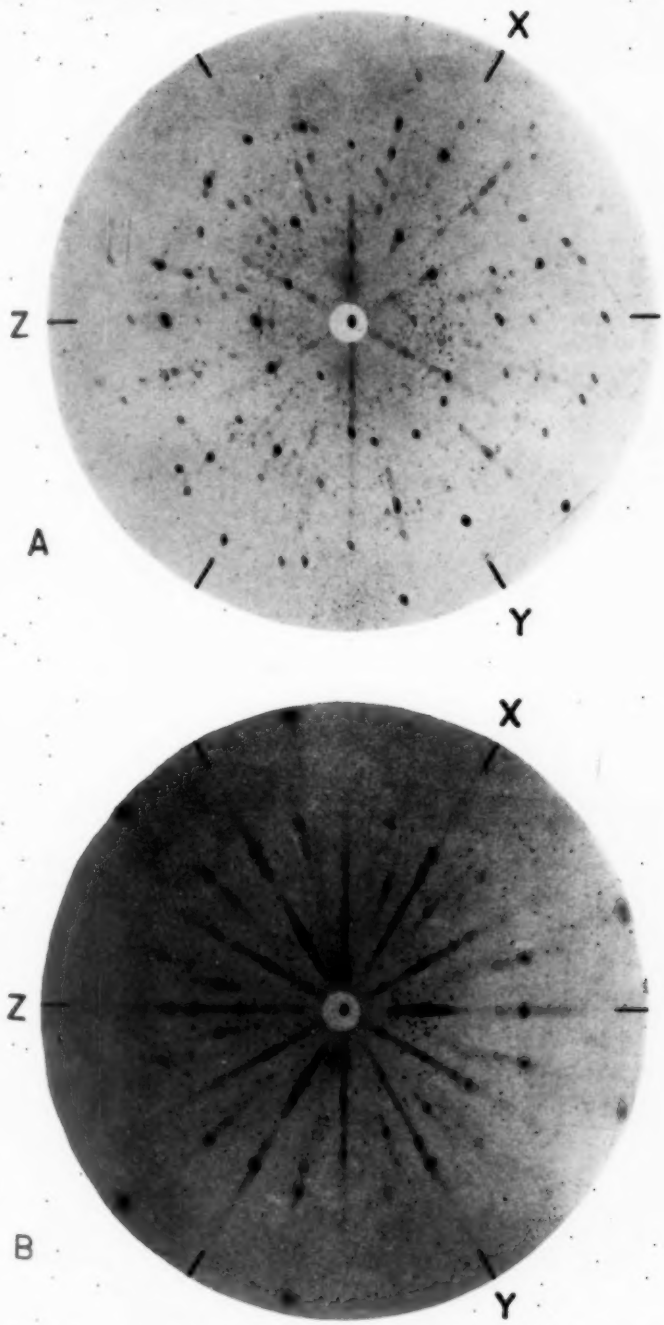

FIGURE 25.—*Laue X-ray diffraction patterns of biotite mica from North Carolina (sample 1713).*

A, Obtained before heating; *B*, typical of patterns obtained at 475°, 580° C, and after cooling to room temperature. The patterns indicate that heating caused a change in crystal symmetry and buckling of thin layers parallel to the principal cleavage plane. Molybdenum target, distance from specimen to film, 5 cm. Reduced ¼.

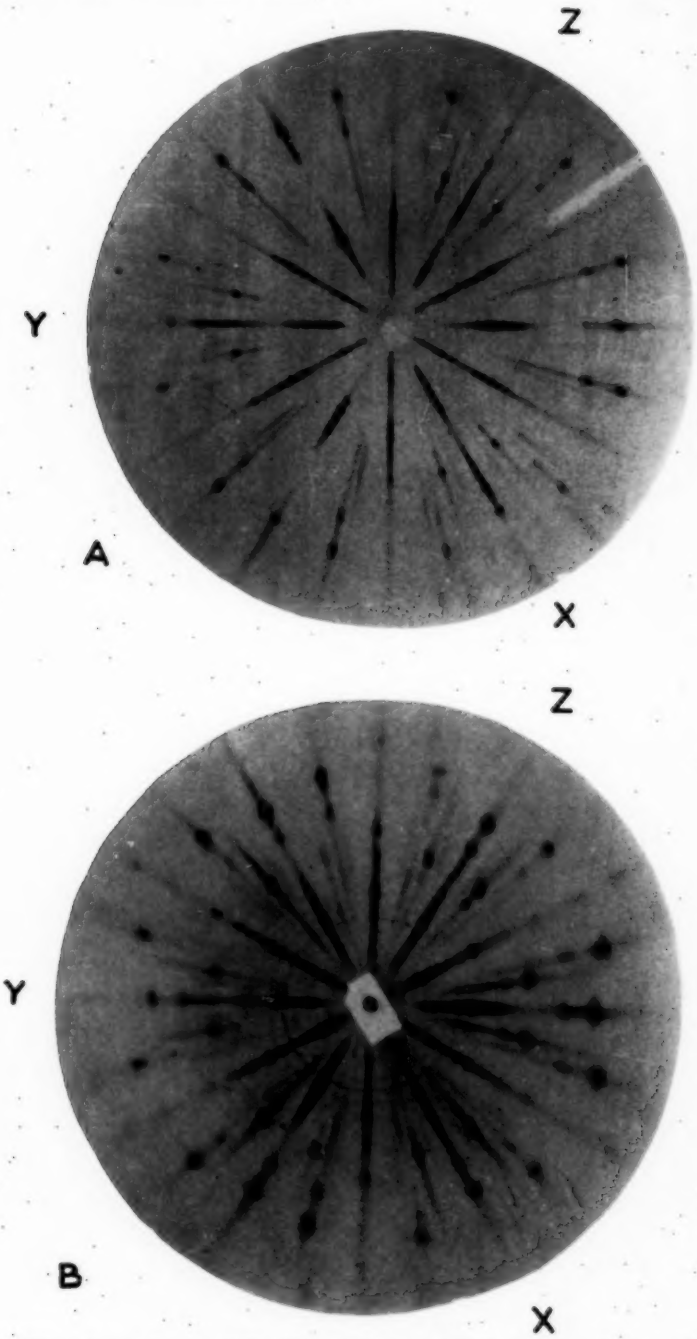

FIGURE 26.—*Laue X-ray diffraction patterns of phlogopite and muscovite mica after heating to 800° C. and cooling to room temperature.*

A, Phlogopite mica from Mozambique (sample 1688); *B*, muscovite mica from Brazil (sample 162). Heating has transformed the structure (fig. 23) of muscovite mica to a structure similar to that of phlogopite mica. Molybdenum target, distance from specimen to film, 6 cm. Reduced ¼.

imately 120°, developed considerable asterism (radial streaks) at elevated temperatures. In the patterns obtained from Madagascar phlogopite, asterism appeared on these zones between 190° and 245° C and became more pronounced at temperatures between 275° and 385° C. However, after Madagascar phlogopite was cooled from 385° C to room temperature a pattern showed that the structure reverted to its initial condition. The behavior of the Mozambique phlogopite was slightly different from that of the Madagascar phlogopite. Asterism on the *X*, *Y*, and *Z* zone lines appeared between 145° and 185° C and did not increase during heating to 385° C. However, after the Mozambique phlogopite was cooled to room temperature a slight amount of asterism was present. Patterns obtained from specimens

TABLE 4.—*Heating cycles and temperatures at which Laue patterns [a] of mica were obtained*

Sample No.	Mica	Heating cycle	Temperatures
			°C
1682 [b]	Muscovite, from Brazil, as received	1	20, 100, 20
		2	20, 145, 20
		3	20, 190, 240, 20
		4	20, 285, 20
1681 [b]	Phlogopite, from Madagascar, as received	1	20, 100, 145, 20
		2	20, 200, 20
		3	20, 245, 275, 20
		4	20, 340, 385, 20
1681A [c]	Phlogopite, from Madagascar, as received	1	20, 100, 135, 20
		2	20, 135, 190, 20
		3	20, 240, 290, 20
		4	20, 340, 385, 20
1688 [b]	Phlogopite from Mozambique, Africa, as received	1	20, 105, 20
		2	20, 145, 185, 20
		3	20, 245, 20
		4	20, 275, 340, 20
		5	20, 385, 20
1713	Biotite, from North Carolina, as received	1	20, 475, 20
		2	20, 590, 20
1713 [d]	Biotite, from North Carolina	1	20, 475, 20
		2	20, 590, 20

[a] See figs. 23 to 26, inclusive.
[b] Laue pattern was also obtained after specimen was heated to 800° C and cooled to room temperature.
[c] From same lot of mica as sample 1681.
[d] After heating incident to thermal expansion determinations. (See fig. 16.)

of phlogopite micas that had been heated and cooled incident to the thermal-expansion determinations showed slightly more asterism than the patterns obtained from specimens that had been heated and cooled in the furnace shown in figure 22. This increase in retained asterism was probably caused by the higher temperature to which the specimens were heated during the thermal-expansion determinations (see page 315). The temperature ranges in which Madagascar and Mozambique phlogopite micas indicated breaks in the expansion and contraction curves (figs. 6, 7, and 9) are in good agreement with the temperature ranges in which a change in structure was indicated.

The structure developed in biotite mica (sample 1713) at elevated temperatures did not revert to its initial condition as did that developed in the muscovite and phlogopite micas. The structure of the biotite mica before and after heating is indicated by the patterns of figure 25. The initial pattern of the biotite mica is similar to the initial patterns of the phlogopite micas. At 475° and 590° C and after cooling to room temperature, the patterns of the biotite mica were alike and had a degree of asterism similar to that shown in

patterns obtained from the phlogopite micas in the range from 185° to 385° C. The permanent change in structure brought about by heating to 475° and 590° C is in agreement with the anomalous thermal expansion and contraction curves obtained for biotite mica (fig. 16).

The fact that samples of muscovite mica indicated very large increases in thickness after heating to 800° C (see page 344) suggested the probable existence of a transition in muscovite mica at elevated temperatures.[14] The stable structure produced in biotite mica at elevated temperatures also suggested that the initial structures of muscovite and phlogopite micas might be altered permanently if heated to a sufficiently high temperature. Accordingly, patterns were obtained from muscovite mica (sample 1682) and phlogopite micas (samples 1681 and 1688) after heating to 800° C and cooling to room temperature. The pattern obtained from Madagascar phlogopite (sample 1681) showed some asterism but in general was similar to pattern *A* in figure 24. However, the pattern obtained from Mozambique phlogopite (sample 1688) shows considerable asterism (pattern *A*, fig. 26) and is similar to the patterns obtained at temperatures between 185° and 385° C (pattern *B*, fig. 24). The pattern obtained from the muscovite mica after heating to 800° C and cooling to room temperature also shows considerable asterism (pattern *B*, fig. 26). Inspection of the specimens showed that heating to 800° C caused little change in the Madagascar phlogopite but had caused the Mozambique phlogopite and the muscovite mica to swell and to separate partly into numerous laminas.

The structures of the micas investigated appeared to be fragmented by heating, as indicated by the asterism of all reflections. The asterism of the type shown in the initial patterns (before heating) was confined to certain crystallographic zones, thereby indicating a destruction in the lattice periodicity perpendicular to the principal cleavage plane [21]. The fragmentation produced in mica as a result of heating appears to be caused by the independent buckling of very thin layers parallel to the principal cleavage plane. The asterism resulting from buckling is superimposed on the asterism resulting from a destruction in the lattice periodicity.

3. POWER FACTORS

By E. L. Hall[15]

The power factors[16] of some samples of muscovite and phlogopite micas were determined at 100 and 1,000 kc/s in terms of a type 722-N General Radio precision condenser. The samples were in the form of 16-mm (⅝-in.)-diameter disks that had been punched from larger pieces of mica. A tinfoil disk approximately 14 mm (9/16 in.) in diameter was cemented to one side of each mica specimen, and a tinfoil disk about 10 mm (⅜ in.) in diameter was cemented to the other side of the specimen with small amounts of clear petroleum jelly, thus forming a small electric condenser. Four test specimens were prepared from each sample. The capacitance of the test specimens ranged between 70 and 200 micromicrofarads, depending upon thickness. Further details of the test method and equipment were published in a recent paper [23]. Table 5 gives the results obtained.

[14] Zwetsch [20] found a change in the X-ray spectra of muscovite mica above 600° C.
[15] Electrical Division, National Bureau of Standards.
[16] A tentative method of test for power factor of mica has been published [22].

TABLE 5.—*Power factors of some muscovite and phlogopite micas before and after treatment*

Sample number	Description	Treatment	Power factors	
			100 kc/s	1,000 kc/s
			Percent	*Percent*
1682 [a]	Muscovite mica from Brazil.	As received	0.16	0.10
			.08	.06
			.04	.03
			.04	.03
			Avg.. 0.08	0.06
1682 [a]	do	After heating to 600° C and cooling to room temperature with load of 30 lb/in.² incident to thermal expansion tests. (See fig. 1.)	0.13	0.10
			.04	.04
			.15	.10
			.09	.06
			Avg.. 0.10	0.08
1689 [a]	Muscovite mica from Guatemala.	As received	0.06	0.06
			.10	.07
			.05	.06
			.08	.06
			Avg.. 0.07	0.06
1689 [a]	do	After heating to 600° C and cooling to room temperature with load of 30 lb/in.² incident to thermal expansion tests. (See fig. 3.)	0.08	0.06
			.08	.06
			.06	.04
			.06	.05
			Avg.. 0.07	0.05
1681 [a]	Phlogopite mica from Madagascar.	As received	0.18	0.07
			.34	.16
			.12	.05
			.28	.11
			Avg.. 0.23	0.10
1681 [a]	do	After heating to 600° C and cooling to room temperature with load of 30 lb/in.² incident to thermal expansion tests. (See fig. 6.)	1.00	0.39
			.93	.37
			.96	.42
			1.25	.62
			Avg.. 1.04	0.45
1681 [b]	do	After heating to 600° C and cooling to room temperature without load.	0.90	0.42
			.42	.18
			.37	.15
			.39	.17
			Avg.. 0.52	0.23
1688 [a]	Phlogopite mica from Mozambique, Africa.	As received	0.95	0.67
			.94	.63
			1.03	.65
			.87	.52
			Avg.. 0.95	0.62
1688 [a]	do	After heating to 600° C and cooling to room temperature with load of 30 lb/in.² incident to thermal expansion tests. (See fig. 9.)	1.93	0.94
			1.77	.88
			2.1	1.06
			2.2	
			Avg.. 2.0	0.96
1688 [b]	do	After heating to 600° C and cooling to room temperature without load.	>3	1.55
			>3	1.53
			>3	1.63
			>3	1.93
			Avg.>3	1.66

[a] Power-factor measurements were made at 25° C and relative humidity of 50 percent.
[b] Power-factor measurements were made at 26° C and relative humidity of 34 percent.

The power factors of nearly all specimens of muscovite mica from Brazil and Guatemala were slightly greater at 100 kc/s than at 1,000 kc/s. The power factor of each specimen of phlogopite mica was considerably greater at 100 kc/s than at 1,000 kc/s. The power factors of the samples of phlogopite mica from Madagascar and Mozambique are considerably larger than the power factors of the samples of muscovite mica from Brazil and Guatemala. Heating the samples of phlogopite and muscovite micas to 600° C, with or without a load on each sample, caused considerable increases in the power factors of the phlogopite micas and only slight changes in the power factors of the muscovite micas. The power factors of the phlogopite mica from Madagascar which was heat treated without a load, are less than the power factors of this mica heat treated with a load. However, the power factors of the phlogopite mica from Mozambique heat treated without a load are considerably greater than the power factors of this mica heat treated with a load.

An examination of table 5 indicates divergent values for the power factors of different specimens of a given mica. These differences were not due to errors of observation but to variations in the specimens. A discussion of differences of the power factors of mica is given in a previous paper [23].

4. EFFECTS OF HEAT TREATMENTS ON THICKNESS, OPACITY, AND COLOR[17]

Five disks (about ⅝-in. diameter) were cut from each of the 30 micas, and their thicknesses were measured to the nearest 0.0001 in. with a Zeiss micrometer that applied a load of 36 oz (1.02 kg) between parallel contacts having 0.315-in. (8.00 mm) diameter. The thicknesses of the disks of mica ranged from 0.0036 to 0.0594 in. (0.092 to 1.51 mm).

One disk from each kind of mica was placed on a slab of flint clay and heated without a load in an electric furnace to 600° C maintained at this temperature for 1 hour, and then allowed to cool in the furnace. A second, third, fourth, and fifth disk of each kind of mica was heated to 700°, 800°, 900°, and 1,000° C, respectively, in a similar manner. After the disks of mica were cooled to room temperature, their thicknesses were measured with the Zeiss micrometer that applied the load indicated above. Table 6 shows the changes in thickness (in percent) of the disks of mica.

All of the muscovite micas except the processed plate mica (sample 1687) indicated changes in thickness of 2 percent or less after heating to 600° C. Nearly all of the muscovite samples indicated the greatest increases (up to 155 percent) after heating to 800° C. These results suggest the probable existence of a transition in muscovite micas between 600° and 800° C or a marked increase in the rate of cleavage in this temperature range. For nearly all of the muscovite samples, the increase in each sample after heating to 900° C is approximately equal to the increase after heating to 1,000° C and these changes are considerably less than those after heating to 800° C. Horton [3] stated that at 400° C, muscovite mica begins to give up minute quantities of its water of crystallization, at 700° C normal muscovites

[17] Designations of opacity and color and their interpretations have been taken from a report on test 43C-97/44 from the Photometry and Colorimetry Section of the National Bureau of Standards.

lose about one-tenth percent of their weight, and as dehydration progresses the mica swells and loses its transparency. The data on muscovite micas (under load) in table 6 are not in agreement with Horton's statement relating to increase in swelling, if applied to temperatures between 800° and 1,000° C.

The changes in thickness of the phlogopite samples ranged from a decrease of 25 percent to an increase of 39 percent. From these results it appears that phlogopite mica resists elevated temperatures better than muscovite mica. Horton [3] indicated that phlogopite micas, particularly light-colored varieties, are more resistant to heat than muscovite micas and will stand a temperature of 800° C without appreciable dehydration, probably because they contain less water of crystallization.

The outstanding feature of three of the four biotite samples is the fact that they show large increases in thickness (17 to 134 percent) after heating to 600° C. The changes of the four biotite samples after heating to higher temperatures indicated increases from 1 to 45 percent of the original thickness.

The maximum change in thickness (increase of 45 percent) of the ripidolite sample was observed after heating to 800° C. For the zinnwaldite sample, the maximum change (increase of 120 percent) was noted after heating to 1,000° C.

Some of the heat-treated specimens of mica when measured without a load were found to have increased 8 to 20 times the original thickness. When measured with the Zeiss micrometer which applied a load of 36 oz, the thickness of these specimens was reduced to less than two times the original thickness (see table 6).

In order to indicate the changes in appearance which each mica had undergone as a result of the heat treatments at elevated temperatures, the color designations of the disks of mica after the heat treatments and of disks that had not been heated are given in table 6. The appearance of each mica disk is indicated by an opacity and a color designation, and if necessary, by a one- or two-word description of texture.

The opacity of each specimen of mica is indicated as clear, translucent, or opaque. If, by looking through the specimen, objects (chimney and trees silhouetted against the sky) could be seen distinctly, the specimen was noted as "clear." If the specimen transmitted a noticeable amount of light but so scattered as to yield indistinct images or no image, it was noted as "translucent." If no noticeable light was transmitted, the specimen was noted as "opaque."

The colors of all specimens not exhibiting metallic luster were designated in accord with the ISCC–NBS method of designating colors described by Judd and Kelly [24] and by Kelly [25]. These designations accord with those used in the National Formulary (7th edition, 1942).

Most of the opaque specimens of mica have a metallic luster and were given a color designation by comparison with polished samples of silver, gold, and copper. These color designations and their meanings are as follows:

Silver.—Substantially the same body color and highlight as polished silver.

Gold.—Substantially the same body color and highlight as polished gold.

TABLE 6.—*Color designations and changes in thickness of 50 samples of mica after heating to elevated temperatures and cooling to room temperature*

The following abbreviations of color terms are those proposed by Nickerson and Newhall [26]. To these have been added abbreviations for metallic colors and terms descriptive of opacity and texture:

B=blue.
b=bluish
Bk=black
Br=brown
br=brownish.
cl=clear.
Cp=copper.
d=dusky.
dk=dark.
G=green.
g=greenish.
Go=gold.
go=golden.
Gr=gray.
lt=light.
mod=moderate.
O=orange.
o=orange.
Ol=olive.
ol=olive.
op=opaque.
p=pale.
Po=polychrome.
R=red.
r=reddish.
Sl=silver.
sl=silvery.
ta=tarnished.
tr=translucent.
v=very.
wk=weak.
Y=yellow.
y=yellowish.

Sample No.	Source	Description of appearance before heating	After heating to 600° and cooling to 20° C.		After heating to 700° and cooling to 20° C.		After heating to 800° and cooling to 20° C.		After heating to 900° and cooling to 20° C.		After heating to 1,000° and cooling to 20° C.	
			Description of appearance	Change in thickness	Description of appearance	Change in thickness	Description of appearance	Change in thickness	Description of appearance	Change in thickness	Description of appearance	Change in thickness
					A. MUSCOVITE MICA							
				Percent		*Percent*		*Percent*		*Percent*		*Percent*
1682	Brazil	cl, v p Br	cl, y Gr, Br spots	1	tr, Sl, y Gr	1	op, Sl	118	op, y Sl	41	op, Sl	44
1684	Canada	cl, v p O	cl, v p O	1	cl, y Gr	0	cl, y Gr	0	tr, Sl, lt br Gr	1	op, y Sl	47
1685	Brazil	cl, y Gr	cl, y Gr	1	tr, p Br, Br spots.	8	op, Sl	115	op, Sl	51	op, y Sl	45
1686	do	cl, v p Br	cl, wk Y	0	tr, Sl, p Br, Po	2	op, Sl	140	op, y Sl	54	op, Sl, p Br	52
1687	Plate mica (processed sheet).	tr, dk Sl	op, dk Sl	22	op, dk Sl	62	op, dk Sl	90	op, dk Sl	68	op, Sl, wk O	66
1689	Guatemala (Verde claro)	cl, p Ol	cl, d YG	1	tr, mod Ol, Po	1	op, sl Go	66	op, r Go	14	op, sl r Go	22
1690	Guatemala (Verde oscuro)	cl, ol Bk	cl, mod Ol	−0	op, sl g Go, Po	9	op, Go	71	op, go Cp	33	op, go Cp	24
1691	Colombia (Black stained)	cl, y Gr	cl, p Ol, Br spots	0	op, y Sl, Po	31	op, sl Go	81	op, r Go	b 64	op, r Go	51
1692	Colombia (Stained or good stained).	cl, p Ol	cl, p Ol	0	op, y Sl, Po	22	op, sl Go	124	op, r Go	46	op, r Go	52
1693	Colombia	cl, p Ol, Bk specks.	cl, wk Ol, Bk specks.	−1	op, y Sl	39	op, Go	126	op, r Go	56	op, sl r Go	44
1694	Peru	cl, y Gr	cl, y Gr	−1	op, Sl	46	op, sl Go	113	op, Go	61	op, sl Go	52
1695	do	cl, y Gr	cl, p Ol	−1	tr, y Sl	23	op, sl Go	65	op, sl Go	46	op, r Go	42
1696	Bolivia	cl, lt y Br	cl, p Br	−1	cl, wk Br, Po stripes.	0	op, dk Sl, Po	66	op, dk r Gr	27	op, r Go	22
1697	do	cl, lt Gr	cl, y Gr	+1	cl, p Ol, Po	−1	op, ta Sl	59	op, dk go Cp	23	op, dk go Cp	29
1698	do	tr, Sl	op, Sl	1	op, Sl	+24	op, y Sl	100	op, Go	44	op, sl r Go	40
1699	New Hampshire (first quality).	cl, p Br	cl, p Ol	0	cl, p Ol, Po, Br spots.	−1	op, y Sl	110	op, sl Go	60	op, sl Go	45

1697	do	cl, lt Gr	cl, y Gr	+1	cl, p Ol, Po	−1	op, ta Sl	59	op, dk go Cp	23	op, dk go Cp	29
1698	do	tr, Sl	op, Sl	1	op, Sl	+24	op, y Sl	100	op, Go	44	op, sl r Go	40
1699	New Hampshire (first quality).	cl, p Br	cl, p Ol	0	cl, p Ol, Po, Br spots.	−1	op, y Sl	110	op, sl Go	50	op, sl Go	45
1700	New Hampshire (second quality).	cl, p Br	cl, wk YG, Y spots.	0	tr, y Sl, Po	+3	op, y Sl	96	op, Go	49	op, sl Go, wk y O.	40
1701	South Dakota (first quality).	cl, p Br	cl, y Gr	0	fr, b Sl	6	op, Sl	106	op, Sl, lt Gr	52	op, Sl lt Gr	58
1702	South Dakota (second quality).	cl, v p Br	cl, p Br	0	op, b Sl	22	op, Sl	104	op, Sl, lt Gr	58	op, Sl, lt Gr	60
1703	North Carolina (first quality).	cl, mod Ol	cl, wk Ol G	1	op, ta Sl, Po	15	op, dk Go	125	op, go Cp	29	op, go Cp	34
1704	North Carolina (second quality).	cl, mod Ol	cl, mod Ol	0	op, ta Sl, Po	28	op, r Go	101	op, go Cp	34	op, go Cp	34
1705	North Carolina (first quality).	cl, p Br	cl, v p Br	1	op, Sl	13	op, y Sl	101	op, sl Go	41	op, sl Go	44
1706	North Carolina (second quality).	cl, v p Br	cl, p Br	1	op, Sl	20	op, y Sl	104	op, sl Go	48	op, sl Go, mod y Br.	44
1707	New Mexico (first quality).	cl, wk YG	cl, wk YG	1	cl, wk YG, Po	−1	op, ta Sl, Po	83	op, dk Go	35	op, sl Go	30
1708	New Mexico (second quality).	cl, wk YG	cl, wk ol G	0	tr, g Sl, Po	+2	op, dk Go, Po	74	op, dk go Cp	31	op, dk go Cp	32
1729	Ontario, Canada	cl, br Bk	cl, br Bk	1	op, ta Sl, Po	9	op, sl Go	[b] 155	op, go Cp	51	op, go Cp	[b] 160
1731	Quebec, Canada	cl, lt y Br	cl, v p Br	0	op, y Sl	101	op, Sl	20	op, y Sl wk y O.	69	op, y Sl, wk y O.	63
1741	Bolivia	cl, y Gr	cl, wk Y	1	cl, wk Y, Po	−2	op, ta Sl	85	op, ta Sl	38	op, ta Sl	38
1742	Argentina (semiclear)	cl, p Br	cl, p Ol	−1	op, Sl	+29	op, sl Go	88	op, Go	51	op, Go	48
1743	Argentina (semistained)	cl, p Ol	cl, p Ol	+1	op, Sl	25	op, Go	91	op, r Go	45	op, r Go	47
1744	Argentina (stained)	cl, p Ol	cl, p Ol	0	op, Sl	40	op, sl Go	72	op, sl Go	47	op, sl Go	49
1745	Argentina	cl, y Gr	cl, y Gr	−1	cl, p Ol, Po	2	op, y Sl	83	op, y Sl	48	op, y Sl	49
1746	Argentina (clear)	cl, y Gr	cl, y Gr	0	tr, Sl, p Br	17	op, Sl	79	op, Sl	56	op, Sl	57
1747	Argentina (semiclear)	cl, v p Br	cl, v p Br	−2	tr, Sl, p Br, Po	16	op, Sl	90	op, y Sl	62	op, y Sl, lt y Br	50
1748	do	cl, y Gr	cl, y Gr, Br spots	0	tr, Sl, p Br	7	op, Sl	53	op, y Sl, mod y Br.	44	op, y Sl, lt y Br.	41
1749	Maine	cl, y Gr									op, Sl, p Br	52

B. PHLOGOPITE MICA

1681	Madagascar	cl. d Br	op, ta Sl	5	tr, ta Sl, d Br	0	op, sl Go	34	op, r Go	10	op, r Go	12
1683	do	op, br Bk	op, br Bk	−1	op, br Bk	−1	op, v dk Go	−1	op, dk Go	2	op, r Go	6
1688	Mozambique, Africa	op, br Bk	op, v dk Go	+1	op, dk Go	+24	op, dk r Go	+39	op, dk r Go	17	op, dk r Go, Sl spots.	9
1709	do	op, br Bk	op, br Bk	−7	op, br Bk	−2	op, br Bk	−4	op, br Bk, Po	4	op, dk go Cp	7
1710	do	tr, y Sl	op, y Sl	+7	op, y Sl	−6	op, sl Go	−6	op, Go	−11	op, sl r Go	−25
1711	Burgess, Canada	op, sl Cp	op, y Sl	5	op, y Sl	+6	op, y Sl	+5	op, y Sl	+3	op, y Sl	+8
1712	New York	cl, v p Br	tr, Sl	5	tr, Sl	0	tr, y Gr	−3	tr, Sl	2	op, Sl, lt Gr	8
1732	Quebec, Canada	op, br Bk	op, br Bk, speckled.	−0	op, br Bk	−1	op, br Bk, Po	0	op, dk r Go	−1	op, dk r Go	2

See footnotes at end of table.

TABLE 6.—*Color designations and changes in thickness* [a] *of 50 samples of mica after heating to elevated temperatures and cooling to room temperature*—Continued

Sample No.	Source	Description of appearance before heating	After heating to 600° and cooling to 20° C.		After heating to 700° and cooling to 20° C.		After heating to 800° and cooling to 20° C.		After heating to 900° and cooling to 20° C.		After heating to 1,000° and cooling to 20° C.	
			Description of appearance	Change in thickness	Description of appearance	Change in thickness	Description of appearance	Change in thickness	Description of appearance	Change in thickness	Description of appearance	Change in thickness
					C. BIOTITE MICA							
				Percent		*Percent*		*Percent*		*Percent*		*Percent*
1713	Newdale, N. C	op, Bk	op, dk go Cp, Po.	[b]75	op, Cp	29	op, go Cp	37	op, Cp	45	op, Cp	11
1730	Ontario, Canada	op, Bk	op, Bk	—0	op, Bk	1	op, Bk, Po	20	op, Bk	23	op, Bk	9
1733	Macon County, N. C	op, br Bk	op, d y Br, flakes.	[b]17	op, dk O flakes, Po.	18	op, Cp	33	op, dk Br	30	op, Cp, Po	7
1734	Oxford County, Maine	op, br Bk	op, dk y Br, flakes.	[b]134	op, Cp	28	op, Cp	[b]37	op, Cp	[b]25	op, mod y Br	34
					D. RIPIDOLITE MICA							
1714	Pennsylvania	op, g Bk	op, ol Bk	1	op, Bk, Po	2	op, ta Sl	45	op, y Sl	14	op, y Sl	9
					E. ZINNWALDITE MICA							
1735	Virginia	tr, dk y Br	tr, mod Br	0	op, wk Br	6	op, wk Br	25	op, br Gr, mat	45	op, dk Gr, mat	120

[a] During the measurement of the thickness of each specimen of mica, the micrometer applied a load of 36 oz between parallel contacts having 0.315-in. diameter. Each negative value in the table indicates a decrease in thickness.

[b] With no load on specimen, the increase in thickness was 8 to 20 times the original thickness.

Copper.—Substantially the same body color and highlight as polished copper.

Yellowish silver.—More like silver than gold.

Silvery gold.—More like gold than silver.

Reddish gold.—More like gold than copper.

Golden copper.—More like copper than gold.

Silvery copper.—More like copper than silver.

Tarnished silver.—Highlight darker and yellower than that of polished silver.

Polychrome.—Many colored, as by interference colors.

Many of the specimens of mica have an appearance partially like polished metal and partially dissimilar. The luster is metallic and the highlight can be described fairly well by the above terms. The body color, however, is lighter than that of the metal on account of light being diffused from the body of the specimen so that the metallic term is only partially applicable. These specimens have accordingly been given a double designation, a designation of the metallic luster by the above terms combined with a body-color designation in accord with the method of designating colors by Judd and Kelly [24].

The specimens of mica were examined by light from the north sky. The designations of body color were found by comparisons with the charts of the Munsell Book of Color, complete 40-hue-chart edition, specimen and charts being illuminated along angles centering on 45 degrees and viewed approximately along the perpendicular. The designations of metallic luster were obtained chiefly by observations in which the specimen and the metallic standard were held in the same plane, illuminated at about 20 degrees from the perpendicular, and viewed at the angle of mirror reflection.

All but two of the specimens of mica exhibited luster, either metallic or vitreous. The two exceptions were designated "mat" in table 6 (sample 1735, heat treated at 900° and 1,000° C).

The appearance of the mica specimens gives a fairly reliable indication of the degree to which heat treatment caused cleavage along crystal planes. The first indication of cleavage is the change from vitreous to a polychrome luster, and for clear specimens the change to translucency. This first indication seems to be quickly followed by a change from polychrome luster to metallic luster, and for clear specimens the change from translucent to opaque. Both of these changes are to be expected from the development of many cleavages. A third stage of cleavage is indicated by the development of a body color lighter than that of the corresponding polished metal. The final stage of disintegration, indicated by a loss of luster, is the breaking up of the crystals into minute elementary crystals. Only the sample of zinnwaldite mica reached this stage; the heat treatment to 1,000° C left it an ashlike, mat dark gray.

The color differences among the original untreated micas seem to be ascribable to inclusions of varying amounts. The spots that develop from the heat treatment suggest segregation of these materials.

Large increases in thickness of nearly all of the muscovite samples accompanied changes from clear or translucent to opaque, or from polychrome to metallic color.

Horton [3] reported data by F. R. Caldwell, of the National Bureau of Standards, on some physical properties (color, condition of surface,

opacity, separation of laminas, texture, and size) of 19 samples of mica (muscovite, phlogopite, and biotite) after heat treatments (without a load) to various temperatures between 600° and 1,200° C. There was no perceptible change in these micas after heating at 600° C except that a biotite mica from South Dakota swelled to 10 times its original thickness and a phlogopite mica from Quebec, Canada, swelled to about 8 times its original thickness. At 800° C all muscovite samples showed radical changes, most of them swelling considerably. Two of the Canadian and all of the Madagascar phlogopites were not notably affected at 800° C. At 1,200° C all the micas blistered and were so changed as to be unsuitable for use.

IV. DISCUSSION

It has been stated by Mohr [6], Lewis, Hall, and Caldwell [27], Horton [3], Houk [28] and Gwinn [29] that muscovite and phlogopite micas withstand heating between 400° and 600° C without appreciable change. The results obtained in the present investigation indicate that there was little change in the samples of muscovite mica when heated to 600° C, but there were appreciable changes in some of the samples of phlogopite mica when heated to 600° C. Some of the samples of phlogopite mica had an enormous thermal expansion when heated to this temperature. Heating some samples of phlogopite mica to 600° C and cooling to room temperature caused appreciable changes in power factors, opacity, and thickness.

There is some evidence [11] indicating that the thermal expansion of the elementary crystals of phlogopite mica is comparatively small. The pronounced increases in the thermal expansion of some phlogopite micas (figs. 6, 7, 9, 12, and 14) and biotite micas (figs. 16 to 19, inclusive) may be ascribed to the displacement or tilting of the elementary crystals of the mica laminas on heating.

Powell and Griffiths [30] investigated the thermal conductivity (under pressure) of some muscovite and phlogopite micas up to a temperature of 600° C, in a direction perpendicular to the cleavage plane. Five specimens of Indian muscovite mica showed slight variations of the thermal conductivity with temperature over the range 100° to 600° C. However, Canadian and Madagascan phlogopite micas indicated a pronounced decrease in thermal conductivity between 150° and 250° C, which was only partially reversible on cooling. Subsequent examination of these micas by Wood [11] by means of X-ray crystal analysis revealed the fact that in these samples that suffered appreciable change in conductivity, the arrangement of the elementary crystals composing the mica laminas became displaced from their ordered setting at approximately the same temperature as the thermal conductivity change. It was considered that the surface crystals became stepped as a result of the heat treatment, even though the surface still appeared to be approximately plane.

Wood [11] concluded that these structural changes alone appeared to be responsible for the anomalies in the thermal conductivity of phlogopite mica. He stated that "The fall in thermal conductivity of these micas at elevated temperatures is to be explained by the physical disturbances in the macrostructure in which an initially perfect crystal disintegrates into innumerable elements, themselves

intrinsically perfect but differing very widely in orientation from the initial uniform formation. It is reasonable to suppose that the extra boundaries thus produced increase the resistance to the heat flow. It is a new and interesting point that such a mosaic formation may be brought about by a rise in temperature and may actually exhibit a partial recovery on cooling, and, as found subsequently, on aging. The tendency to recovery and the critical temperature required suggest that the fragmentation is not due to escape of gas, known to be evolved by heated mica, but rather associated more intimately with the atomic structure."

In view of the fact that certain micas possess tremendously high thermal expansion in a direction perpendicular to the cleavage plane, it is possible to use them in temperature responsive devices.[18] For example, one or more disks of a high-expanding mica in combination with a metal, alloy, or nonmetallic material may be employed so that when this combination is heated or cooled, a large differential expansion or contraction occurs. The large differential expansion and contraction offer a basis for controlling and indicating temperatures over a wide, useful range. The action caused by the differential expansion or contraction can be converted into a linear or angular movement. The enormous thermal expansion, many times that of any other known solid material, makes it possible to use a considerably smaller expanding element in a temperature responsive device than is possible with a so-called "high-expanding" element of any other solid material. When high-expanding mica is used to operate thermal responsive devices it may not be necessary to depend on mechanical magnification which is often required with other materials.

The high-expanding micas, which can be used to operate temperature responsive devices, may present serious difficulties when used for some other purposes. For example, the use of such micas as insulating parts in electric devices where large dimensional changes are not desired, would affect the usefulness of the devices when subjected to large temperature changes. Furthermore, the use of high-expanding micas in locked or rigidly bound parts of a device subject to large temperature changes would undoubtedly result in permanent injury to the device.

V. SUMMARY AND CONCLUSION

This paper gives data on the linear thermal expansion, changes in structure, power factors, and effects of heat treatments on thickness, opacity, and color of micas (muscovite, phlogopite, biotite, ripidolite, and zinnwaldite) from different domestic and foreign sources.

The results obtained on the thermal expansion of 30 samples of micas in a direction perpendicular to the cleavage plane when subjected to a load over the range 20° to 600° C (or 700° C) are indicated in figures 1 to 21, inclusive. Tremendous expansion was noted for some of the samples of phlogopite and biotite micas. The maximum coefficients of expansion of the samples of phlogopite and biotite micas are 0.0552 (between 100° and 114° C) and 0.00411 (between 500° and

[18] During the preparation of the present paper, the attention of the authors was called to U. S. Patent 2,246,536, which was granted to Josef Reinthaler on June 24, 1941. His invention relates to thermostat and other thermomotive means by the use of a pile of plates of muscovite mica to 600° C and of phlogopite mica to 1,200° C. The present authors tested the 36 muscovite micas indicated in table 1 between 20° and 600° C, and did not find any that are suitable in this temperature range for temperature responsive devices.

600° C) per degree centigrade, respectively. The coefficients of expansion of the samples of muscovite, ripidolite, and zinnwaldite micas are comparatively low. The maximum coefficient of expansion of the samples of these three types of mica is 0.000036 per degree centigrade.

Laue X-ray diffraction patterns of a few samples of micas (muscovite, phlogopite, and biotite), at room temperature and at elevated temperatures, are shown in figures 23 to 26. The transitions shown in the expansion curves of two phlogopite samples and a biotite sample at elevated temperatures appear to be related to the structural changes indicated in the X-ray diffraction patterns in figures 24 and 25. These changes may be ascribed to the buckling of very thin layers during heating, resulting in the displacement or tilting of the elementary crystals of the mica laminas.

The power factors of two samples of phlogopite mica from Madagascar and Mozambique were found to be considerably greater at 100 kc/s than at 1,000 kc/s. The power factors of these samples are considerably larger than the power factors of two samples of muscovite mica from Brazil and Guatemala. Heat treatment of the samples of phlogopite and muscovite micas to 600° C with or without a load, caused considerable increases in the power factors of the former and only slight changes in the latter.

The effects of heat treatments on the thickness, opacity, and color of 50 samples of various micas are indicated in table 6. Nearly all of the muscovite samples showed the greatest increases in thickness (up to 155 percent) after heat treatment at 800° C. The results on the changes in thickness of the phlogopite and muscovite samples indicate that the former resist elevated temperatures better than the latter. The large increases in thickness of nearly all of the muscovite samples accompanied changes from clear or translucent to opaque, or from polychrome to metallic color.

None of the species of mica can be considered as a substance or material of fixed and reproducible properties. There are wide variations in such properties as thermal expansion, power factor, and color. These properties of mica depend largely upon the chemical composition, the nature of the crystals, their magnitude and their orientation, the presence of impurities, the way in which these enter the structure, the heat treatment, etc.

Some of the phlogopite and biotite micas, which possess tremendously high thermal expansion in a direction perpendicular to the cleavage plane, may have decided advantages when used for high-expanding elements in temperature responsive devices.

The authors are greatly indebted to the corporations and Government agencies listed in table 1 for the samples of mica used in this research. The assistance of the following members of the staff of the National Bureau of Standards is also acknowledged: Deane B. Judd, for the determination of opacity and color of the specimens of mica; Henry W. Bearce and Wilmer Souder, for valuable suggestions; and James F. Pfau for the preparation of the illustrations on thermal expansion.

VI. REFERENCES

[1] G. Agricola, Da natura fossilium (1546).
[2] B. De Boot, Gemmarum et lapidarum historia (1647).
[3] F. W. Horton, Mica, U. S. Bureau of Mines Information Circular 6822, revised edition (August 1941). This circular includes data obtained on dielectric strength, power factors, and physical changes of mica by A. B. Lewis, E. L. Hall, and F. R. Caldwell of the National Bureau of Standards.
[4] S. B. Hendricks and M. E. Jefferson, Polymorphism of the micas; with optical measurements, Am. Mineral. **24**, 729 (1939).
[5] L. Pauling, The structure of the micas and related minerals, Proc. Nat. Acad. Sci. **16**, 123 (1930).
[6] H. Mohr, Der Nutzglimmer (Verlag von Gebrüder Borntraeger, Berlin, 1930).
[7] J. W. Mellor, A comprehensive treatise on inorganic and theoretical chemistry, vol. VI, 603 (1925).
[8] P. Hidnert and W. T. Sweeney, Thermal expansion of magnesium and some of its alloys, BS J. Research **1**, 771 (1928) RP29.
[9] W. Souder and P. Hidnert, Measurements on the thermal expansion of fused silica, BS Sci. Pap. **21**, 1 (1926–27) S524.
[10] H. D. Megaw, The thermal expansion of certain crystals with layer lattices, Proc. Roy. Soc. London, [A] **142**, 198 (1933).
[11] W. A. Wood, The variation with temperature of the thermal conductivity and the X-ray structure of some micas. II.—The X-ray examination of the structure, Proc. Roy. Soc. London, [A] **163**, 199 (1937).
[12] P. Braesco, Cuisson des argiles, Compt. rend. **157**, 123 (1913).
[13] P. Braesco, Étude des points de transformation par une méthode dilatométrique, Ann. phys. **14**, 5 (1920).
[14] W. Souder and W. T. Sweeney, data obtained at National Bureau of Standards (1925).
[15] H. Ebert, Ausdehnungsmessungen, Z. Instrumentenk. **47**, 324 (1927).
[16] H. Ebert, Ausdehnungsmessungen bei tiefen Temperaturen, Z. Physik **47**, 712 (1928).
[17] R. A. Heindl, Linear thermal expansion of muscovite mica, NBS Tech. News Bul. 181, p. 46 (May 1932).
[18] H. Ebert, Ausdehnungsbestimmungen, Physik. Z. **36**, 258 (1935).
[19] R. Rieke and Pu-Yi Wen, Die Wirkung von Kaliglimmer in Porzellanmassen, Ber. deut. keram. Gesell. **20**, 43 (1939).
[20] A. Zwetsch, Röntgenuntersuchungen in der Keramik, Ber. deut. keram. Gesell. **15**, 2 (1934).
[21] S. B. Hendricks, Variable structures and continuous scattering of X-rays from layer silicate lattices, Phys. Rev. **57**, 448 (1940).
[22] Tentative method of test for power factor and dielectric constant of natural mica, ASTM Designation 351–42 T, ASTM Standards, part III, Nonmetallic materials, p. 1207 (1942) (Am. Soc. Testing Materials, Philadelphia, Pa.).
[23] E. L. Hall, Equipment and method for measurement of power factor of mica, Proc. Inst. Radio Engrs. **32**, 393 (1944).
[24] D. B. Judd and K. L. Kelly, Method of designating colors, J. Research NBS **23**, 355 (1939) RP1239.
[25] K. L. Kelly, Instructions for determining color names for drugs and chemicals, Bul. Nat. Formulary Comm. **8**, 11 (1940).
[26] D. Nickerson and S. M. Newhall, Central notations for ISCC–NBS color names, J. Opt. Soc. Am. **31**, 587 (1941).
[27] A. B. Lewis, E. L. Hall, and F. R. Caldwell, Some electrical properties of foreign and domestic micas and the effect of elevated temperatures on micas, BS J. Research **7**, 403 (1931) RP347.
[28] L. G. Houk, Marketing strategic mica, U. S. Bureau of Mines Information Circular 7219 (September 1942).
[29] G. R. Gwinn, Strategic mica, U. S. Bureau of Mines Information Circular 7258 (September 1943).
[30] R. W. Powell and E. Griffiths, The variation with temperature of the thermal conductivity and the X-ray structure of some micas. I.—The thermal conductivity up to 600° C, Proc. Roy. Soc. London, [A] **163**, 189 (1937).

WASHINGTON, March 24, 1945